Exploring the Quantum Regime of Nanoelectromechanical Systems

**Dissertation zur Erlangung des
naturwissenschaftlichen Doktorgrades der
Bayerischen Julius-Maximilians-Universität Würzburg**

vorgelegt von

Stefan Walter

aus Würzburg

Würzburg 2012

Eingereicht am: . . . .

bei der Fakultät für Physik und Astronomie

1. Gutachter: . . . .

2. Gutachter: . . . .

3. Gutachter: . . . .

der Dissertation

1. Prüfer: . . . .

2. Prüfer: . . . .

3. Prüfer: . . . .

4. Prüfer: . . . .

im Promotionskolloquium

Tag des Promotionskolloquiums: . . . .

Doktorurkunde ausgehändigt am: . . . .

To my parents.

Zusammenfassung

Diese Arbeit beschäftigt sich mit den quantenmechanischen Aspekten von nanoelektromechanischen Systemen. In nanomechanischen Systemen koppelt ein nahezu makroskopischer mechanischer Freiheitsgrad an einen elektronischen Freiheitsgrad. Ohne weitere Einschränkungen kann der mechanische Freiheitsgrad mit der fundamentalen Anregung eines harmonischen Oszillators beschrieben werden. Auf Grund der Größenordnung von beteiligten Längen- und Energieskalen spielt die Quantenmechanik eine sehr wichtige und nicht zu vernachlässigende Rolle in der Beschreibung dieser Systeme. In dieser Arbeit untersuchen wir elektrische Transporteigenschaften in solchen nanomechanischen Elementen, wobei unser Fokus in der Quantennatur dieser Systeme liegt. Um quantenmechanische Effekte gänzlich zu berücksichtigen, verwenden wir Nichtgleichgewichts-Methoden wie zum Beispiel den Keldysh Formalismus. Wir konzentrieren uns hauptsächlich auf Systeme, in denen der nanomechanische Oszillator Teil eines Tunnelkontaktes ist. In solchen Anordnungen wird die Tunnelbarriere durch den Oszillator moduliert, was zur Folge hat, dass auch die elektronischen Transporteigenschaften beeinflusst werden. Durch Signaturen in Transportgrößen der Elektronik, wie zum Beispiel des mittleren Tunnel-Stroms oder des Stromrauschens, ist es nun möglich den nanomechanischen Oszillator zu untersuchen und zu charakterisieren. Die Wechselwirkung zwischen dem mechanischem Freiheitsgrad und anderen Freiheitsgraden ermöglicht es diese anderen Freiheitsgrade zu charakterisieren. Folglich kann der nanomechanische Oszillator als Detektor benutzt werden. In dieser Arbeit zeigen wir, dass der nanomechanische Oszillator als Detektor für sehr exotische physikalische Freiheitsgrade verwendet werden kann. Diese exotischen Freiheitsgrade sind sogenannte gebundene Majoranazustände, die kürzlich in der theoretischen und experimentellen Physik viel Aufsehen erregt haben. Hier spielt die quantenmechanische Beschreibung des Systems wiederum eine große Rolle. Eines der wichtigsten und faszinierendsten Phänomene der Quantenmechanik ist die quantenmechanische Verschränkung zweier Quantensysteme. Die Verschränkung von quantenmechanischen Systemen mit wenigen (diskreten) Freiheitsgraden ist ein theoretisch und experimentell sehr gut verstandenes Phänomen. Wir untersuchen Verschränkung zwischen zwei makroskopischen Systemen mit kontinuierlichen Freiheitsgraden in zwei verschiedenen Anordnungen, die es erlauben zwei nanomechanische Oszillatoren zu verschränken, die nicht direkt miteinander gekoppelt sind. Schließlich fassen wir unsere Ergebnisse zusammen und diskutieren offene Fragen und künftige Entwicklungen, die sich mit der Quantennatur nanoelektromechanischer Systeme beschäftigen.

Summary

This thesis deals with nanoelectromechanical systems in the quantum regime. Nanoelectromechanical systems are systems where a mechanical degree of freedom of rather macroscopic size is coupled to an electronic degree of freedom. The mechanical degree of freedom can without any constraints be modeled as the fundamental mode of a harmonic oscillator. Due to their size and the energy scales involved in the setting, quantum mechanics plays an important role in their description. We investigate transport through such nanomechanical devices where our focus lies on the quantum regime. We use non-equilibrium methods to fully cover quantum effects in setups where the mechanical oscillator is part of a tunnel junction. In such setups, the mechanical motion influences the tunneling amplitude and thereby the transport properties through the device. The electronics in these setups can then be used to probe and characterize the mechanical oscillator through signatures in transport quantities such as the average current or the current noise. The interplay between the mechanical motion and other physical degrees of freedom can also be used to characterize these other degrees of freedom, i.e., the nanomechanical oscillator can be used as a detector. In this thesis, we will show that a nanomechanical oscillator can be used as a detector for rather exotic degrees of freedom, namely Majorana bound states which recently attracted great interest, theoretically as well as experimentally. Again, the quantum regime plays an essential role in this topic. One of the major manifestations of quantum mechanics is entanglement between two quantum systems. Entanglement of quantum systems with few (discrete) degrees of freedom is a well established and understood subject experimentally as well as theoretically. Here, we investigate quantum entanglement between two macroscopic continuous variable systems. We study different setups where it is possible to entangle two nanomechanical oscillators which are not directly coupled to each other. We conclude with reviewing the obtained results and discuss open questions and possible future developments on the quantum aspects of nanomechanical systems.

Contents

Part I

Introduction

Introduction to nanoelectromechanical systems

Our everyday world is predominantly governed by the laws of classical mechanics that describe the motion of macroscopic objects under the influence of forces acting on them. The basic physical and mathematical laws of classical mechanics were established in 1686 by Sir Isaac Newton who also built upon research done by Johannes Kepler and Galileo Galilei a hundred years earlier. Also being part of our everyday world but far from our usual experience is the atomic and subatomic world. For objects as for instance single electrons and atoms, the theory established by Newton no longer applies but quantum mechanics sets the laws for the behavior of atomic and subatomic particles and objects. It is intuitive to assume that there is a separation of length scales. There is the macroscopic and the atomic regime which are exceptionally well described and tested by the theory of classical and quantum mechanics, respectively. If we would take a macroscopic object and decrease its size, we could imagine that at some point its properties and its interaction with other objects start to differ. This regime is called the mesoscopic regime, an intermediate regime where system sizes vary from a few atoms to micrometers.

In his famous 1959 talk "There's plenty of room at the bottom", Richard Feynman invited us "[...] to enter a new field of physics." and talked about "[...] the problem of manipulating and controlling things at the small scale." [Feynman60]. This new field of physics envisaged by Feynman back in 1959, today is no longer just an imagination but the frontier of technical applications and realizations of theoretical proposals. Micro- and nanotechnology led to a second industrial revolution with applications ranging from microchips to micromechanical sensors for, e.g., force, pressure, and acceleration.

We are most interested in mechanical systems on the mesoscopic length scale called nanoelectromechanical system (NEMS), i.e., these systems are not of atomic size but they consist of a considerably low number of atoms. Nanomechanical systems are right in the regime between macroscopic and atomic. Already on the mesoscopic length scale, quantum mechanics, as we will see, can play a non negligible role. As the name "nanoelectromechanical" already suggests, we deal with systems that have a mechanical degree of freedom coupled to an electronic system which could either be used to control and manipulate the mechanical degree of freedom or be used to gain information on the mechanical degree of freedom. One might claim that Coulomb's mechanical torsion balance was the first electromechanical system used as a practical measurement device to discover the $1/\text{distance}^2$ dependence of the force between two electrical charges. Nowadays, nanomechanical systems are used as highly sensitive detectors for, e.g., mass [Yang06, Jensen08, Lassagne08, Chiu08, Naik09] and force [Mamin01].

Typical geometries of nanoelectromechanical systems include simple beam-like structures that are either clamped on both ends or just on one end of the beam [Kleckner06, Flowers-Jacobs07]. Recently, there are also more advanced geometries as drum-like structures [O'Connell10, Teufel11]. The properties of the mechanical motion depend strongly on the dimensional parameters as well as the material used for fabrication. These systems effectively act as a harmonic oscillator when we take the limit of small amplitude oscillations. Typical beam-like structures are around $1\,\mu$m long, $20\,$nm wide and $60\,$nm thick. The drum in Ref. [O'Connell10] has a diameter of $60\,\mu$m. The description of the nanomechanical resonator depends very much on its geometry and the fabrication material. For nanome-

chanical resonators of cantilever-form or doubly clamped beams, the fundamental flexural mode corresponds to the fundamental mode of a harmonic oscillator [Cleland02]. In typical experiments with these kinds of resonators it is usually only the fundamental mode that is excited. There are also very interesting experiments where the in-plane as well as the out-of-plane mode of a doubly clamped beam can be excited [Rieger12]. This can lead to novel effects arising from an interplay between the two modes [Faust12]. In this thesis, however, we will focus on the case where only one mode is excited.

In order to give a comprehensive introduction to mechanical systems close to the quantum regime, we briefly want to mention the field of nanooptomechanics. In nanooptomechanics the interplay between an optical mode and a mechanical mode is being studied. The general setup of a nanooptomechanical system consists of two mirrors forming an optical cavity where one of the mirrors is movable. The cavity is now driven with a laser. The laser light induces radiation pressure acting on the movable mirror and thereby deflecting it. The deflection changes the length of the optical cavity and therefore the optical mode frequency. This interplay, induced by the radiation pressure force, leads to an interaction between the photons in the cavity and the phonons (which are the quantum excitations of the movable mirror). Due to the exceptional high level of control of laser light and the possibility to produce mirrors of basically any size, shape, and mass, there are a lot of cutting edge experiments with optomechanical systems, see for instance Refs. [Kippenberg07, Kippenberg08, Marquardt09, Aspelmeyer10] for brief introductory reviews on optomechanics.

Nanomechanical systems in the quantum regime

With recent experiments of nanoelectromechanical systems softening the boundary between the macroscopic and the quantum world, experimentalists as well as theorists are able to explore this very exciting intermediate regime, where it is possible to see quantum mechanics work on mesoscopic length scales. It is this intermediate regime that allows us to study fundamental questions as for instance: What characterizes the boarder classical/quantum? What causes the quantum to classical transition? How do macroscopic objects behave in the quantum regime? Is there a macroscopic Schrödinger's cat state?

In order to give a flavor of state of the art experiments which investigate this regime, we may mention two of the pioneering experiments. The first experiment was done by O'Connell et al. [O'Connell10] which brought a mechanical dilatation resonator of size of the diameter of a human's hair ($\sim 60 \, \mu$m) to its quantum mechanical ground state. The great challenge in bringing a mesoscopic resonator to its quantum ground states lies in the need for sufficiently low environmental temperatures T_{env}. Freezing out internal thermal phonons of the device and thereby entering the quantum regime requires environmental temperatures $T_{\mathrm{env}} \ll \hbar\Omega/k_B$ where Ω is the oscillator's resonance frequency. For usual resonance frequencies of around hundreds of megahertz this prerequisite is very hard to achieve with standard cryogenic techniques. O'Connell et al. circumvented this problem by building a high frequency dilatation drum resonator of $\Omega/2\pi \approx 6$ GHz for which a standard dilution refrigerator with a base temperature of $T_{\mathrm{env}} \approx 25$ mK was sufficient to meet the condition $T_{\mathrm{env}} \ll \hbar\Omega/k_B$. Furthermore, strong coupling to a Josephson phase qubit allowed for a readout of the oscillator's state in this experiment.

The second experiment was performed by Teufel et al. [Teufel11] where a nanomechanical drum (made out of aluminum) of diameter $\sim 10\,\mu$m was also cooled to is quantum mechanical ground state. Ground state cooling in this experiment was not done passively as in the experiment by O'Connell et al. but actively with a technique called sideband cooling which is similar to the laser cooling technique of atoms.

Not quite in the quantum regime but interesting in its own right due to the kind of coupling between the mechanical degree of freedom and the electronic degree of freedom, is the experiment by Flowers-Jacobs et al. [Flowers-Jacobs07]. They showed that the position power spectrum of a conducting nanomechanical oscillator (fabricated from gold) which is coupled via an atomic point contact to a metallic lead, is directly related to the finite frequency current noise spectrum through the atomic point contact. Therefore, simple transport measurements can be used to characterize the nanomechanical oscillator. The experimental realization of the doubly clamped nanomechanical beam resonator used in Ref. [Flowers-Jacobs07] is shown in Fig. 0.1.
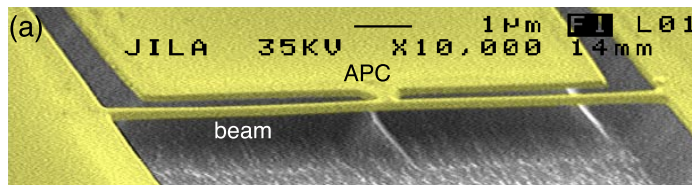
Figure 0.1: Experimental realization of a nanoelectromechanical system. A doubly clamped beam fabricated out of gold is coupled to a macroscopic detector via an atomic point contact (APC). Due to the motion of the beam, the tunnel coupling changes with the position of the beam. In this experiment the gap of the APC is ≈ 1 nm and the amplitude of the resonator's oscillation is of order of picometers. Adapted from Ref. [Flowers-Jacobs07].

We can ask, what is the difference between a classical harmonic oscillator and a quantum harmonic oscillator and what does it make so interesting to study a nanomechanical oscillator close to the quantum regime?

A classical harmonic oscillator such as a pendulum is a well studied problem in physics. The total energy of the pendulum being a conserved quantity is the sum of its potential energy and its kinetic energy. The total energy of a classical harmonic oscillator can take any value. It could also be zero, meaning that the oscillator performs no motion. We can describe the classical harmonic oscillator in terms of the commuting quantities x and p, being the position and momentum of the oscillator, respectively.

For a quantum mechanical harmonic oscillator, things are very different. The two most prominent differences are that the quantities x and p become non-commuting quantum mechanical operators $\hat{x}$ and $\hat{p}$ and that the energy of the quantum mechanical harmonic oscillator can no longer take any value. The energy of the quantum harmonic oscillator becomes quantized in multiples of $\hbar\Omega$ and takes values $E_n = \hbar\Omega(n + 1/2)$ where $n = 0, 1, 2, \ldots$. From this we also see that in quantum mechanics the energy of the oscillator can never be zero. Even at zero temperature the so-called zero-point motion survives, leading to the zero-point energy of the quantum harmonic oscillator of $E_0 = \hbar\Omega/2$. The probability of finding the quantum harmonic oscillator in a state with n quanta is given by $p(n) = \exp(-n\hbar\Omega/k_B T_{\text{env}})\left[1 - \exp(-\hbar\Omega/k_B T_{\text{env}})\right]$. This equation also dictates us that

for low environmental temperatures T_{env}, the probability of having $n = 0$ is highest, i.e., this reflects the condition for observing quantum effects $T_{\text{env}} \ll \hbar\Omega/k_B$ which we already mentioned above.

Now that we know how to bring a nanomechanical device in its quantum ground state and that very recent experiments also achieved this tremendous task, new possibilities open up. We can wonder what interesting properties and aspects of quantum theory we envision to explore with nanomechanical systems in the quantum regime.

The control of nano-sized objects in comparison to controlling single atoms which nowadays is routinely done, would be an exceptional achievement and could open new doors in the direction of quantum information processing. Proposals range from superconducting qubits coupled to nanoelectromechanical oscillators [Cleland04, Geller05] to quantum spin transducers [Rabl10].

Hybrid systems where the mechanical degree of freedom couples to a different physical degree of freedom broaden the range of possible applications even more. For instance, a nanomechanical resonator can couple to a macroscopic spin [Kovalev11]. It can also be coupled to just a single spin in a nitrogen-vacancy center in diamond [Rabl09]. Here, the mechanical motion could be used to coherently control the electronic spin degree of freedom [Hong12] or vice versa, meaning that the mechanical motion can be monitored using the single spin [Bennett12]. Nanomechanical resonators can even be coupled to a Bose-Einstein condensate [Treutlein07] or Rydberg atoms [Gao11].

Nanomechanical systems furthermore allow to study manifestations of quantum mechanics as for instance entanglement, quantum state engineering, and superposition of quantum mechanical states on a mesoscopic length scale. Possible routes towards entanglement are given in Refs. [Eisert04, Vitali07b, Bose06, Schmidt10, Ludwig10, Joshi10, Barzanjeh11, Børkje11].

With nanomechanical systems raising the length scale on which quantum mechanical effects become visible, they are excellent candidate systems for testing foundations of quantum mechanics on scales larger than an atom. These systems could also be used to answer the question where and how the transition from the quantum regime to the classical regime takes place [Penrose96, Leggett05] and could maybe eliminate the Schrödinger's cat paradox [Schrödinger35a]. In Refs. [Katz07, Katz08], this classical to quantum transition is investigated for driven nonlinear nanomechanical oscillators.

It is exactly the above discussed quantum regime which we aim to study in this thesis in the context of nanoelectromechanical systems. In Chap. 3, we describe a nanomechanical resonator in the non-Markovian regime with a focus on possible momentum detection. We continue in Chap. 4 by showing that a nanomechanical resonator can be used as a detector for exotic states of matter. Finally, we study in Chap. 5 the generation of non-classical correlations between two nanomechanical resonators, exploring one of the most fascinating quantum mechanical phenomena, entanglement, in a mesoscopic regime.

Part II

Theoretical methods for quantum transport

Chapter 1

The Keldysh diagrammatic technique

When we study transport in mesoscopic systems, we in general have in mind a total system that consists of a central region (the actual system of interest), leads that are attached to the central region, and of course a part that couples the central region to the leads. For reasons of simplicity, we stick to a two terminal device with one central region attached to two leads. Such a system is most easily described by the Hamiltonian

$$H = H_{\text{leads}} + H_{\text{cen}} + H_{\text{tun}} \tag{1.1}$$

and schematically depicted in Fig. 1.1. Many transport properties such as the average current through the system are readily defined with the knowledge of the above Hamiltonian, e.g., the current operator I is defined as the change of electrons in, e.g., the left lead

$$I = \frac{d}{dt} N_l = i\,[H, N_l]\ ,$$

where N_l counts electrons in the left lead (we set $e = \hbar = 1$). From this point of view, we already can see that in order to calculate average values of transport quantities, the Green's function or propagator will play a central role, cf. Chap. 3 and 4. The knowledge of the Green's functions of the underlying Hamiltonian in principle allows us to calculate the transport properties.

Since in all realistic experiments the current through the system is driven by applying a bias voltage across the sample, i.e., choosing different chemical potentials for the leads, and sometimes finite temperature also plays a crucial role, such systems are said to be in a non-equilibrium state.

In the following, we give a short review of how such systems are treated with what is called the non-equilibrium Keldysh technique rather than the usual equilibrium Green's function
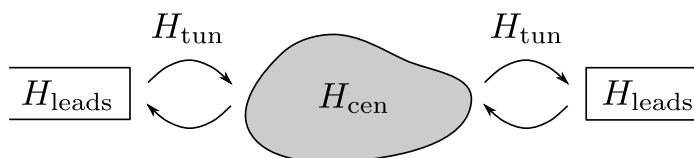
Figure 1.1: Schematics of a generic mesoscopic transport setup consisting of a central region of interest (gray) that is coupled to two non-interacting metallic leads. The coupling is induced via a tunneling Hamiltonian. The two leads are held at different chemical potentials which drives the system in the central region out-of-equilibrium.

technique which as we will shortly explain, fails for systems out-of-equilibrium.

1.1 Equilibrium Green's functions

In quantum mechanics, the time dependence of a quantum mechanical system can be treated within three different pictures. In the Schrödinger picture (denoted by the subscript S), the complete time dependence is carried by the quantum mechanical states and the quantum mechanical operators are time-independent. The Heisenberg picture (operators/states without a subscript) is opposite to the Schrödinger picture, i.e., the states are time-independent and all time dependence is carried by the operators which evolve according to

$$O(t) = e^{iHt} O_S e^{-iHt} \tag{1.2}$$

with H being the system's Hamiltonian. If the Hamiltonian of the system can be decomposed into a diagonalizable part H_0 and an interaction part V, the interaction picture (denoted by the subscript I) is the most convenient language. Here, both, the states and the operators are time-dependent and operators evolve according to

$$O_I(t) = e^{iH_0 t} O_S(t) e^{-iH_0 t} \,,$$

where the operators in the Schrödinger picture still may have an explicit time dependence that is not considered in Eq. (1.2). In the interaction picture, the Schrödinger equation

$$i\frac{\partial}{\partial t}|\psi(t)\rangle_I = V_I(t)|\psi(t)\rangle_I \tag{1.3}$$

dictates the time evolution of the quantum mechanical states. By integrating Eq. (1.3), we obtain the relation between states at time t and $t = 0$ given by the time evolution operator

$$|\psi(t)\rangle_I = U(t)|\psi(0)\rangle_I$$

with

$$U(t) = T e^{-i\int_0^t dt' \, V_I(t')} \,.$$

The time-ordering operator T sorts two arbitrary operators O_1 and O_2 according to their time variable in the following way

$$T\left[O_1(t_1)O_2(t_2)\right] = \begin{cases} O_1(t_1)O_2(t_2) & \text{if } t_1 > t_2 \\ \pm O_2(t_2)O_1(t_1) & \text{if } t_2 > t_1 \\ : O_1(t_1)O_2(t_2) : & \text{if } t_1 = t_2 \end{cases} \,, \tag{1.4}$$

where the $+$ and $-$ sign is taken for bosonic and fermionic operators, respectively, and the colons denote normal ordering, meaning that all creation operators have to be moved left of all annihilation operators.

1.1.1 Time-ordered equilibrium Green's functions

In equilibrium as well as in non-equilibrium many-body theory, a central goal is the calculation of real time correlation functions among which the time-ordered Green's function in the Heisenberg picture

$$iG(x,t;x',t') = \left\langle T\psi(x,t)\psi^\dagger(x',t') \right\rangle = \mathrm{Tr}\left[\tilde{\rho}T\psi(x,t)\psi^\dagger(x',t')\right] \tag{1.5}$$

is of major interest and well suited for the purpose of our discussion. Here, the density matrix $\tilde{\rho}$ is the equilibrium density matrix at zero temperature and given by

$$\tilde{\rho} = \rho = |G_H\rangle\langle G_H| \tag{1.6}$$

with $|G_H\rangle$ being the ground state of the full Hamiltonian under consideration $H = H_0 + V$. H_0 is a quadratic Hamiltonian and V contains possible interactions. Textbook Feynman-Dyson perturbation theory [Mahan00] tells us that the time-ordered Green's function is then given by

$$iG(x,t;x',t') = \frac{\langle G_0|TS(\infty,-\infty)\psi_I(x,t)\psi_I^\dagger(x',t')|G_0\rangle}{\langle G_0|S(\infty,-\infty)|G_0\rangle}\,, \tag{1.7}$$

where the subscript I denotes operators in the interaction picture with respect to H_0, $|G_0\rangle$ is the ground state of the Hamiltonian H_0, and the S-matrix containing the interactions V is given by

$$S(\infty,-\infty) = Te^{-i\int_{-\infty}^{\infty} dt'\, V_I(t')}\,.$$

Generally speaking, the S-matrix propagates a state from time t' to time t and is defined as $S(t,t') = U(t)U^\dagger(t')$, having the following group like properties

$$S(t,t) = 1\,, \tag{1.8}$$

$$S(t,t') = S^\dagger(t',t)\,, \tag{1.9}$$

$$S(t,t')S(t',t'') = S(t,t'')\,. \tag{1.10}$$

1.1.2 Failure of the equilibrium technique for non-equilibrium states

So far, we did not say anything why in the equilibrium case the Feynman-Dyson technique allowed us to calculate the time-ordered Green's function. In the following, we will provide the missing explanation and along the way show that the equilibrium technique is not suitable to describe a non-equilibrium state. One might right away ask the question why the conventional technique fails to describe non-equilibrium situations. The answer is that in general the density matrix is not a projector on the ground state of the Hamiltonian as in Eq. (1.6). Because this might not be easy to grasp, we will consider an arbitrary density

matrix

$$\tilde{\rho} = \rho' = \sum_{\Gamma} p_{\Gamma} |\Gamma\rangle\langle\Gamma|$$

with $|\Gamma\rangle$ being an arbitrary state and $\{|\Gamma\rangle\}$ forms a complete basis of the corresponding Hilbert space. We now take this density matrix in order to compute the time-ordered Green's function in Eq. (1.5) for a particular state $|\Gamma\rangle$

$$iG_{\Gamma}(x,t;x',t') = \langle\Gamma|T\psi(x,t)\psi^{\dagger}(x',t')|\Gamma\rangle \,. \tag{1.11}$$

The Hamiltonian we consider is given by $\mathcal{H}(t) = H + h(t)$ with H being the unperturbed equilibrium Hamiltonian (which can still contain interactions). $h(t)$ describes the non-equilibrium perturbation and contains all time dependence. The operators $\psi(x,t)$ transform to the interaction picture according to

$$\psi_I(x,t) = e^{iHt}\psi(x)e^{-iHt} \,,$$

and to the Heisenberg picture as

$$\psi(x,t) = \mathcal{U}^{\dagger}(t)\psi(x)\mathcal{U}(t) = \mathcal{S}(0,t)\psi_I(x,t)\mathcal{S}(t,0) \,.$$

The notation is chosen in such a way that the curly $\mathcal{U}$ and $\mathcal{S}$ contain the non-equilibrium perturbation $h(t)$. They are given by

$$\mathcal{S}(t,t') = e^{iHt}\mathcal{U}(t,t')e^{-iHt'} = Te^{-i\int_{t'}^{t} d\tilde{t}\, h_I(\tilde{t})}$$

with

$$\mathcal{U}(t,t') = Te^{-i\int_{t'}^{t} d\tilde{t}\, \mathcal{H}(\tilde{t})} \,,$$

and the interaction picture representation of $h_I(t)$ reads

$$h_I(t) = e^{iHt}h(t)e^{-iHt} \,.$$

With all of the above relations we can rewrite Eq. (1.11) in the following way

$$iG_{\Gamma}(x,t;x',t') = \langle\Gamma|T\mathcal{S}(0,t)\psi_I(x,t)\mathcal{S}(t,0)\mathcal{S}(0,t')\psi_I^{\dagger}(x',t')\mathcal{S}(t',0)|\Gamma\rangle \,. \tag{1.12}$$

The state $|\Gamma\rangle$ in the interaction picture is represented as

$$|\Gamma(t)\rangle_I = \mathcal{S}(t,0)|\Gamma(0)\rangle_I = \mathcal{S}(t,0)|\Gamma\rangle \,,$$

where the last equality sign hold because we chose $t = 0$ as the time where all three pictures coincide. With that we can connect $|\Gamma\rangle$ with an interaction picture state at $t = \pm\infty$

$$|\Gamma\rangle = \mathcal{S}(0,\pm\infty)|\Gamma(\pm\infty)\rangle_I \,,$$

which allows us to write Eq. (1.12) as

$$iG_\Gamma(x,t;x',t') = {}_I\langle\Gamma(\infty)|T\mathcal{S}(\infty,-\infty)\psi_I(x,t)\psi_I^\dagger(x',t')|\Gamma(-\infty)\rangle_I\,, \tag{1.13}$$

where we made use of the properties in Eqs. (1.8 - 1.10).

Now, we already see a relation between the zero-temperature equilibrium Green's function in Eq. (1.7) and the Green's function in Eq. (1.13) for an arbitrary quantum state. The above derivation of the time-ordered Green's function $G_\Gamma(x,t;x',t')$ even holds for a non-equilibrium situation, however the problem is that we need to know the state in the remote past and future. In the equilibrium situation, the states $|\Gamma(\infty)\rangle$ and $|\Gamma(-\infty)\rangle$ have a rather simple relationship and only differ by a phase which breaks down in a general non-equilibrium setting.

At this point, it is valuable to recall the various assumptions that are made for the perturbative treatment to be valid and to review what is called the adiabatic theorem [Born28] and the Gell-Mann Low theorem [Gell-Mann51]. First, we need to say that if the time evolution operator has no series representation, the problem is non-perturbative. In the usual textbooks, the adiabatic theorem is often introduced as the basis of a valid perturbative treatment of a physical problem. However, it is of importance to remember that this is not the whole truth, because an adiabatic switching on and off, of interactions giving rise to phenomena such as BCS [1]-superconductivity or the macroscopic ground state of a Bose-Einstein condensate does not allow for a perturbative treatment of these problems. An elaborate discussion for perturbation theory to be applicable is that the Fermi surface when going from the unperturbed system to the interacting one does not change. A very nice discussion on this rather seldom stated argument is given in Chapter 5 of Ref. [Nozieres64]. Now, assuming that we exclude such perturbations from our discussion we go on with the adiabatic theorem which is best explained in the original formulation of Born and Fock: "If we label the states of a quantum system with quantum numbers corresponding to their energy levels, the adiabatic theorem states, that if the system has initially been in a state with a well defined quantum number and is then adiabatically perturbed, the transition probability to a state with a different quantum number is negligibly small. However, the energy levels after the perturbation can differ by a finite amount.".

The Gell-Mann Low theorem links eigenstates (any eigenstate not only the ground state) of the unperturbed Hamiltonian H_0 to eigenstates of the interacting Hamiltonian H. In the equilibrium case, the Gell-Mann Low theorem is applied to the ground state of the unperturbed Hamiltonian and connects this known ground state to the ground state of the interacting problem. We will continue in the discussion by considering the adiabatic switching on and off of the perturbation according to

$$\mathcal{H}_\varepsilon = H + e^{-\varepsilon|t|}h$$

with $\varepsilon \to 0^+$. This ensures that the system stays in an eigenstate (the eigenstate it has been in, before the interaction was adiabatically switched on) while it becomes interacting. In the equilibrium situation the state $|\Gamma\rangle$ is chosen to be a non-degenerate ground state $|G\rangle$ of the

---

[1]BCS stands for Bardeen Cooper Schrieffer who in 1957 established a microscopic theory of superconductivity [Bardeen57].

Hamiltonian $\mathcal{H} = H + h$. The adiabatic theorem then ensures that (the limit $\varepsilon \to 0$ is called the adiabatic limit)

$$|\Gamma(\pm\infty)\rangle_I = \lim_{\varepsilon\to 0} \mathcal{S}_\varepsilon(\pm\infty, 0)|G\rangle$$

are both eigenstates of H and since we have assumed a non-degenerate ground state, the states at $t = \pm\infty$ can only differ by a phase

$$|\Gamma(\infty)\rangle_I = \mathcal{S}(\infty, -\infty)|\Gamma(-\infty)\rangle_I = e^{iL}|\Gamma(-\infty)\rangle_I.$$

By setting $|G_0\rangle = |\Gamma(-\infty)\rangle_I$, i.e., in the remote past the perturbation is switched off and we know the ground state $|G_0\rangle$ of the unperturbed Hamiltonian, we can identify the phase factor as

$$e^{iL} = \langle G_0|\mathcal{S}(\infty, -\infty)|G_0\rangle,$$

which is exactly the denominator in Eq. (1.7) and therefore drops out. We can conclude that with the adiabatic theorem, we can use Eq. (1.13) and obtain the conventional equilibrium Green's function. Now, it should also be obvious why the conventional equilibrium method fails for non-equilibrium states: out of equilibrium, the adiabatic theorem is no longer justified and the states in the remote past and future are no longer related by just a phase.

1.2 The Keldysh contour and non-equilibrium Green's functions

The cure to the non-equilibrium problem was pioneered and put forward by Schwinger, Kadanoff and Baym, Keldysh, and Craig [Schwinger61, Kadanoff62, Keldysh65, Craig68] and consists of avoiding any reference to the state in the asymptotic future and solely base the expansion on the known state in the remote past. A modern and comprehensive introduction to the Keldysh technique is given in Ref. [Rammer07].

We start by introducing the following identity in order to get rid of the state in the future

$$|\Gamma(\infty)\rangle_I = \mathcal{S}(\infty, -\infty)|\Gamma(-\infty)\rangle_I,$$

rewinding the time evolution to the remote past and with that we can write the time-ordered Green's function as

$$iG_\Gamma(x, t; x', t') = {}_I\langle\Gamma(-\infty)|\mathcal{S}(-\infty, \infty)T\mathcal{S}(\infty, -\infty)\psi_I(x, t)\psi_I^\dagger(x', t')|\Gamma(-\infty)\rangle_I. \tag{1.14}$$

We now have a part describing the backward evolution $\mathcal{S}(-\infty, \infty)$ and a part describing the forward evolution $\mathcal{S}(\infty, -\infty)$ and the time-ordering operator between them, which prevents us from pushing the backward evolution past it. The crucial step was to introduce a two-branch contour $\mathcal{C}$ and ordering along this contour by the contour-ordering operator T_c. The Schwinger-Keldysh contour is depicted in Fig. 1.2, it consist of two branches, a forward branch $\mathcal{C}_+$ extending from $-\infty$ to ∞ and a backward branch $\mathcal{C}_-$ extending from ∞ to $-\infty$. In order to better distinguish times lying on the real time axis and times lying on the contour, we use t and τ, respectively and define the so-called contour-ordered Green's
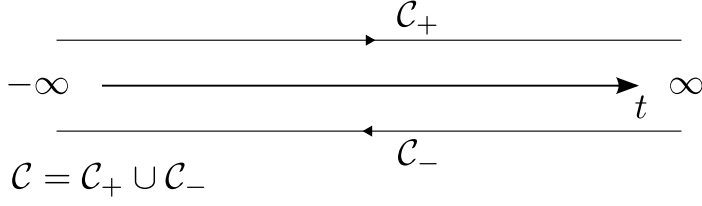
Figure 1.2: The Schwinger-Keldysh contour.

function $\mathcal{G}$ in the Heisenberg picture

$$i\mathcal{G}(x,\tau,x',\tau') = \left\langle T_c \psi(x,\tau)\psi^\dagger(x',\tau') \right\rangle = \mathrm{Tr}\left[\rho T_c \psi(x,\tau)\psi^\dagger(x',\tau')\right].$$

With the S-matrix defined on the contour by

$$\mathcal{S}_c(-\infty,-\infty) = T_c e^{-i\int_{\mathcal{C}} d\tau' h'_I(\tau')},$$

where the integral is along the contour, the Green's function in Eq. (1.14) in the interaction picture on the contour can be written as

$$i\mathcal{G}_\Gamma(x,\tau;x',\tau') = {}_I\langle\Gamma(-\infty)|T_c\mathcal{S}_c(-\infty,-\infty)\psi_I(x,t)\psi_I^\dagger(x',t')|\Gamma(-\infty)\rangle_I.$$

The full Green's function on the contour in the interaction picture becomes with the definition of the density matrix $\rho(-\infty) = \sum_\Gamma p_\Gamma |\Gamma(-\infty)\rangle_{II}\langle\Gamma(-\infty)|$

$$i\mathcal{G}(x,\tau;x',\tau') = \mathrm{Tr}\left[\rho(-\infty)T_c\mathcal{S}_c(-\infty,-\infty)\psi_I(x,t)\psi_I^\dagger(x',t')\right],$$

where we now have cured the problem of the non-equilibrium case by referring only to the interaction picture state in the remote past. As Eq. (1.7) in the equilibrium case allows for a controlled perturbative expansion in the (small) interaction term appearing in the exponent of the S-matrix, so does the Green's function $\mathcal{G}$ in the non-equilibrium case.

Real time formalism

A last step we have to perform is expressing the contour Green's function $\mathcal{G}(x,\tau;x',\tau')$ as real time Green's functions $G(x,t;x',t')$, where we label times lying on the contour $\mathcal{C}$ with τ and t denote real times. Depending on the locations of the times τ and τ' on the contour $\mathcal{C}$, we get four real time Green's functions

$$\mathcal{G}(x,\tau;x',\tau') = \begin{cases} G^{++}(x,t;x',t') &= -i\left\langle T\psi(x,t)\psi^\dagger(x',t')\right\rangle \text{ for } \tau,\tau' \in \mathcal{C}_+ \\ G^{-+}(x,t;x',t') &= \pm i\left\langle \psi^\dagger(x',t')\psi(x,t)\right\rangle \text{ for } \tau \in \mathcal{C}_+,\tau' \in \mathcal{C}_- \\ G^{+-}(x,t;x',t') &= -i\left\langle \psi(x,t)\psi^\dagger(x',t')\right\rangle \text{ for } \tau \in \mathcal{C}_-,\tau' \in \mathcal{C}_+ \\ G^{--}(x,t;x',t') &= -i\left\langle \bar{T}\psi(x,t)\psi^\dagger(x',t')\right\rangle \text{ for } \tau,\tau' \in \mathcal{C}_- \end{cases}.$$

Here, T is the time-ordering operator as defined in Eq. (1.4) and $\bar{T}$ is the anti-time ordering-operator bringing the operators in reverse order than the operator T does. A common notation is to define a matrix containing all four real time Green's functions

$$\mathbf{G} = \begin{pmatrix} G^{--} & G^{-+} \\ G^{+-} & G^{++} \end{pmatrix},$$

where the following identities also called Keldysh identities hold

$$G^R = G^{--} - G^{-+} = G^{+-} - G^{++},$$
$$G^A = G^{--} - G^{+-} = G^{-+} - G^{++},$$
$$G^K = G^{+-} + G^{-+} = G^{--} + G^{++},$$
$$0 = G^{--} + G^{++} - G^{-+} - G^{+-},$$

where $G^{A/R}$ is the advanced/retarded Green's function and G^K is the Keldysh Green's function. With the above identities we see that the entries of the Keldysh matrix $\mathbf{G}$ are not independent and we can perform a unitary transformation with

$$\mathbf{R} = \frac{1}{\sqrt{2}} \begin{pmatrix} 1 & -1 \\ 1 & 1 \end{pmatrix},$$

in order to obtain

$$\hat{\mathbf{G}} = \mathbf{R}\boldsymbol{\sigma}_z \mathbf{G}\mathbf{R}^T = \begin{pmatrix} G^R & G^K \\ 0 & G^A \end{pmatrix},$$

where $\boldsymbol{\sigma}_z$ is the third Pauli matrix.

1.3 Non-equilibrium nanoelectromechanical systems in the quantum regime

Having outlined the general theory of non-equilibrium quantum states, we now want to sketch why and how we seek to employ this technique in the study of nanoelectromechanical systems. This section should merely set the stage for Chap. 3 of this thesis, where nanoelectromechanical systems in the quantum regime are studied in detail. In general, the problems we study are of the generic form described by the Hamiltonian H in Eq. (1.1). For a better visualization, we show in Fig. 1.3 a schematics of an archetype setup we have in mind. The central part becomes the nanoelectromechanical oscillator which is considered conducting and acting as one of the leads. As pointed out in the Introduction, for low oscillation amplitudes the nanomechanical oscillator is modeled by the fundamental mode of a harmonic oscillator

$$H_{\text{cen}} = H_{\text{osc}} = \frac{\hat{p}^2}{2m} + \frac{1}{2}m\Omega^2\hat{x}^2.$$
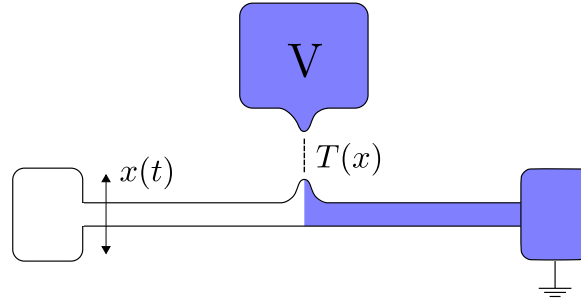
Figure 1.3: Schematics of an archetype of a NEMS where the tunneling amplitude $T(x)$ is modulated by the motion of the nanomechanical oscillator. The nanomechanical oscillator itself serves as one of the leads that in this case is grounded, the other lead is held at bias voltage V. Blue indicates the conducting region in the setup, where current is flowing.

This resonator is tunnel coupled to a second lead, held at a different chemical potential. The two leads in the setup are characterized by the Hamiltonian of a non-interacting Fermi liquid

$$H_{\text{leads}} = \sum_{\alpha,k} \varepsilon_k \psi_{\alpha,k}^\dagger \psi_{\alpha,k} \,,$$

where $\alpha = \{l, r\}$ for the left or right lead and k are the momenta of electrons in lead α. We suppress the spin index, since in our analysis it does not play any role. For the coupling we assume that the average distance between the lead and the nanomechanical resonator is large compared to the amplitude of oscillations of the resonator. The coupling is then best described in a tunneling Hamiltonian approach where the tunneling amplitude depends on the position of the oscillator

$$H_{\text{tun}} = \sum_k T(x) \psi_{l,k}^\dagger \psi_{r,k} + \text{H.c.}$$

with an energy and momentum independent tunneling amplitude $T(x)$. In general, the tunneling amplitude $T(x)$ has an exponential dependence on the position of the oscillator

$$T(x) = \tilde{t} e^{-x/x_0} \,.$$

In the limit of small oscillation amplitudes, we can expand the exponential function to linear order

$$T(x) = t_0 + t_1 \hat{x} \,, \tag{1.15}$$

where we call $t_0 = \tilde{t}$ and $t_1 = -\tilde{t}/x_0$. Note that in Eq. (1.15) we promoted x to the quantum mechanical operator $\hat{x}$ indicating that we explicitly treat the oscillator and its influence on the tunneling quantum mechanical. We will only focus on the regime of small oscillation amplitudes as this limit is also suggested by, e.g., the experiment in Ref. [Flowers-Jacobs07], where the oscillation amplitude is of the order of a few picometer and the tunneling gap is of order of a few nanometer. Therefore, we will later use the tunneling amplitude given in Eq. (1.15) where tunneling depends only linearly on the position of the oscillator. Note that

there are also theoretical studies of NEMS investigating the regime of exponential dependent tunneling [Smirnov03].

The theoretical studies of nanoelectromechanical systems widely use the Born and Markov approximations, meaning that the coupling is treated in second order perturbation theory and that the fermionic bath (represented by the leads) has a correlation time that is small compared to the time scale of the system given by $1/\Omega$ which then is the dominant time scale in the problem. Making these assumptions however does not cover the true quantum regime, where all involved energy scales of the system should be of the same order $\hbar\Omega \approx eV \approx k_B T_{\text{env}}$. The involved energy scales being the oscillator energy ($\hbar\Omega$), the energy scale that is due to the applied bias (eV), and an energy scale that is due to a possible coupling to an additional thermal environment ($k_B T_{\text{env}}$) giving rise to a damping of the mechanical resonator. With recent experiments approaching the regime $\hbar\Omega \approx eV \approx k_B T_{\text{env}}$, it is this very limit we are interested in. In Chap. 3, we study in detail signatures of the nanomechanical oscillator in non-equilibrium transport properties such as the finite frequency current noise and the average tunnel current for an arbitrary hierarchy of energy scales.

Chapter 2

Master equation techniques

In the previous chapter, we were concerned about how we can analytically treat quantum transport in nanoelectromechanical systems. The formulation there relied on Green's functions which are related to transport quantities and can be calculated using the (perturbative) Keldysh technique. We now want to introduce the notion of open quantum systems which not only in the realm of NEMS is a noteworthy subject. For open quantum systems, in contrast to closed systems, the dynamics can in general not be represented by a unitary time evolution. Instead, if we consider an open quantum system, consisting of a quantum system with few degrees of freedom that is coupled to a larger quantum system (called reservoir or bath), and if we are only interested in the dynamics of the smaller quantum system – in the presence of the bath – its behavior can be described by an equation of motion of the reduced density matrix $\rho_S = \text{Tr}_B[\rho_{\text{tot}}]$. The general setting of an open quantum system is schematically shown in Fig. 2.1. The core of an open quantum system approach is the so-called "master equation" for the system's reduced density matrix ρ_S. With the master equation, the time evolution of the system is then given under the influence of the bath. The
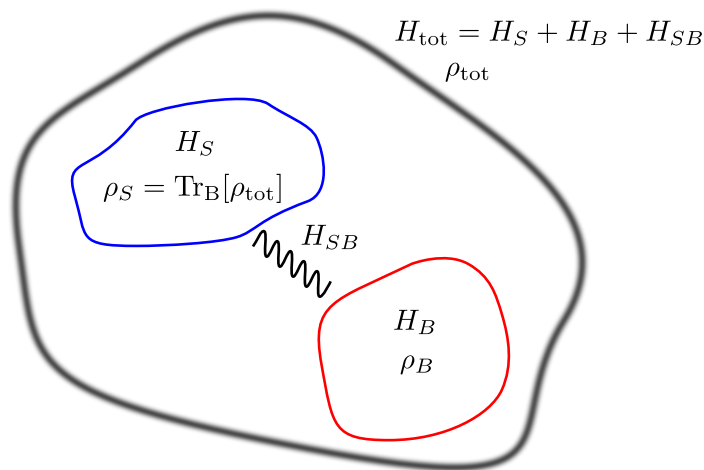
Figure 2.1: Schematics of an open quantum system consisting of a system and a bath part described by H_S and H_B, respectively. The coupling between system and bath is mediated via H_{SB}.

Hamiltonian of the total system H_{tot} is given by

$$H_{\text{tot}} = H_S + H_B + H_{SB}\,, \tag{2.1}$$

where the system of interest and the bath are described by the Hamiltonian H_S and H_B, respectively. The coupling between the system and the bath is mediated via the Hamiltonian H_{SB}. The total system's density matrix is denoted by ρ_{tot} and obeys the von Neumann equation (we set $\hbar = 1$)

$$\frac{d}{dt}\rho_{\text{tot}}(t) = -i\left[H_{\text{tot}}(t), \rho_{\text{tot}}(t)\right]. \tag{2.2}$$

Later we will use the master equation approach to study NEMS under the influence of a bath. The bath in our case will be the detector the NEMS couples to which in our setting is a tunnel junction detector, cf. Fig. 1.3. However, in principle, the detector does not need to be the only bath the nanomechanical oscillator couples to. In addition to the detector, it could also couple to another (bosonic) heat bath. Such an additional heat bath can be modeled within a Caldeira-Leggett model and leads to damping/a finite Q factor [1] of the nanomechanical oscillator. The effects of the bath on the dynamics of the system crucially depend on the type of bath, the type of coupling, and on the involved time scales of the problem.

In the study of NEMS, there are mainly two different types of scenarios we will focus on, the Markovian and non-Markovian one. What this means will become clearer later, for now, we will introduce in Sec. 2.1 for a generic system-bath Hamiltonian the master equation formalism in the weak system-bath coupling (Born) and Markov limit, and in Sec. 2.2 we will discuss the non-Markovian master equation.

2.1 Markovian master equations

In the following, we review the Born Markov master equation in the spirit of Ref. [Breuer02]. We consider a quantum mechanical system weakly coupled to a reservoir. The total system is described by the Hamiltonian in Eq. (2.1) and the dynamics is governed by the von Neumann equation (2.2). In the interaction picture representation with respect to $H_S + H_B$, the von Neumann equation reads

$$\frac{d}{dt}\hat{\rho}_{\text{tot}}(t) = -i\left[\hat{H}_{SB}(t), \hat{\rho}_{\text{tot}}(t)\right], \tag{2.3}$$

where operators in the interaction picture carry a hat and

$$\hat{\rho}_{\text{tot}}(t) = U^\dagger(t)\rho_{\text{tot}}(t)U(t),$$
$$\hat{H}_{SB}(t) = U^\dagger(t)H_{SB}U(t),$$

with

$$U(t) = e^{-i(H_S + H_B)t}.$$

---

[1] The Q or quality factor is a dimensionless parameter. It is the ratio of the oscillator's bandwidth and its resonance frequency. It characterizes the rate at which the oscillator loses energy. High-Q oscillators have low damping rates.

By integration of Eq. (2.3) we obtain the von Neumann equation in integral form

$$\hat{\rho}_{\text{tot}}(t) - \hat{\rho}_{\text{tot}}(0) = -i \int_0^t dt' \left[\hat{H}_{SB}(t'), \hat{\rho}_{\text{tot}}(t') \right] ,$$

which we insert back into Eq. (2.3) in order to obtain

$$\frac{d}{dt}\hat{\rho}_{\text{tot}}(t) = -i \left[\hat{H}_{SB}(t), \hat{\rho}_{\text{tot}}(0) \right] - \int_0^t dt' \left[\hat{H}_{SB}(t), \left[\hat{H}_{SB}(t'), \hat{\rho}_{\text{tot}}(t') \right] \right] . \tag{2.4}$$

Since we are only interested in the dynamics of the system described by H_S under the influence of the bath, we trace out the bath degrees of freedom in order to obtain the reduced density matrix of the system $\hat{\rho}_S$

$$\hat{\rho}_S(t) = \text{Tr}_B \left[\hat{\rho}_{\text{tot}}(t) \right] .$$

As an initial condition we assume that system and bath are uncorrelated, meaning that the total density matrix factorizes and is given by the direct product

$$\rho_{\text{tot}}(0) = \rho_S(0) \otimes \rho_B . \tag{2.5}$$

Tracing both sides of Eq. (2.4) over the bath then yields

$$\frac{d}{dt}\hat{\rho}_S(t) = - \int_0^t dt' \, \text{Tr}_B \left\{ \left[\hat{H}_{SB}(t), \left[\hat{H}_{SB}(t'), \hat{\rho}_{\text{tot}}(t') \right] \right] \right\} ,$$

where we assumed $\text{Tr}_B \left[\hat{H}_{SB}(t)\hat{\rho}_{\text{tot}}(0) \right] = \text{Tr}_B \left[\hat{H}_{SB}(t)\rho_S(0) \otimes \rho_B \right] = 0$ which is always true for the system-bath couplings considered in this thesis. Now, we make use of the weak coupling approximation by extending Eq. (2.5) to finite times t which in the context of open quantum systems is known as the Born approximation

$$\hat{\rho}_{\text{tot}}(t) \approx \hat{\rho}_S(t) \otimes \rho_B .$$

Within the weak coupling approximation we have made the assumption that the bath's density matrix is not influenced by the interaction with the system at any time. The system's density matrix however can change significantly under the coupling to the bath. With this, the equation of motion of the reduced density matrix becomes an integro-differential equation

$$\frac{d}{dt}\hat{\rho}_S(t) = - \int_0^t dt' \, \text{Tr}_B \left\{ \left[\hat{H}_{SB}(t), \left[\hat{H}_{SB}(t'), \hat{\rho}_S(t') \otimes \rho_B \right] \right] \right\} , \tag{2.6}$$

which is in general only solvable numerically since it is nonlocal in time. The system's time evolution also depends explicitly on the history from $t' = 0$ to $t' = t$. However, by applying further approximations which take into account the time scales of the problem, it is possible to arrive at a differential equation for $\hat{\rho}_S(t)$ which is considerably easier to solve. The approximation we will make in the following is oftentimes just called Markov approximation, but as we will see later the Markov approximation actually consists of two approximations, better coined first and second Markov approximation.

The first Markov approximation comprises replacing $\hat{\rho}_S(t')$ with $\hat{\rho}_S(t)$ in Eq. (2.6) which yields a local in time master equation known as the Redfield equation [Redfield57]

$$\frac{d}{dt}\hat{\rho}_S(t) = -\int_0^t dt' \operatorname{Tr}_B\left\{\left[\hat{H}_{SB}(t),\left[\hat{H}_{SB}(t'),\hat{\rho}_S(t)\otimes\rho_B\right]\right]\right\},\qquad(2.7)$$

where only the present state $\hat{\rho}_S(t)$ governs the time evolution of the reduced system's density matrix. It is said that the system looses its memory on the past. Let us now bring into play the involved time scales of the problem and see what the first Markov approximation actually means in terms of them. We therefore introduce correlation functions by writing the system-bath coupling in a very general form as

$$H_{SB} = \sum_n S_n E_n\,,$$

where the S_n and E_n are system and bath operators only acting on the Hilbert space of the system and bath, respectively. The transformation to the interaction picture is straight forward and yields

$$\hat{H}_{SB}(t) = \sum_n S_n(t)E_n(t)$$

with $X_n(t) = \exp(iH_X t)X_n\exp(-iH_X t)$ where $X = \{S,E\}$. With this we can write Eq. (2.7) as

$$\frac{d}{dt}\hat{\rho}_S(t) = -\sum_{n,m}\int_0^t dt'\ [S_n(t)S_m(t')\hat{\rho}_S(t) - S_m(t')\hat{\rho}_S(t)S_n(t)]\operatorname{Tr}_B\left\{E_n(t)E_m(t')\rho_B\right\}$$
$$- [S_n(t)\hat{\rho}_S(t)S_m(t') - \hat{\rho}_S(t)S_m(t')S_n(t)]\operatorname{Tr}_B\left\{E_m(t')E_n(t)\rho_B\right\}.$$

Now, we consider the time correlation functions of the bath $\langle E_n(t)E_m(t')\rangle$ which characterize the overlap/correlation between interactions at time t and t'. As we said earlier, we assume a large bath that quickly relaxes, i.e., the bath is not influenced by the interaction with the system. In terms of the correlation functions, this means, that there will be some correlations during the small time interval $t - t' \leq \tau_B$, where τ_B is the correlation time of the bath and depends very much on the type and structure of the bath. For $t - t' > \tau_B$ the correlations decrease and finally for $t - t' \gg \tau_B$ they become zero, i.e., the time τ_B sets a time scale on which some memory of the interactions is kept, even in the master equation in Eq. (2.7). Going back to Eq. (2.6) we can now argue that the integral is only nonzero for times $t - t' \leq \tau_B$ [2], i.e., the influence of $\hat{\rho}_S(t')$ outside this interval on $\dot{\hat{\rho}}_S(t)$ is negligible. If we now introduce a time scale $\tau_r \sim 1/\gamma$ [3] which originates, e.g., from damping characterized by the damping rate γ, we can argue that the Markov approximation is valid, i.e., that $\rho_S(t') \approx \rho_S(t)$ holds, if

$$\tau_B \ll 1/\gamma\,.$$

---

[2]i.e., between times $t' \approx t - \tau_B$ and $t' = t$

[3]τ_r refers to a characteristic time scale on which $\rho_S(t)$ changes considerably, meaning that τ_r can be associated with a relaxation time of the system

This is also known as a coarse graining of the time axis, because we are not able to describe the system's dynamics on time scales comparable to the bath correlation time τ_B. This is what we would call the second Markov approximation because with this we can substitute $t' \to t - t'$ and let the upper integration limit in Eq. (2.7) go to infinity. We then obtain the so-called Born Markov master equation for the reduced system's density matrix in the interaction picture

$$\frac{d}{dt}\hat{\rho}_S(t) = - \int_0^\infty dt' \, \text{Tr}_B \left\{ \left[\hat{H}_{SB}(t), \left[\hat{H}_{SB}(t - t'), \hat{\rho}_S(t) \otimes \rho_B \right] \right] \right\},$$

which in the Schrödinger picture reads

$$\frac{d}{dt}\rho_S(t) = -i\left[H_S, \rho_S(t) \right] - \int_0^\infty dt' \, \text{Tr}_B \left\{ \left[H_{SB}, \left[H_{SB}(-t'), \rho_S(t) \otimes \rho_B \right] \right] \right\}.$$

Since we have made several approximations when deriving the Born Markov master equation, it is obvious that the regime of validity is limited. For most applications concerning nanomechanical systems, the Born Markov master equation nevertheless describes the physics in good accuracy. However, when it comes to memory effects or a special structure of the reservoir, the Born Markov master equation fails. The regimes where also the bath is influenced by the time evolution of the system or where the reservoir has a given spectral density are however among the most interesting ones. We therefore introduce in the following section the time convolutionless master equation technique which allows us to capture non-Markovian effects in the time evolution of the reduced system.

2.2 Non-Markovian master equations

Besides the Keldysh formalism which we discussed in Chap. 1 and showed that it is a suitable method to treat systems out-of-equilibrium, there are also master equation techniques which cover systems out-of-equilibrium. As we have already seen in the previous chapter, master equations can either be nonlocal or local in time. The so-called Nakajima-Zwanzig master equation [Nakajima58, Zwanzig60] is for instance a nonlocal in time master equation, where the memory kernel depends on the reduced density operator at all previous times. There are also local in time master equations as the time convolutionless master equation, which is an exact master equation describing the full dynamics of the reduced system's density matrix but is, as said, local in time and therefore easier to treat analytically. The time convolutionless master equation technique is due to Shibata et al. [Shibata77, Chaturvedi79, Shibata80]. Here, we will focus on the time convolutionless master equation and introduce the subject along the lines of Ref. [Breuer02]. We will also briefly review the Nakajima-Zwanzig equation from which the time convolutionless master equation follows more naturally.

As before, the combined system-bath open quantum system is characterized by the density matrix ρ_{tot} and governed by the Hamiltonian $H = H_S + H_B + \lambda H_{SB}$, here we explicitly introduce λ as a small dimensionless expansion parameter. The von Neumann equation in

the interaction picture (denoted by a hat) with respect to $H_S + H_B$ is given by

$$\frac{d}{dt}\hat{\rho}_{\text{tot}}(t) = -i\lambda \left[\hat{H}_{SB}(t), \hat{\rho}_{\text{tot}}(t) \right] \equiv \lambda \mathcal{L}(t)\hat{\rho}_{\text{tot}}(t) \,, \tag{2.8}$$

where we defined the Liouville super-operator $\mathcal{L}(t)$. The core of the derivation uses projection super-operators. A first projection operator $\mathcal{P}$ projects the density matrix of the system to the relevant part which then can be used to gain information on the reduced system's density matrix $\hat{\rho}_S$. Relevant in this context means that with the relevant part of the density matrix ρ_{tot}, it is possible to calculate the correct quantum mechanical expectation values of system operators. Here, the projection is just a formal operation equivalent to tracing over the bath degrees of freedom. A complementary super-operator $\mathcal{Q}$ projects on the irrelevant part of the open system. They are given by

$$\hat{\rho}_{\text{tot}} \mapsto \mathcal{P}\hat{\rho}_{\text{tot}} = \text{Tr}_B \left\{ \hat{\rho}_{\text{tot}} \right\} \otimes \rho_B = \hat{\rho}_S \otimes \rho_B \,,$$
$$\mathcal{Q}\hat{\rho}_{\text{tot}} = \hat{\rho}_{\text{tot}} - \mathcal{P}\hat{\rho}_{\text{tot}} \,.$$

The super-operator being introduced as projectors have the following properties

$$\mathcal{P} + \mathcal{Q} = \mathbb{1} \,, \tag{2.9}$$
$$\mathcal{P}^2 = \mathcal{P} \,,$$
$$\mathcal{Q}^2 = \mathcal{Q} \,,$$
$$\mathcal{P}\mathcal{Q} = \mathcal{Q}\mathcal{P} = 0 \,.$$

The density matrix of the bath can be an arbitrary state of the environment that however has to be known. In contrast to the Markovian master equation we however do not have to assume factorizing initial conditions as in Eq. (2.5). The following assumption will greatly simplify the later derivation

$$\text{Tr}_B \left\{ \hat{H}_{SB}(t_1)\hat{H}_{SB}(t_2)...\hat{H}_{SB}(t_{2n+1})\rho_B \right\} = 0 \,,$$

which means that all odd moments of the system-bath coupling Hamiltonian with respect to ρ_B vanish ($n = 0, 1, 2, ...$). In super-operator language, this leads to

$$\mathcal{P}\mathcal{L}(t_1)\mathcal{L}(t_2)...\mathcal{L}_{2n+1}\mathcal{P} = 0 \,. \tag{2.10}$$

This assumption is however not a requirement for the derivation.

The Nakajima-Zwanzig master equation

We apply the projection operators $\mathcal{P}$ and $\mathcal{Q}$ to the von Neumann equation Eq. (2.8), to obtain

$$\frac{d}{dt}\mathcal{P}\hat{\rho}_{\text{tot}}(t) = \lambda\mathcal{P}\mathcal{L}(t)\hat{\rho}_{\text{tot}}(t)\,,$$

$$\frac{d}{dt}\mathcal{Q}\hat{\rho}_{\text{tot}}(t) = \lambda\mathcal{Q}\mathcal{L}(t)\hat{\rho}_{\text{tot}}(t)\,,$$

and by inserting the identity Eq. (2.9) we further obtain

$$\frac{d}{dt}\mathcal{P}\hat{\rho}_{\text{tot}}(t) = \lambda\mathcal{P}\mathcal{L}(t)\mathcal{P}\hat{\rho}_{\text{tot}}(t) + \lambda\mathcal{P}\mathcal{L}(t)\mathcal{Q}\hat{\rho}_{\text{tot}}(t)\,, \tag{2.11}$$

$$\frac{d}{dt}\mathcal{Q}\hat{\rho}_{\text{tot}}(t) = \lambda\mathcal{Q}\mathcal{L}(t)\mathcal{P}\hat{\rho}_{\text{tot}}(t) + \lambda\mathcal{Q}\mathcal{L}(t)\mathcal{Q}\hat{\rho}_{\text{tot}}(t)\,. \tag{2.12}$$

Solving Eq. (2.12) by integrating it once we get

$$\mathcal{Q}\hat{\rho}_{\text{tot}}(t) = G(t,t_0)\mathcal{Q}\hat{\rho}_{\text{tot}}(t_0) + \lambda\int_{t_0}^t dt' G(t,t')\mathcal{Q}\mathcal{L}(t')\mathcal{P}\hat{\rho}_{\text{tot}}(t')\,, \tag{2.13}$$

where the propagator $G(t,t')$ is defined as

$$G(t,t') = Te^{\lambda\int_{t'}^t d\tau\,\mathcal{Q}\mathcal{L}(\tau)} \tag{2.14}$$

with T being the time-ordering operator, ordering super-operators with larger time arguments chronologically left of those with smaller time arguments. With the help of the solution to the irrelevant part of the density matrix, we are able to write down the Nakajima-Zwanzig equation by plugging Eq. (2.13) into Eq. (2.11)

$$\frac{d}{dt}\mathcal{P}\hat{\rho}_{\text{tot}}(t) = \lambda\mathcal{P}\mathcal{L}(t)G(t,t_0)\mathcal{Q}\hat{\rho}_{\text{tot}}(t_0) + \lambda\mathcal{P}\mathcal{L}(t)\mathcal{P}\hat{\rho}_{\text{tot}}(t)$$

$$+ \lambda^2\int_{t_0}^t dt'\mathcal{P}\mathcal{L}(t)G(t,t')\mathcal{Q}\mathcal{L}(t')\mathcal{P}\hat{\rho}_{\text{tot}}(t')\,.$$

Using Eq. (2.10) and defining the memory kernel $\mathcal{K}(t,t') = \lambda^2\mathcal{P}\mathcal{L}(t)G(t,s)\mathcal{Q}\mathcal{L}(t')\mathcal{P}$, we can write the Nakajima-Zwanzig equation as

$$\frac{d}{dt}\mathcal{P}\hat{\rho}_{\text{tot}}(t) = \lambda\mathcal{P}\mathcal{L}(t)G(t,t_0)\mathcal{Q}\hat{\rho}_{\text{tot}}(t_0) + \int_{t_0}^t dt'\mathcal{K}(t,t')\mathcal{P}\hat{\rho}_{\text{tot}}(t')\,. \tag{2.15}$$

This equation is an exact master equation for the relevant part of the open quantum system. Still, Eq. (2.15) might be as hard to solve as the von Neumann equation, but it serves as a starting point for various perturbative expansions, as for instance expansions in the coupling constant λ. This simplifies the structure of the Nakajima-Zwanzig equation considerably, but it nevertheless is a nonlocal in time master equation, cf. the time convolution in the memory kernel $\mathcal{K}(t,t')$. The purpose of this brief discussion of the Nakajima-Zwanzig equation is to show how the time convolutionless master equations can be gained from the Nakajima-

Zwanzig equation. The interested reader might find more details on the Nakajima-Zwanzig equation and a perturbative expansion of the memory kernel $\mathcal{K}(t, t')$ in Ref. [Breuer02].

The time convolutionless master equation

The time convolutionless master equation technique removes the time convolution of the memory kernel $\mathcal{K}(t, t')$ in the Nakajima-Zwanzig equation, making the resulting master equation a local in time one. In order to transform the Nakajima-Zwanzig equation to a local in time master equation, we have to eliminate the time dependence on the history of the system which is achieved by introducing a propagator similar to the one in Eq. (2.14)

$$\bar{G}(t, t') = \bar{T} e^{-\lambda \int_{t'}^{t} d\tau \mathcal{L}(\tau)}, \tag{2.16}$$

where $\bar{T}$ is the anti-time-ordering operator. The propagator $\bar{G}(t, t')$ in comparison to $G(t, t')$ is a backward propagator, describing the inverse of the time evolution of the open system. With Eq. (2.16) we can write the density matrix at time t' as

$$\hat{\rho}_{\text{tot}}(t') = \bar{G}(t, t') \left[\mathcal{P} + \mathcal{Q}\right] \hat{\rho}_{\text{tot}}(t),$$

which we plug into Eq. (2.13) to obtain

$$\mathcal{Q}\hat{\rho}_{\text{tot}}(t) = G(t, t_0)\mathcal{Q}\hat{\rho}_{\text{tot}}(t_0) + \lambda \int_{t_0}^{t} dt' G(t, t') \mathcal{Q}\mathcal{L}(t')\mathcal{P}\bar{G}(t, t') \left[\mathcal{P} + \mathcal{Q}\right] \hat{\rho}_{\text{tot}}(t). \tag{2.17}$$

We introduce another super-operator

$$\mathcal{S}(t) = \lambda \int_{t_0}^{t} dt' G(t, t') \mathcal{Q}\mathcal{L}(t')\mathcal{P}\bar{G}(t, t') \tag{2.18}$$

with the properties

$$\mathcal{S}(t_0) = 0, \tag{2.19}$$

$$\mathcal{S}(t)|_{\lambda=0} = 0, \tag{2.20}$$

and rewrite Eq. (2.17) for the irrelevant part as

$$\left[1 - \mathcal{S}(t)\right] \mathcal{Q}\hat{\rho}_{\text{tot}}(t) = G(t, t_0)\mathcal{Q}\hat{\rho}_{\text{tot}}(t_0) + \mathcal{S}(t)\hat{\rho}_{\text{tot}}(t).$$

With the properties of $\mathcal{S}(t)$ in Eq. (2.19) and (2.20) it possible to invert $\left[1 - \mathcal{S}(t)\right]$ for moderate couplings λ and small times $t - t_0$, i.e., we get an equation for the irrelevant part of the density matrix in terms of the relevant part

$$\mathcal{Q}\hat{\rho}_{\text{tot}}(t) = \left[1 - \mathcal{S}(t)\right]^{-1} G(t, t_0)\mathcal{Q}\hat{\rho}_{\text{tot}}(t_0) + \left[1 - \mathcal{S}(t)\right]^{-1} \mathcal{S}(t)\hat{\rho}_{\text{tot}}(t). \tag{2.21}$$

The time convolutionless master equation is then obtained by Eq. (2.21) together with Eq. (2.11)

$$\frac{d}{dt}\mathcal{P}\hat{\rho}_{\text{tot}}(t) = \mathcal{K}(t)\mathcal{P}\hat{\rho}_{\text{tot}}(t) + \mathcal{I}(t)\mathcal{Q}\hat{\rho}_{\text{tot}}(t_0)\,, \tag{2.22}$$

where the kernel $\mathcal{K}(t)$ is now local in time

$$\mathcal{K}(t) = \lambda\mathcal{P}\mathcal{L}(t)\left[1 - \mathcal{S}(t)\right]^{-1}\mathcal{P}\,, \tag{2.23}$$

and an inhomogeneity $\mathcal{I}$

$$\mathcal{I}(t) = \lambda\mathcal{P}\mathcal{L}(t)\left[1 - \mathcal{S}(t)\right]^{-1}G(t,t_0)\mathcal{Q}\,.$$

The inhomogeneous part in Eq. (2.22) in the case of factorizing initial conditions $\hat{\rho}_{\text{tot}}(t_0) = \hat{\rho}_S(t_0) \otimes \rho_B$ will be zero since we have $\mathcal{P}\hat{\rho}_{\text{tot}}(t_0) = \hat{\rho}_{\text{tot}}(t_0)$ which implies $\mathcal{Q}\hat{\rho}_{\text{tot}}(t_0) = 0$. The Eq. (2.22) can then be used as a starting point for a perturbative expansion in the coupling parameter λ. Expanding $\left[1 - \mathcal{S}(t)\right]^{-1}$ into a geometric series, we write Eq. (2.23) as

$$\mathcal{K}(t) = \lambda\sum_{n=0}^{\infty}\mathcal{P}\mathcal{L}(t)\mathcal{S}(t)^n\mathcal{P} = \sum_{n=1}^{\infty}\lambda^n\mathcal{K}_n(t)\,,$$

where we now can associate $\mathcal{K}_n(t)$ the n-order contribution to the kernel $\mathcal{K}(t)$ by expanding $\mathcal{S}(t)$ also in powers of λ

$$\mathcal{S}(t) = \sum_{n=1}^{\infty}\lambda^n\mathcal{S}_n(t)\,.$$

The expansion to second order in λ yields for the memory kernels $\mathcal{K}_n(t)$ (here we set $t_0 = 0$)

$$\mathcal{K}_1(t) = \mathcal{P}\mathcal{L}(t)\mathcal{P} = 0\,,$$
$$\mathcal{K}_2(t) = \mathcal{P}\mathcal{L}(t)\mathcal{S}_1(t)\mathcal{P} = \int_0^t dt'\mathcal{P}\mathcal{L}(t)\mathcal{L}(t')\mathcal{P}\,,$$

and the time convolutionless master equation in the interaction picture to second order in the coupling λ becomes

$$\frac{d}{dt}\hat{\rho}_S(t) = -\lambda^2\int_0^t dt'\,\text{Tr}_B\left\{\left[\hat{H}_{SB}(t),\left[\hat{H}_{SB}(t'),\hat{\rho}_S(t) \otimes \rho_B\right]\right]\right\}\,. \tag{2.24}$$

We can compare Eq. (2.24) with the Redfield equation Eq. (2.7), and notice that they are actually the same. Later, in Chap. 5 we will discuss where exactly the non-Markovian effects are contained in the master equation when we want to describe non-Markovian effects in nanomechanical systems.

2.3 Nanoelectromechanical systems as open quantum systems

From the perspective of open quantum systems, the actual nanomechanical oscillator is viewed as the reduced system that is coupled to a mesoscopic conductor (detector) acting as the reservoir. The electric current through the system is then influenced by the motion of the oscillator.

If we assume weak coupling between the mechanical and electronic degree of freedom, the influence of the detector on the mechanical resonator is equivalent to that of an equilibrium heat bath [Mozyrsky02, Mozyrsky04, Armour04b, Utami04, Clerk04b, Clerk04a, Blencowe05a, Wabnig05, Blencowe05b, Clerk05]. For a nanomechanical resonator which is coupled to a quantum/atomic point contact where the tunneling amplitude depends linearly on the position of the oscillator, the heating and damping effects of the electronic reservoir on the oscillator were found to be of Caldeira-Leggett form. It is therefore possible to assign an effective temperature and damping to the resonator which stem from the electronic reservoir.

These studies mainly employ Born Markov master equation techniques, either to gain information on transport properties or to study effects of the bath on the nanomechanical resonator. In order to access transport properties such as the average current or the current noise, a method called, the charge reduced density matrix formalism has to be used [Clerk04b, Wabnig05, Armour04a]. Non-Markovian effects of a nanomechanical resonator linearly coupled to a mesoscopic conductor using a master equation approach have been studied in Ref. [Chen11a].

In nanoelectromechanical setups, there are in principal two reservoirs which we have to be taken into account. First, there is an external bosonic heat bath that gives rise to damping and a finite Q-factor of the mechanical mode. This bosonic bath can be described within a Caldeira-Leggett model. Second, we have a fermionic bath which is due to the electronic mesoscopic detector. The fermionic bath is of special interest when we study for instance in Chap. 5 the generation of entanglement. It is described by the bias voltage and the coupling to the mechanical degree of freedom can be of a form that non-Markovian effects play a crucial role. The bosonic heat bath which could also serve as a medium to generate entanglement of two mechanical modes [Liu07, Isar10] is a somehow academic approach for entanglement generation due to the lack of experimental feasibility. A fermionic bath can in principle be easily controlled experimentally. Having a fermionic bath at hand, we can also imagine to engineer certain processes which lead to interesting effects. For instance, we could use a superconducting lead as a reservoir to which two nanomechanical oscillators are tunnel coupled. The superconductor serves as a source of Cooper-pairs. The tunneling electrons of the Cooper-pair spin singlet can then lead to an effective coupling between the two oscillators cf. Chap. 5.

Part III

Applications of nanoelectromechanical systems in the quantum regime

Chapter 3

Non-Markovian effects in nanoelectromechanical systems

The motivation for this chapter of the thesis is to study an experimentally feasible setup in which the quantum nature of NEMS can be probed by current noise measurements of a tunnel junction detector. A quantum NEMS can be described by a quantum harmonic oscillator which is a continuous variable system characterized by two non-commuting operators $\hat{x}$ and $\hat{p}$. The theoretical treatment of NEMS widely uses a Markovian master equation approach [Clerk04b, Wabnig05, Doiron07, Doiron08] with a few exceptions, for instance, the work by Wabnig et al. [Wabnig07] and Rastelli et al. [Rastelli10] where a Keldysh perturbation theory has been employed. Here, we also make use of the Keldysh technique (cf. Chap. 1) because it allows us to treat the non-equilibrium system fully quantum mechanically. Furthermore, using the Keldysh technique, we are able to carefully investigate the dynamics of the combined system for an arbitrary ratio of $eV/\hbar\Omega$, where V is the applied bias of the tunnel junction and Ω the eigenfrequency of the oscillator. In this sense, we go beyond the Markov approximation of previous works where these parameters were restricted to the regime $eV/\hbar\Omega \gg 1$. We also go beyond the Born approximation by expanding the finite frequency current noise of the tunnel junction up to fourth order in the tunneling amplitudes. Since we are interested in the quantum nature of the oscillator, it is important that the environmental temperature T_{env} and the applied bias V of the tunnel junction are not much larger than the eigenfrequency Ω of the oscillator, cf. Introduction. Otherwise, the oscillator would be heated and low energy properties inaccessible.

In order to probe the quantum nature of the continuous variable system, it is desirable to have a detector at hand that can measure expectation values with respect to $\hat{x}$-dependent observables, $\hat{p}$-dependent observables, as well as observables that depend on both $\hat{x}$ and $\hat{p}$. In Ref. [Doiron08], Doiron et al. have proposed a setup which could be used for position and momentum detection of NEMS. This setup consists of two tunnel junctions forming an Aharonov-Bohm (AB) loop. There, it is possible to tune the relative phase between the tunnel amplitudes (where one depends on $\hat{x}$ and the other one not) via a magnetic flux penetrating the AB loop, see Fig. 3.1 for the schematic setup. In such a setup, the symmetrized current noise

$$S_{\text{sym}}(\omega) = \frac{1}{2} \int dt\, e^{i\omega t} \left\langle \left\{ \Delta\hat{I}(t), \Delta\hat{I}(0) \right\} \right\rangle \tag{3.1}$$

(with the current fluctuation operator $\Delta\hat{I}(t) = \hat{I}(t) - \langle\hat{I}\rangle$) of the tunnel junction detector

can either contain information on the oscillator's position spectrum

$$S_x(\omega) = \frac{1}{2} \int dt\, e^{i\omega t} \left\langle \{\hat{x}(t), \hat{x}(0)\} \right\rangle, \tag{3.2}$$

then $S_{\mathrm{sym}}(\omega) \sim S_x(\omega)$, or the oscillator's momentum spectrum

$$S_p(\omega) = \frac{1}{2} \int dt\, e^{i\omega t} \left\langle \{\hat{p}(t), \hat{p}(0)\} \right\rangle, \tag{3.3}$$

then $S_{\mathrm{sym}}(\omega) \sim S_p(\omega)$ depending on the flux through the AB loop, see also Eq. (3.23). The former case has been coined x-detector and the latter case p-detector.The current noise $S_{\mathrm{sym}}(\omega)$ can also contain information on both, the position and the momentum of the oscillator. We note that $S_{\mathrm{sym}}(\omega)$, $S_x(\omega)$, and $S_p(\omega)$ are properly defined above in Eqs. (3.1)-(3.3) for a stationary problem. In the non-stationary case, which is also subject of discussion in this chapter, these quantities do not only depend on a single frequency ω but on one frequency argument and one time argument instead, see Eq. (3.12) below.

To be more specific, we call an x-detector, a detector that allows to measure expectation values of the oscillator's position operator $\hat{x}$, i.e., $\langle \hat{x} \rangle$, $\langle \hat{x}\hat{x} \rangle$, etc. Similarly, we call a p-detector, a detector that allows to measure expectation values of $\hat{p}$, the oscillator's momentum operator, i.e., $\langle \hat{p} \rangle$, $\langle \hat{p}\hat{p} \rangle$, etc. In Ref. [Doiron08], switching from the x-detector to the p-detector is then accomplished by tuning the relative phase between the tunnel amplitudes. The main difficulty of this setup is the need of long coherence times and lengths in the AB loop to make the switching possible. Here, we show that the AB setup can be avoided. We find that the current noise of the coupled oscillator-junction system with one tunnel junction only, already can be used for momentum detection due to the complex nature of the current noise when the oscillator is in a non-stationary state.

We further investigate the current noise stemming from a stationary oscillator up to fourth order in the tunneling amplitudes, thereby going beyond the Born approximation. Most importantly, we extend previous results of Ref. [Doiron08] to the non-Markovian regime without any restrictions on the relative magnitude of the energy scales eV, $\hbar\Omega$, and $k_B T_{\mathrm{env}}$.

We show that peaks in the finite frequency current noise at $\omega = \pm\Omega$ (both for the x-detector and the p-detector) are a fourth order effect. In the Markovian regime, the peaks in the position detector signal are always much larger than the ones in the momentum detector signal. This is different in the non-Markovian regime. There, we even find a larger signal for the momentum detector compared to the position detector, clearly demonstrating that the non-Markovian regime is the preferred regime to operate the momentum detector. The detailed understanding of the x-detector and the p-detector allows us to uniquely identify the quantum state of the oscillator by a finite frequency noise measurement. [1]

3.1 Overview of the theoretical model

The system we consider consists of a nanomechanical harmonic oscillator coupled to a biased tunnel junction. In Ref. [Flowers-Jacobs07] an experimental realization is shown, where

---

[1]This chapter of the thesis is built upon the published article in Ref. [Walter11b].
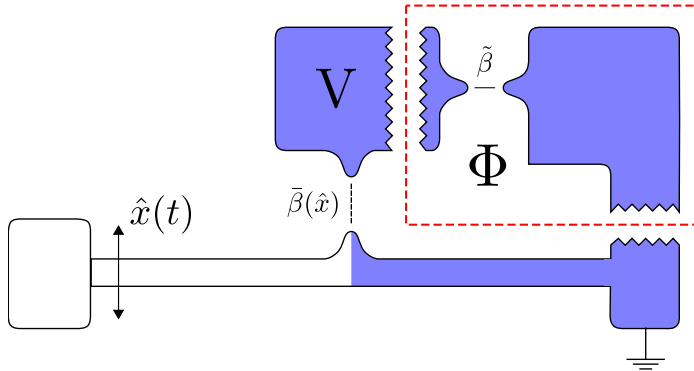
Figure 3.1: Schematic setup for the realization of a position detector which can be extended by the parts enclosed in the red dashed box to a momentum detector. The total tunnel amplitude in the case of the position detector (setup without parts in the red dashed box) is given by just $\bar{\beta}(\hat{x}) = t_0 + t_1 \hat{x}$. In the case of the momentum detector a second tunnel junction $\tilde{\beta}$ is added which leads to a relative phase η between t_0 and t_1 that can be tuned via a magnetic flux Φ penetrating the AB loop. If the oscillator is in a non-stationary state, already the parts without the elements in the red dashed box serve as a position as well as a momentum detector.

electrons can tunnel from an atomic point contact (APC) onto a conducting oscillator. The coupled system is described by the following Hamiltonian

$$\hat{H} = \hat{H}_{\text{osc}} + \hat{H}_{\text{res}} + \hat{H}_{\text{tun}} \,.$$

The unperturbed Hamiltonian $\hat{H}_0 = \hat{H}_{\text{res}} + \hat{H}_{\text{soc}}$ consists of

$$\hat{H}_{\text{osc}} = \frac{\hat{p}^2}{2m} + \frac{1}{2} m \Omega^2 \hat{x}^2 \,,$$
$$\hat{H}_{\text{res}} = \sum_{l,r} \varepsilon_l \, \hat{c}_l^\dagger \, \hat{c}_l + \varepsilon_r \, \hat{c}_r^\dagger \, \hat{c}_r \,,$$

where $\hat{H}_{\text{osc}}$ describes the oscillator with $\hat{x}$ and $\hat{p}$ being the position and momentum operator of the oscillator with mass m and frequency Ω, respectively. $\hat{H}_{\text{res}}$ contains the fermionic reservoirs of the left and right contacts where $\hat{c}_\alpha$ ($\hat{c}_\alpha^\dagger$) annihilates (creates) an electron in reservoir $\alpha = l, r$ and l/r are electron momenta in the left/right lead. The oscillator couples to the tunnel junction via the tunneling Hamiltonian

$$\hat{H}_{\text{tun}} = \sum_{l,r} \beta \, \hat{c}_l^\dagger \, \hat{c}_r + \text{H.c.} \,.$$

Motivated by the experimental setup in Ref. [Flowers-Jacobs07], we take the oscillator to act as one of the fermionic reservoirs. Therefore, the tunneling gap depends on the position of the oscillator, modifying the tunneling amplitude of the APC. For small oscillator displacements x, we assume linear coupling of the oscillator to the tunnel junction with a tunnel amplitude β_1. Hence we obtain $\beta = [\beta_0 + \beta_1 \hat{x}]$, with β_0 being the bare tunneling amplitude. Here, we allow for complex tunnel amplitudes β_0 and β_1 as previously discussed

in Refs. [Doiron08, Schmidt10]. With η we denote the relative phase between the tunnel amplitudes, i.e., we write $\beta_0 = t_0$ and $\beta_1 = t_1 e^{i\eta}$ where $t_0, t_1 \in \mathbb{R}$. A possible experimental realization of the finite and tunable phase η is discussed in Ref. [Doiron08]. There, it was shown that by adding a second tunneling junction as shown in Fig. 3.1 and threatening the resulting loop with a magnetic flux Φ leads to a tunable phase of the tunneling amplitudes. The tunneling amplitudes of the two junctions in Fig. 3.1 are given by a position dependent one $\bar{\beta}(\hat{x}) = t_0 + t_1 \hat{x}$ and a position independent one $\tilde{\beta}$. The AB-effect caused by threading the loop with a flux causes a phase shift of the electronic wave function. This phase shift can be absorbed in the tunneling amplitudes and the total tunneling amplitude is then given by $\beta_t = \bar{\beta}(\hat{x}) + \tilde{\beta} \exp(-i\Phi/\Phi_0)$ with $\Phi_0 = h/e$. The position independent parts of the tunneling amplitude are just related by a constant $c \in \mathbb{R}$, i.e., we can write $\tilde{\beta} = ct_0$. With this the total tunneling amplitude is given by (up to a global irrelevant phase) $\beta_t = \sqrt{1 + c^2} t_0 + t_1 \hat{x} \exp(-i\phi)$ with $\phi = \arg(1 + c \exp(-i\Phi/\Phi_0))$. As a consequence the phase ϕ can be tuned with the flux Φ. For all practical purposes we use the simplified notation introduced before $\beta = t_0 + t_1 e^{i\eta} \hat{x}$. This phase η as we will see later gives rise to the possibility to detect the oscillator's momentum expectation value $\langle \hat{p}^2 \rangle$, present in the current noise.

The true non-equilibrium, non-Markovian quantum behavior of the coupled system is the subject of our interest. Therefore, we make use of the Keldysh formalism for our calculation. The quantities being accessible in the experiment are for instance the tunnel current and the current-current correlator, the noise of the tunnel junction. These will also be the main objects of interest in this chapter. We employ a perturbation theory in the tunnel Hamiltonian $\hat{H}_{\mathrm{tun}}$ and calculate the noise up to fourth order in the tunneling.

We start with introducing the current operator in a convenient notation, it is given by $\hat{I} = -e \frac{d}{dt} \hat{N}_l$, where $\hat{N}_l = \hat{c}_l^\dagger \hat{c}_l$ counts electrons in the left reservoir. We then write the current operator as

$$\hat{I} = e \left[\hat{j}_0 + \hat{x}\hat{j}_1 \right] ,$$

and similarly for the tunnel Hamiltonian

$$\hat{H}_{\mathrm{tun}} = \hat{h}_0 + \hat{x}\hat{h}_1 ,$$

with $\hat{j}_i = i \left[\hat{\mathcal{T}}_i - \hat{\mathcal{T}}_i^\dagger \right]$ and $\hat{h}_i = \hat{\mathcal{T}}_i + \hat{\mathcal{T}}_i^\dagger$. The operator $\hat{\mathcal{T}}_i$ is given by $\hat{\mathcal{T}}_i = \sum_{l,r} \beta_i \hat{c}_l^\dagger \hat{c}_r$ with $i \in \{0, 1\}$.

Details on the reservoir Green's functions

The fermionic Green's functions of the left and right reservoirs (free electron gas) $G_{l,r}$, are given on the Keldysh contour $\mathcal{C}$ by $G_{l,r}(t, t') = -i \left\langle T_c \hat{c}_{l,r}(t) \hat{c}_{l,r}^\dagger(t') \right\rangle$. See Fig. 1.2 for the Keldysh contour $\mathcal{C}$. Here however, the time ordered branch is $\mathcal{C}_-$ and the anti-time ordered one is $\mathcal{C}_+$. A Fourier transformation of the real time Green's functions then leads to the following Green's functions

$$G_{l,r}(\omega) = \begin{pmatrix} G_{l,r}^{--}(\omega) & G_{l,r}^{-+}(\omega) \\ G_{l,r}^{+-}(\omega) & G_{l,r}^{++}(\omega) \end{pmatrix} = 2\pi i \rho_0 \begin{pmatrix} n_{l,r}(\omega) - 1/2 & n_{l,r}(\omega) \\ n_{l,r}(\omega) - 1 & n_{l,r}(\omega) - 1/2 \end{pmatrix} .$$

Here we made use of time translation invariance and assumed a constant density of states in the left and right reservoir $\rho_l = \rho_r = \rho_0$. We make the reasonable assumption that the fermionic bath relaxes much faster than the system into a steady state, justifying that the fermionic bath correlation functions do not depend on absolute times but only on the time difference. The applied finite bias $\mu_r - \mu_l = eV$ is included in the Fermi distribution functions

$$n_l = n(\omega - eV/2) = [\exp(\beta(\omega - eV/2) + 1]^{-1} \,,$$
$$n_r = n(\omega + eV/2) = [\exp(\beta(\omega + eV/2) + 1]^{-1} \,.$$

The inverse temperature of electrons in the reservoirs is $\beta = 1/k_B T$ and we use units where $\hbar = 1$. Expectation values of products of the fermionic operators $\hat{h}_i$ and $\hat{j}_i$ which we will need for the perturbative expansion can be expressed by the Keldysh Green's functions $G_{l,r}(t, t')$ as

$$\left\langle T_c \hat{h}_i(t)\, \hat{j}_j(t') \right\rangle_0 \equiv -i\, \bar{\mathcal{G}}_{ij}(t, t') = -i \left[\beta_i \beta_j^* G_r(t, t') G_l(t', t) - \beta_i^* \beta_j G_r(t', t) G_l(t, t') \right] \,,$$
$$\left\langle T_c \hat{h}_i(t)\, \hat{h}_j(t') \right\rangle_0 \equiv \mathcal{G}_{ij}(t, t') = \left[\beta_i \beta_j^* G_r(t, t') G_l(t', t) + \beta_i^* \beta_j G_r(t', t) G_l(t, t') \right] \,,$$
$$\left\langle T_c \hat{j}_i(t)\, \hat{j}_j(t') \right\rangle_0 \equiv \mathcal{G}_{ij}(t, t') = \left[\beta_i \beta_j^* G_r(t, t') G_l(t', t) + \beta_i^* \beta_j G_r(t', t) G_l(t, t') \right] \,,$$

where the average is taken with respect to the unperturbed Hamiltonian $\hat{H}_0$. The Fourier transform of the function $\mathcal{G}_{ij}(t, t')$ and $\bar{\mathcal{G}}_{ij}(t, t')$ can be calculated in the usual way, yielding

$$\mathcal{G}_{ij}^{-+}(\omega) = \tag{3.4}$$
$$2\pi\rho_0^2 \left\{ \beta_i\, \beta_j^* \frac{eV + \omega}{2} \left[-1 + \coth\left(\beta \frac{eV + \omega}{2} \right) \right] + \beta_i^* \beta_j \frac{eV - \omega}{2} \left[1 + \coth\left(\beta \frac{eV - \omega}{2} \right) \right] \right\} \,,$$
$$\mathcal{G}_{ij}^{+-}(\omega) = \tag{3.5}$$
$$2\pi\rho_0^2 \left\{ \beta_i\, \beta_j^* \frac{eV + \omega}{2} \left[1 + \coth\left(\beta \frac{eV + \omega}{2} \right) \right] + \beta_i^* \beta_j \frac{eV - \omega}{2} \left[-1 + \coth\left(\beta \frac{eV - \omega}{2} \right) \right] \right\} \,,$$
$$\bar{\mathcal{G}}_{ii}^{--}(\omega) =$$
$$\beta_i\, \beta_i^* \int \frac{d\omega_1}{2\pi} \left[G_r^{--}(\omega_1 + \omega) G_l^{--}(\omega_1) - G_r^{--}(\omega_1) G_l^{--}(\omega_1 + \omega) \right] = 2\pi\rho_0^2\, \beta_i\, \beta_i^*\, \sigma^-(\omega, V) \,,$$
$$\bar{\mathcal{G}}_{ii}^{++}(\omega) = \bar{\mathcal{G}}_{ii}^{--}(\omega) \,,$$

where we defined the functions

$$\sigma^{\pm}(\xi, V) = \frac{eV + \xi}{2} \coth\left(\beta \frac{eV + \xi}{2} \right) \pm \frac{eV - \xi}{2} \coth\left(\beta \frac{eV - \xi}{2} \right) \,. \tag{3.6}$$

The functions $\sigma^{\pm}(\xi, V)$ also allow us to distinguish the Markovian from the non-Markovian regime. For $T \to 0$, we find

$$\sigma^-(\xi, V) = \begin{cases} \operatorname{sgn}(V)\, \xi & \text{for } e|V| > \xi \\ \operatorname{sgn}(V)\, e|V| & \text{for } e|V| < \xi \end{cases} \,,$$

and

$$\sigma^+(\xi, V) = \begin{cases} e|V| & \text{for} \quad e|V| > \xi \\ \xi & \text{for} \quad e|V| < \xi \end{cases},$$

where T here is the temperature of electrons in the leads. Later, the parameter ξ can be Ω and therefore the functions $\sigma^\pm(\xi, V)$ will depend on the ratio V/Ω, thereby allowing to distinguish Markovian from non-Markovian.

Details on the oscillator

Since the oscillator modulates the tunneling of electrons and therefore has impact on the measured average current and current-current correlator, it is important to understand the significance of the oscillator's state. We distinguish between an oscillator in a stationary state and one in a non-stationary state. We justify this differentiation by arguing that for short times after the measurement, the oscillator will certainly be non-stationary. The dominating time scale here is the one given by the oscillator itself, $1/\Omega$, which has to be compared to time scales on which the damping of the oscillator due to the tunnel junction and the external heat bath happens. In the non-stationary case, we cannot make use of time translation invariance in the oscillator's correlation function $D(t, t')$ defined in Eq. (3.7). For longer times however, the assumption of stationarity is justified since the oscillator can equilibrate with the environment and reach a steady state. The oscillator's correlation function then only depends on the time difference $t - t'$.

We work in the following with the oscillator operators given in the Heisenberg picture as $\hat{x}(t) = \hat{x}\cos(\Omega t) + \hat{p}/(m\Omega)\sin(\Omega t)$ and $\hat{p}(t) = \hat{p}\cos(\Omega t) - \hat{x}(m\Omega)\sin(\Omega t)$. We also define the aforementioned oscillator correlation function $D(t, t')$ in Keldysh space as

$$D(t, t') = -i \langle T_c \, \hat{x}(t)\hat{x}(t') \rangle . \tag{3.7}$$

When we later investigate the second order noise we consider both the stationary situation and the non-stationary situation. The following relation then is a very useful one

$$\hat{x}(t + t') = \hat{x}(t')\cos(\Omega t) + \frac{\hat{p}(t')}{m\Omega}\sin(\Omega t). \tag{3.8}$$

For calculations up to second order in the tunneling, we look at the influence of stationary and non-stationary oscillator states on the current noise. In fourth order, we restrict ourselves to the stationary case. Hence, we are interested in a clear definition of the oscillator's correlation functions and spectral functions in the stationary case, which will be addressed now.

Oscillator correlation functions in the stationary case

Considering the stationary case, we give useful expressions for the oscillator's correlation functions which later on allow us to identify the oscillator's power spectrum in x denoted by $S_x(\omega)$ and in p denoted by $S_p(\omega)$. From Eq. (3.7) the correlation function where $t \in \mathcal{C}_+$ and

$t' \in \mathcal{C}_-$ is given by

$$iD^{+-}(t,t') = \langle \hat{x}(t)\hat{x}(t') \rangle$$
$$= \frac{1}{2}\Big\langle \bar{x}_+^2 \cos(\Omega(t-t')) + \frac{[\hat{p},\hat{x}]}{m\Omega}\sin(\Omega(t-t')) + \bar{x}_-^2 \cos(\Omega(t+t')) + \frac{\{\hat{p},\hat{x}\}}{m\Omega}\sin(\Omega(t+t')) \Big\rangle,$$

and similar for $t \in \mathcal{C}_-$ and $t' \in \mathcal{C}_+$

$$iD^{-+}(t,t') = \langle \hat{x}(t')\hat{x}(t) \rangle$$
$$= \frac{1}{2}\Big\langle \bar{x}_+^2 \cos(\Omega(t-t')) - \frac{[\hat{p},\hat{x}]}{m\Omega}\sin(\Omega(t-t')) + \bar{x}_-^2 \cos(\Omega(t+t')) + \frac{\{\hat{p},\hat{x}\}}{m\Omega}\sin(\Omega(t+t')) \Big\rangle,$$

where we defined

$$\bar{x}_\pm^2 = \hat{x}^2 \pm \frac{\hat{p}^2}{m^2\Omega^2}\,.$$

Since, here we deal with the stationary case, the expectation values $\langle \bar{x}_-^2 \rangle$ and $\langle \{p,x\} \rangle$ appearing as prefactors of functions depending on $t+t'$ equal zero which one can easily check by using any stationary state, e.g., number-states. As one would expect, the correlation function now is a function of the time difference $t-t'$ only. The Fourier transform of the correlation functions then yields

$$iD^{+-}(\omega) = \frac{1}{2}\Big\langle \bar{x}_+^2 \mathcal{R}_\gamma^+(\omega,\Omega) + \frac{i\,[\hat{p},\hat{x}]}{m\Omega}\mathcal{R}_\gamma^-(\omega,\Omega) \Big\rangle,$$
$$iD^{-+}(\omega) = \frac{1}{2}\Big\langle \bar{x}_+^2 \mathcal{R}_\gamma^+(\omega,\Omega) - \frac{i\,[\hat{p},\hat{x}]}{m\Omega}\mathcal{R}_\gamma^-(\omega,\Omega) \Big\rangle.$$

Additionally, we introduce the two momentum correlation functions $iP^{+-}(t,t') = \langle \hat{p}(t)\hat{p}(t') \rangle$ and $iP^{-+}(t,t') = \langle \hat{p}(t')\hat{p}(t) \rangle$. The same arguments as for $iD^{\pm\mp}(t,t')$ lead here to the following Fourier transforms

$$iP^{+-}(\omega) = \frac{1}{2}\Big\langle \bar{p}_+^2 \mathcal{R}_\gamma^+(\omega,\Omega) + m\Omega i\,[\hat{p},\hat{x}]\mathcal{R}_\gamma^-(\omega,\Omega) \Big\rangle,$$
$$iP^{-+}(\omega) = \frac{1}{2}\Big\langle \bar{p}_+^2 \mathcal{R}_\gamma^+(\omega,\Omega) - m\Omega i\,[\hat{p},\hat{x}]\mathcal{R}_\gamma^-(\omega,\Omega) \Big\rangle,$$

where similar to above

$$\bar{p}_\pm^2 = m^2\Omega^2 \hat{x}^2 \pm \hat{p}^2\,.$$

We introduce the functions $\mathcal{R}_\gamma^\pm(\omega,\Omega)$ as

$$\mathcal{R}_{\gamma\to 0}^+(\omega,\Omega) = \pi\left[\delta(\omega+\Omega) + \delta(\omega-\Omega)\right], \tag{3.9}$$
$$\mathcal{R}_{\gamma\to 0}^-(\omega,\Omega) = \pi\left[\delta(\omega-\Omega) - \delta(\omega+\Omega)\right]. \tag{3.10}$$

The coupling of the oscillator to two environments, namely an external heat bath and the tunnel junction, being at temperatures T_{env} and $k_B T_{\mathrm{junc}} = eV/2$ [Mozyrsky02], respectively,

introduces a damping of the oscillator with damping coefficients γ_0 and γ_+, respectively. The oscillator dynamics due to the coupling to the tunnel junction can be calculated by solving a Dyson equation for the oscillator correlation function $D(t, t')$ where the self-energy is taken to lowest non-vanishing order in the tunnel Hamiltonian, i.e., $\Sigma(t, t') = -i \left\langle T_c \, \hat{h}_1(t) \hat{h}_1(t') \right\rangle$. Using the Keldysh technique as done in Refs. [Wabnig07, Clerk04a] the oscillator dynamics and the damping coefficient $\gamma_+ = \pi \rho_0^2 t_1^2 / m$ can be calculated. The coupling to the external heat bath can be added phenomenologically, or explicitly as an interaction with a bath of harmonic oscillators. The total damping then follows as $\gamma_{\text{tot}} = \gamma_0 + \gamma_+$. We can assign an effective temperature T_{eff} to the oscillator with $\gamma_{\text{tot}} T_{\text{eff}} = \gamma_+ T_{\text{junc}} + \gamma_0 T_{\text{env}}$ [2]. This leads to the general case for $\mathcal{R}_\gamma^\pm$ by replacing the δ-functions in Eqs. (3.9, 3.10) by a Lorentzian, where we include both sources of damping and an oscillator frequency $\Omega \to \sqrt{\Omega^2 - \gamma^2}$. For this damped case we can write for $\mathcal{R}_\gamma^+(\omega, \Omega)$

$$\mathcal{R}_\gamma^+(\omega, \Omega) = \frac{2\gamma_{\text{tot}}(\omega^2 + \Omega^2)}{4\gamma_{\text{tot}}^2 \omega^2 + (\omega^2 - \Omega^2)^2} \,,$$

and for $\mathcal{R}_\gamma^-(\omega, \Omega)$

$$\mathcal{R}_\gamma^-(\omega, \Omega) = \frac{4\gamma_{\text{tot}} \, \omega \, \sqrt{\Omega^2 - \gamma_{\text{tot}}^2}}{4\gamma_{\text{tot}}^2 \omega^2 + (\omega^2 - \Omega^2)^2} \,.$$

We want to stress that we have not made any assumption on the initial time as, e.g., $t' = 0$, allowing us later to study the current noise in the non-stationary case. This concludes our discussion on the oscillator correlation functions. We now turn to the spectral functions $S_x(\omega)$ and $S_p(\omega)$.

The oscillator's spectra in the stationary case

The symmetrized power spectrum, in general defined as $\frac{1}{2} \int dt \, e^{i\omega t} \left\langle \{\hat{\Upsilon}(t), \hat{\Upsilon}(t')\} \right\rangle$ of the oscillator quantities $\hat{\Upsilon} = \hat{x}, \hat{p}$ is an observable that can be measured by, e.g., current noise measurements (as discussed below). Both $S_x(\omega)$ and $S_p(\omega)$ can be measured through the current noise $S_{\text{sym}}(\omega)$. The expressions for these power spectra are given by

$$S_x(\omega) = \frac{1}{2} \int dt \, e^{i\omega t} \left\langle \{\hat{x}(t), \hat{x}(t')\} \right\rangle = \frac{1}{2} \left\langle \bar{x}^2 \right\rangle \mathcal{R}_\gamma^+(\omega, \Omega) \,,$$
$$S_p(\omega) = \frac{1}{2} \int dt \, e^{i\omega t} \left\langle \{\hat{p}(t), \hat{p}(t')\} \right\rangle = \frac{1}{2} \left\langle \bar{p}^2 \right\rangle \mathcal{R}_\gamma^+(\omega, \Omega) \,.$$

The momentum and position spectrum are related via the relation

$$S_p(\omega) = m^2 \Omega^2 S_x(\omega) \,.$$

---

[2]In typical experiments carried out in a cryogenic environment, the environmental temperature T_{env} and the electronic temperature T are in a first approximation of the same order, i.e., $T_{\text{env}} \approx T$.

We can also write down the spectra using the Keldysh Green's function

$$D^K(\omega) = D^{+-}(\omega) + D^{-+}(\omega)$$

which yields

$$S_x(\omega) = \frac{1}{2}\, i D^K(\omega)\,,$$
$$S_p(\omega) = \frac{1}{2} m^2 \Omega^2\, i D^K(\omega)\,.$$

To further simplify the notation, we introduce

$$Q(\omega) = \frac{i}{2}\left[\Upsilon^{+-}(\omega) - \Upsilon^{-+}(\omega)\right] = \frac{1}{2m\Omega}\mathcal{R}_\gamma^-(\omega,\Omega)\,,$$

where $\Upsilon = D, P$ which we later use in the fourth order current noise calculation.

3.2 Current noise calculations

Brief overview

In this section, we cover a variety of aspects when dealing with the current noise. For all different aspects we find expressions for the current noise which are valid for an arbitrary η and therefore include the x-detector as well as the p-detector.

The first section, Sec. 3.2.1, is dedicated to the current noise in second order perturbation theory, where we furthermore make the distinction between a stationary harmonic oscillator and a non-stationary one. Besides the Markovian regime ($eV \gg \hbar\Omega$), the Keldysh formalism also allows us to investigate the non-Markovian regime ($eV \ll \hbar\Omega$). The main result in this section is that the current noise for a non-stationary oscillator can in principle be complex. In this case, a detectable complex noise would allow for a nearly complete determination of the oscillator's covariance matrix $\sigma_{ij} = \text{Tr}\,[\hat{\rho}\,\{\hat{\Upsilon}_i, \hat{\Upsilon}_j\}/2]$, where $\hat{\Upsilon} = (\hat{x}, \hat{p})^T$. The covariance matrix allows for a complete description of the oscillator's quantum state, cf. Chap. 5.

For the stationary oscillator, we recover a noise that is real and in accordance with the Wiener-Khinchin theorem. This noise is the well known noise of a bare biased tunnel junction which shows kinks at $|\omega| = |V|$ [Schoelkopf97, Blanter00], modified by the oscillator leading to kinks at $|\omega| = |V \pm \Omega|$.

In Sec. 3.2.2, we deal with the noise up to fourth order in the tunneling amplitudes, where we restrict ourselves to the stationary case. On the one hand, the fourth order contributions modify the kinks, on the other hand, they give rise to resonances stemming from the oscillator correlation functions [Clerk04b, Wabnig07, Doiron08].

Importantly, we study the problem over the whole parameter range. Thus, we go, e.g., beyond Ref. [Wabnig05] where a Markov approximation was employed and lead to the constraint $\Omega \ll \max(k_B T, eV)$ for the high frequency current noise. Before we introduce the perturbation theory leading to the noise expression, we want to clarify the term second and fourth order perturbation theory. When we talk about these two cases we want to indicate that we expanded the quantities which we calculate to second and forth order in

the tunneling amplitudes. Our results, especially in Sec. 3.2.2 are of higher order than the actual expansion since we used the oscillator Green's function Eq. (3.7) which is obtained by solving the Dyson equation with the proper self-energy as discussed in Sec. 3.1.

General expressions for the current noise and the average current

In general, the expression for the current-current correlator in the Keldysh formalism is given by

$$S(\tau_3, \tau_4) = \left\langle T_c\, e^{-i\int_c d\tilde{\tau}\hat{H}_{\text{tun}}(\tilde{\tau})}\hat{I}(\tau_3)\hat{I}(\tau_4)\right\rangle_0 - \left\langle\hat{I}(\tau_3)\right\rangle_0\left\langle\hat{I}(\tau_4)\right\rangle_0,$$

where expectation values are taken with respect to the unperturbed Hamiltonian $\hat{H}_0$. Since we consider only the second and fourth order current noise we write

$$S(\tau_3, \tau_4) = S^{(2)}(\tau_3, \tau_4) + S^{(4)}(\tau_3, \tau_4),$$

where the second order term is given by

$$S^{(2)}(\tau_3, \tau_4) = \left\langle T_c\,\hat{I}(\tau_3)\hat{I}(\tau_4)\right\rangle_0, \tag{3.11}$$

and the fourth order term reads

$$S^{(4)}(\tau_3, \tau_4) = -\frac{1}{2}\int_c d\tau_1 d\tau_2\left\langle T_c\,\hat{H}_{\text{tun}}(\tau_1)\hat{H}_{\text{tun}}(\tau_2)\hat{I}(\tau_3)\hat{I}(\tau_4)\right\rangle_0$$
$$+ \int_c d\tau_1 d\tau_2\left\langle T_c\,\hat{H}_{\text{tun}}(\tau_1)\hat{I}(\tau_3)\right\rangle_0\left\langle T_c\hat{H}_{\text{tun}}(\tau_2)\hat{I}(\tau_4)\right\rangle_0.$$

First, we are going to review the average current in the setup. The general expression for the average current from which we start employing the perturbation expansion is given by

$$\langle I(t)\rangle = \left\langle T_c\, e^{-i\int_c d\tau\hat{H}_{\text{tun}}(\tau)}\hat{I}(t)\right\rangle_0.$$

To second order in the tunneling amplitudes, the average current can be calculated by

$$\langle I(t)\rangle = -i\int_c d\tau\left\langle T_c\,\hat{H}_{\text{tun}}(\tau)\hat{I}(t)\right\rangle_0,$$

for which we obtain the following expression in accordance with Ref. [Doiron08]

$$\langle I(t)\rangle = 2\pi\rho_0^2 e\Big\{t_0^2 eV + 2\cos(\eta)t_0 t_1 eV\left\langle\hat{x}(t)\right\rangle + \sin(\eta)t_0 t_1\frac{\langle\hat{p}(t)\rangle}{m}$$
$$+ t_1^2 eV\left\langle\hat{x}(t)\hat{x}(t)\right\rangle - \frac{t_1^2}{2m\Omega}\sigma^-(\Omega, V)\Big\},$$

where $\sigma^-(\Omega, V)$ is given in Eq. (3.6).

The current noise we calculate is always the frequency-dependent (and in the non-stationary

case also time-dependent) symmetrized current noise, defined as

$$
S_{\text{sym}}(\omega, t') = \frac{1}{2} \int dt \, e^{i\omega t} \left[S^{-+}(t, t') + S^{+-}(t, t') \right] ,
\tag{3.12}
$$

where for $S^{-+}(t, t')$, $t \in \mathcal{C}_-$ and $t' \in \mathcal{C}_+$ and similar for $S^{+-}(t, t')$. The debate whether the symmetrized or unsymmetrized current noise of the detector is accessible in an experiment has been discussed in Refs. [Lesovik97, Gavish00]. We focus on the symmetrized version of the current noise, since leading experiments as in Refs. [Schoelkopf97, Flowers-Jacobs07] showed that the symmetrized current noise is measurable and since the focus of this chapter lies in the characterization of the nanomechanical resonator.

3.2.1 Current noise to second order in the tunneling amplitudes

We now turn to the calculation of the current noise to second order. With the current operator $\hat{I}$ already being first order in the tunneling amplitudes, the current noise in the Born approximation is given by the following expression

$$
S^{(2)ij}(t, t') = \left\langle T_c \, \hat{I}(t + t')_i \hat{I}(t')_j \right\rangle ,
$$

where we used a slightly different definition of the current noise as compared to Eq. (3.11). This definition will be useful when examining the non-stationary case. Due to this definition the time dependence on t' in the symmetrized current noise is only present in the oscillator's quantum mechanical expectation values.

The general expression for the current noise to second order in the tunneling amplitudes in Keldysh space reads

$$
\begin{aligned}
S^{(2)ij}(t, t') = e^2 \Big[&\mathcal{G}_{00}(t + t', t') + \langle \hat{x}(t') \rangle \, \mathcal{G}_{01}(t + t', t') \\
&+ \langle \hat{x}(t + t') \rangle \, \mathcal{G}_{10}(t + t', t') + iD(t + t', t') \, \mathcal{G}_{11}(t + t', t') \Big] .
\end{aligned}
\tag{3.13}
$$

Now, we only make use of time translation invariance in the $\mathcal{G}_{ij}(t, t')$ functions and the oscillator is taken as non-stationary. The starting point for the calculation is Eq. (3.13), together with Eqs. (3.7, 3.8) the symmetrized current noise in the non-stationary case can be written as

$$
\begin{aligned}
S_{\text{sym}}^{(2)}(\omega, t') = \frac{e^2}{2} \int dt \, e^{i\omega t} \Big\{ &\mathcal{G}_{00}^{-+}(t) + \mathcal{G}_{00}^{+-}(t) \\
&+ \langle \hat{x}(t') \rangle \left[\mathcal{G}_{01}^{-+}(t) + \mathcal{G}_{01}^{+-}(t) \right] + \langle \hat{x}(t') \rangle \cos(\Omega t) \left[\mathcal{G}_{10}^{-+}(t) + \mathcal{G}_{10}^{-+}(t) \right] \\
&+ \frac{\langle \hat{p}(t') \rangle}{m\Omega} \sin(\Omega t) \left[\mathcal{G}_{10}^{-+}(t) + \mathcal{G}_{10}^{+-}(t) \right] + \langle \hat{x}(t') \hat{x}(t') \rangle \cos(\Omega t) \left[\mathcal{G}_{11}^{-+}(t) + \mathcal{G}_{11}^{+-}(t) \right] \\
&+ \frac{\langle \hat{x}(t') \hat{p}(t') \rangle}{m\Omega} \sin(\Omega t) \mathcal{G}_{11}^{-+}(t) + \frac{\langle \hat{p}(t') \hat{x}(t') \rangle}{m\Omega} \sin(\Omega t) \mathcal{G}_{11}^{+-}(t) \Big\} .
\end{aligned}
\tag{3.14}
$$

The further calculation is straightforward by using Eq. (3.4) and (3.5). Finally, the current

noise $S_{\text{sym}}^{(2)}(\omega, t')$ in Eq. (3.14) can be written as

$$
\begin{aligned}
S_{\text{sym}}^{(2)}(\omega, t') = \frac{e^2}{2} \Big\{ & \mathcal{G}_{00}^{-+}(\omega) + \mathcal{G}_{00}^{+-}(\omega) + \langle \hat{x}(t') \rangle \left[\mathcal{G}_{01}^{-+}(\omega) + \mathcal{G}_{01}^{+-}(\omega) \right] \\
& + \frac{1}{2} \langle \hat{x}(t') \rangle \left[\mathcal{G}_{10}^{-+}(\omega + \Omega) + \mathcal{G}_{10}^{-+}(\omega - \Omega) + \mathcal{G}_{10}^{+-}(\omega + \Omega) + \mathcal{G}_{10}^{+-}(\omega - \Omega) \right] \\
& - \frac{i}{2m\Omega} \langle \hat{p}(t') \rangle \left[\mathcal{G}_{10}^{-+}(\omega + \Omega) - \mathcal{G}_{10}^{-+}(\omega - \Omega) + \mathcal{G}_{10}^{+-}(\omega + \Omega) - \mathcal{G}_{10}^{+-}(\omega - \Omega) \right] \\
& + \frac{1}{2} \langle \hat{x}(t') \hat{x}(t') \rangle \left[\mathcal{G}_{11}^{-+}(\omega + \Omega) + \mathcal{G}_{11}^{-+}(\omega - \Omega) + \mathcal{G}_{11}^{+-}(\omega + \Omega) + \mathcal{G}_{11}^{+-}(\omega - \Omega) \right] \\
& - \frac{i}{2m\Omega} \langle \hat{x}(t') \hat{p}(t') \rangle \left[\mathcal{G}_{11}^{-+}(\omega + \Omega) - \mathcal{G}_{11}^{-+}(\omega - \Omega) \right] \\
& - \frac{i}{2m\Omega} \langle \hat{p}(t') \hat{x}(t') \rangle \left[\mathcal{G}_{11}^{+-}(\omega + \Omega) - \mathcal{G}_{11}^{+-}(\omega - \Omega) \right] \Big\} .
\end{aligned}
$$

The final result we obtain for the symmetrized current noise to second order in the tunneling amplitudes reads

$$
\begin{aligned}
S_{\text{sym}}^{(2)}(\omega, t') = 2\pi \rho_0^2 e^2 \Big\{ & t_0^2 \sigma^+(\omega, V) \\
& + \langle \hat{x}(t') \rangle t_0 t_1 \cos(\eta) \left[\sigma^+(\omega, V) + \frac{1}{2} \left(\sigma^+(\omega + \Omega, V) + \sigma^+(\omega - \Omega, V) \right) \right] \\
& - \langle \hat{x}(t') \rangle t_0 t_1 i \sin(\eta) \left[\sigma^-(\omega, V) - \frac{1}{2} \left(\sigma^-(\omega + \Omega, V) + \sigma^-(\omega - \Omega, V) \right) \right] \\
& - \langle \hat{p}(t') \rangle \frac{t_0 t_1}{2m\Omega} \sin(\eta) \left[\sigma^-(\omega + \Omega, V) - \sigma^-(\omega - \Omega, V) \right] \\
& - \langle \hat{p}(t') \rangle \frac{t_0 t_1}{2m\Omega} i \cos(\eta) \left[\sigma^+(\omega + \Omega, V) - \sigma^+(\omega - \Omega, V) \right] \\
& + \langle \hat{x}(t') \hat{x}(t') \rangle \frac{t_1^2}{2} \left[\sigma^+(\omega + \Omega, V) + \sigma^+(\omega - \Omega, V) \right] - \frac{t_1^2}{2m} \\
& - \langle \{ \hat{x}(t'), \hat{p}(t') \} \rangle \frac{i\, t_1^2}{4m\Omega} \left[\sigma^+(\omega + \Omega, V) - \sigma^+(\omega - \Omega, V) \right] \Big\}, \quad (3.15)
\end{aligned}
$$

where we separated the real and imaginary part using the relative phase η between the tunneling amplitudes.

We want to note the important aspect of the current noise that it possibly can have a complex valued character which we discuss later. The gained expression is quite lengthy but provides us with the full quantum mechanical non-equilibrium characteristics of the current noise in the Markovian as well as in the non-Markovian regime. We made no assumptions on the state of the oscillator, which now gives us the possibility to identify momentum properties of the nanomechanical resonator using the current noise spectrum $S_{\text{sym}}^{(2)}(\omega, t')$. In the next section, we discuss this new possibility of a *p*-detector which involves measuring a complex valued current noise.

Complex current noise and the p-detector in the non-stationary case

The expression in Eq. (3.15) allows for a comparison with results obtained in Ref. [Doiron08] where it was possible with a phase of $\eta = \pi/2$ to determine the momentum of the oscillator. In Ref. [Doiron08], an Aharonov-Bohm setup allows for the tuning of the relative phase η. The full current noise spectrum there is proportional to the position spectrum $S_x(\omega)$ which is peaked at $\omega = \pm\Omega$ in the case of $\eta = 0$ and in the case of $\eta = \pi/2$ is proportional to the momentum spectrum $S_p(\omega)$ also showing peaks at $\omega = \pm\Omega$. This peaked structure of the current noise spectrum is a fourth order effect, as we will see and discuss later when dealing with the fourth order corrections to the current noise.

As one can see from Eq. (3.15), already the second order current noise allows to determine the expectation value of the oscillator's momentum and in addition to that of the anticommutator $\{\hat{x}, \hat{p}\}$, even if the phase $\eta = 0$, i.e., the Aharonov-Bohm setup becomes obsolete in our case. The signature of the oscillator's momentum $\hat{p}$ in our case is however different than the one in Ref. [Doiron08]. Instead of the peaked structure, we find a kink-like structure which stems from the fact that we deal with second order perturbation theory.

In order to understand how one can use this to identify the momentum, we have to understand the meaning of a complex current noise. As stated in Ref. [Dicarlo06] a complex valued current noise is in principle a measurable quantity. To have a relevant measurable quantity, we would have to average the time-dependent current noise $S_{\text{sym}}^{(2)}(\omega, t')$ over the measurement time ΔT. We could do this in the following way

$$\bar{S}_{\text{sym}}^{(2)}(\omega) = \frac{1}{\Delta T} \int_{-\Delta T/2}^{\Delta T/2} dt' S_{\text{sym}}^{(2)}(\omega, t') . \tag{3.16}$$

Since the time dependence of the current noise is only visible in the expectation values of the oscillator's variables, it is important for the actual measurement to consider the time scales which are involved. If the measurement time ΔT is less than the time scale of the oscillator $(1/\Omega)$, the measured time averaged current noise $\bar{S}_{\text{sym}}^{(2)}(\omega)$ will be time-dependent. If however, the oscillator undergoes multiple oscillation cycles during the measurement time, the current noise will be time-independent. In this case we could as well take the oscillator to be in a stationary state. For a damped oscillator the time scales on which the damping happens have also to be taken into account as mentioned already in Sec. 3.1.

Let us briefly discuss the involved time scales for the experiment in Ref. [Flowers-Jacobs07]. The oscillator with a quality factor of $Q_0 \approx 5000$ at frequency $\Omega \approx 60\,\text{MHz}$ has a typical relaxation time scale of $\tau_{\text{osc}} \approx 100\,\mu\text{s}$. For low temperatures the quasiparticle relaxation rate of the fermionic reservoirs can be estimated by usual Fermi-Liquid theory $(1/\tau_{\text{res}} \sim T^2)$ [Nozieres64] which leads for $250\,\text{mK}$ used in the experiment to a relaxation time scale τ_{res} of order μs. Hence, $\tau_{\text{res}} \ll \tau_{\text{osc}}$ in Ref. [Flowers-Jacobs07]. Furthermore, the detector in Ref. [Flowers-Jacobs07] has a high enough resolution of measuring displacements on time scales less than $10\,\text{ns}$ in order to dissolve the dynamics of a non-stationary oscillator.

We conclude with remarks on the interesting non-stationary case, where we can also take $\eta = 0$ without losing the information on $\langle \hat{p}(t') \rangle$ and in addition obtain information on $\langle \{\hat{x}(t'), \hat{p}(t')\} \rangle$. We intend to give an idea of how to access the information on $\langle \hat{p}(t') \rangle$ and $\langle \{\hat{x}(t'), \hat{p}(t')\} \rangle$ available through the complex current noise. The expectation value of $\langle \hat{p}(t') \rangle$

with respect to number states or a linear combination of them, will always vanish when averaging over time according to Eq. (3.16). However, this is different for coherent states $|\alpha\rangle = \exp(-|\alpha|^2/2) \sum_{n=0}^{\infty} \alpha^n/n!|n\rangle$, where we can write $\alpha = |\alpha| \exp(i\,\delta)$ with $|\alpha|$ being the amplitude and δ the phase of the coherent state, respectively. The time averaged expectation value $\langle \hat{p}(t') \rangle$ with respect to $|\alpha\rangle$ yields

$$\langle \hat{p}(t') \rangle_{av} = \sqrt{2m\Omega} \frac{2|\alpha|}{\Omega \Delta T} \sin(\delta) \sin(\Omega \Delta T/2)\,,$$

and for $\langle \{\hat{x}(t'), \hat{p}(t')\} \rangle$

$$\langle \{\hat{x}(t'), \hat{p}(t')\} \rangle_{av} = \frac{2|\alpha|^2}{\Omega \Delta T} \sin(2\delta) \sin(\Omega \Delta T)\,.$$

For short measurement times $\Delta T < 1/\Omega$ we can write

$$\lim_{\Delta T \to 0} \langle \hat{p}(t') \rangle_{av} = \sqrt{2m\Omega}|\alpha| \sin(\delta)\,,$$

and

$$\lim_{\Delta T \to 0} \langle \{\hat{x}(t'), \hat{p}(t')\} \rangle_{av} = 2|\alpha|^2 \sin(2\delta)\,.$$

We separate the current noise $\bar{S}_{\mathrm{sym}}^{(2)}(\omega) = \bar{S}_{\mathrm{sym},R}^{(2)}(\omega) + \bar{S}_{\mathrm{sym},I}^{(2)}(\omega)$ into real and imaginary part where we observe that the imaginary part $\bar{S}_{\mathrm{sym},I}^{(2)}(\omega)$ only contains information on the oscillator's momentum $\langle \hat{p}(t') \rangle$ and the anticommutator $\langle \{\hat{x}(t'), \hat{p}(t')\} \rangle$

$$\begin{aligned}
\bar{S}_{\mathrm{sym},I}^{(2)}(\omega) = 2\pi\rho_0^2 e^2 \Big\{ & \\
& \frac{1}{\sqrt{2m\Omega}} t_0 t_1 |\alpha| \sin(\delta) \left[\sigma^+(\omega+\Omega, V) - \sigma^+(\omega-\Omega, V) \right] \\
& - \frac{t_1^2 |\alpha|^2}{2m\Omega} \sin(2\delta) \left[\sigma^+(\omega+\Omega, V) - \sigma^+(\omega-\Omega, V) \right] \Big\}\,.
\end{aligned} \tag{3.17}$$

The phase δ of the coherent state now allows for a determination of the oscillator's momentum. For $\delta = \pi/2$, the signature in the imaginary part of the time averaged noise $\bar{S}_{\mathrm{sym},I}^{(2)}(\omega)$ stems only from the oscillator's momentum. The signal in the non-Markovian regime is more pronounced than in the Markovian regime, see Eq. (3.17).

Current noise in the stationary case

Contrary to the non-stationary case, we now also assume time translation invariance in the oscillator correlation function, i.e., $D(t, t') = D(t - t')$. One can then see that the calculation in the stationary case goes along the same lines as in the non-stationary case. The only difference will be that oscillator expectation values are now taken at time $t' = 0$, i.e., we encounter for instance $\langle \hat{x}(0) \rangle$ instead of $\langle \hat{x}(t') \rangle$.

When interpreting the result for the stationary case we have to keep the constraints on oscillator expectation values in mind. These constraints lead to vanishing expectation

values of the anticommutator $\langle \{\hat{x}, \hat{p}\} \rangle$ and vanishing expectation values for $\langle \hat{x} \rangle$ and $\langle \hat{p} \rangle$. The current noise to second order is then equivalent to the ones previously obtained in Refs. [Wabnig07, Schmidt10], cf. Eq. (C.4) in Ref. [Schmidt10] with $\gamma_2 = \langle x \rangle = \langle p \rangle = 0$.

3.2.2 Current noise to fourth order in the tunneling amplitudes

We now turn to the investigation of the fourth order current noise. Since the fourth order perturbation theory involves a large amount of terms we use a diagrammatic approach. In the case of the fourth order current noise we restrict ourselves to the stationary case for simplicity. We start with giving the whole expression for the current noise to fourth order in the tunneling amplitudes

$$
\begin{aligned}
S^{(4)}(\tau_3, \tau_4) = -\frac{e^2}{2} \int_c d\tau_1 \, d\tau_2 \; \Big\{ \\
\mathcal{M}_{0,0,0,0}(\tau_1, \tau_2, \tau_3, \tau_4) \\
+ \mathcal{M}_{0,0,0,1}(\tau_1, \tau_2, \tau_3, \tau_4) \langle \hat{x}(\tau_4) \rangle + \mathcal{M}_{0,0,1,0}(\tau_1, \tau_2, \tau_3, \tau_4) \langle \hat{x}(\tau_3) \rangle \\
+ \mathcal{M}_{0,1,0,0}(\tau_1, \tau_2, \tau_3, \tau_4) \langle \hat{x}(\tau_2) \rangle + \mathcal{M}_{1,0,0,0}(\tau_1, \tau_2, \tau_3, \tau_4) \langle \hat{x}(\tau_1) \rangle \\
+ \mathcal{M}_{0,0,1,1}(\tau_1, \tau_2, \tau_3, \tau_4) \langle T_c \, \hat{x}(\tau_3)\hat{x}(\tau_4) \rangle + \mathcal{M}_{0,1,0,1}(\tau_1, \tau_2, \tau_3, \tau_4) \langle T_c \, \hat{x}(\tau_2)\hat{x}(\tau_4) \rangle \\
+ \mathcal{M}_{0,1,1,0}(\tau_1, \tau_2, \tau_3, \tau_4) \langle T_c \, \hat{x}(\tau_2)\hat{x}(\tau_3) \rangle + \mathcal{M}_{1,0,0,1}(\tau_1, \tau_2, \tau_3, \tau_4) \langle T_c \, \hat{x}(\tau_1)\hat{x}(\tau_4) \rangle \\
+ \mathcal{M}_{1,0,1,0}(\tau_1, \tau_2, \tau_3, \tau_4) \langle T_c \, \hat{x}(\tau_1)\hat{x}(\tau_3) \rangle + \mathcal{M}_{1,1,0,0}(\tau_1, \tau_2, \tau_3, \tau_4) \langle T_c \, \hat{x}(\tau_1)\hat{x}(\tau_2) \rangle \\
+ \mathcal{M}_{0,1,1,1}(\tau_1, \tau_2, \tau_3, \tau_4) \langle T_c \, \hat{x}(\tau_2)\hat{x}(\tau_3)\hat{x}(\tau_4) \rangle + \mathcal{M}_{1,0,1,1}(\tau_1, \tau_2, \tau_3, \tau_4) \langle T_c \, \hat{x}(\tau_1)\hat{x}(\tau_3)\hat{x}(\tau_4) \rangle \\
+ \mathcal{M}_{1,1,0,1}(\tau_1, \tau_2, \tau_3, \tau_4) \langle T_c \, \hat{x}(\tau_1)\hat{x}(\tau_2)\hat{x}(\tau_4) \rangle + \mathcal{M}_{1,1,1,0}(\tau_1, \tau_2, \tau_3, \tau_4) \langle T_c \, \hat{x}(\tau_1)\hat{x}(\tau_2)\hat{x}(\tau_3) \rangle \\
+ \mathcal{M}_{1,1,1,1}(\tau_1, \tau_2, \tau_3, \tau_4) \langle T_c \, \hat{x}(\tau_1)\hat{x}(\tau_2)\hat{x}(\tau_3)\hat{x}(\tau_4) \rangle \Big\} \\
+ \int_c d\tau_1 \, d\tau_2 \left\langle T_c \, \hat{H}_{\text{tun}}(\tau_1)\hat{I}(\tau_3) \right\rangle \left\langle T_c \hat{H}_{\text{tun}}(\tau_2)\hat{I}(\tau_4) \right\rangle ,
\end{aligned}
\tag{3.18}
$$

where the we introduced

$$
\begin{aligned}
\mathcal{M}_{i_1,i_2,i_3,i_4}(\tau_1, \tau_2, \tau_3, \tau_4) &= \left\langle T_c \, \hat{h}_{i_1}(\tau_1)\hat{h}_{i_2}(\tau_2)\hat{j}_{i_3}(\tau_3)\hat{j}_{i_4}(\tau_4) \right\rangle \\
&= \left\langle T_c \, \hat{\mathcal{T}}_{i_1}^\dagger(\tau_1)\hat{\mathcal{T}}_{i_2}(\tau_2)\hat{\mathcal{T}}_{i_3}(\tau_3)\hat{\mathcal{T}}_{i_4}^\dagger(\tau_4) + (3 \leftrightarrow 4) - (2 \leftrightarrow 4) + \text{H.c.} \right\rangle .
\end{aligned}
\tag{3.19}
$$

The index i_j determines whether we are dealing with the complex tunneling amplitudes β_0 or β_1, $i_j \in \{0, 1\}$

A first reduction of terms in Eq. (3.18) is done by only focusing on the stationary case. This allows us to drop terms which are proportional to $\langle \hat{x}(t) \rangle$ in Eq. (3.18) and only keep terms proportional to $D(t, t')$ and $D(t, t') \, D(t'', t''')$. Unlinked diagrams which appear in this expression are canceled by the $\hat{I}^2$ term which is always of the bubble type.

In what follows we give a short explanation of the diagrammatics. It is only necessary to evaluate the first expectation value in Eq. (3.19) using Wick's theorem, the other ones follow

as indicated by $(3 \leftrightarrow 4)$, $(2 \leftrightarrow 4)$ and hermitian conjugation. This first term leads to

$$
\left\langle T_c \, \hat{\mathcal{T}}_{i_1}^\dagger(\tau_1)\hat{\mathcal{T}}_{i_2}(\tau_2)\hat{\mathcal{T}}_{i_3}(\tau_3)\hat{\mathcal{T}}_{i_4}^\dagger(\tau_4) \right\rangle = \beta_{i_1}^* \beta_{i_2} \beta_{i_3} \beta_{i_4}^* \tag{3.20}
$$
$$
\times \left[G_l(\tau_1, \tau_2)G_l(\tau_4, \tau_3) - G_l(\tau_1, \tau_3)G_l(\tau_4, \tau_2) \right] \left[G_r(\tau_2, \tau_1)G_r(\tau_3, \tau_4) - G_r(\tau_3, \tau_1)G_r(\tau_2, \tau_4) \right] .
$$

Similar to Ref. [Wabnig07] we use a diagrammatic representation for the expression in Eq. (3.19). As an example, we show the diagrams emerging from the expression in Eq. (3.20) in Fig. 3.2 and explain the components of the diagrams. Fermionic Green's functions of the reservoirs are represented by solid lines and vertices are depicted by a dot, labeled with a time variable and a Keldysh index indicating on which branch of the Keldysh contour the time lies. An integration over internal times τ_1 and τ_2 is implicit. In addition, we also have to sum over the two internal Keldysh indices k and l. We recognize that we have to deal
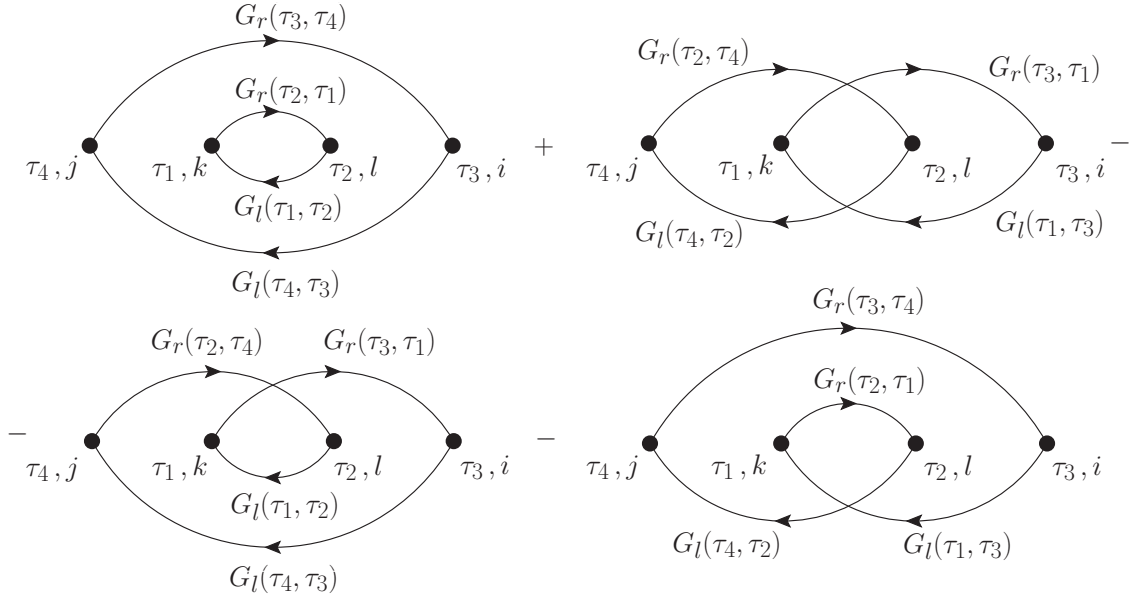

Figure 3.2: Diagrammatic representation for Eq. (3.20) where we omitted the factor $\beta_{i_1}^* \beta_{i_2} \beta_{i_3} \beta_{i_4}^*$, note that Eq. (3.20) only contains fermionic Green's functions. Every vertex (black dots) comes with a contour time τ_i and a Keldysh index indicating the branch of the contour. Integration (summation) over internal times (Keldysh indices) is implicit.

with two types of diagrams: diagrams which consist of one closed fermion loop (diagrams in the lower panel of Fig. 3.2) and diagrams consisting of two closed fermion loops/bubbles (diagrams in the upper panel of Fig. 3.2). These two different types of diagrams give very different contributions to the current noise which we will discuss below. We include the oscillator correlation function $D(t, t')$ in diagrams by a wiggly line connecting two vertices. In Fig. 3.3, we give an example of diagrams in frequency space containing one oscillator correlation function. Here, integration over the two internal frequencies ω_1 and ω_2 as well as summation over the internal Keldysh indices k and l is implied. In frequency space, the difference between the closed loop diagrams in Fig. 3.3(b) and the bubble diagrams in Fig. 3.3(a) becomes clear: for the closed loop diagrams, the oscillator line always appears

under integration of an internal frequency, whereas for the bubble diagrams, there is no integration over the oscillator line. This is the reason for the different kind of contribution to the current noise of closed loop and bubble diagrams. As we will show below, bubble diagrams lead to peaks in the current noise, whereas closed loop diagrams lead to the afore mentioned kinks in the current noise. We reduce the number of diagrams by only keeping
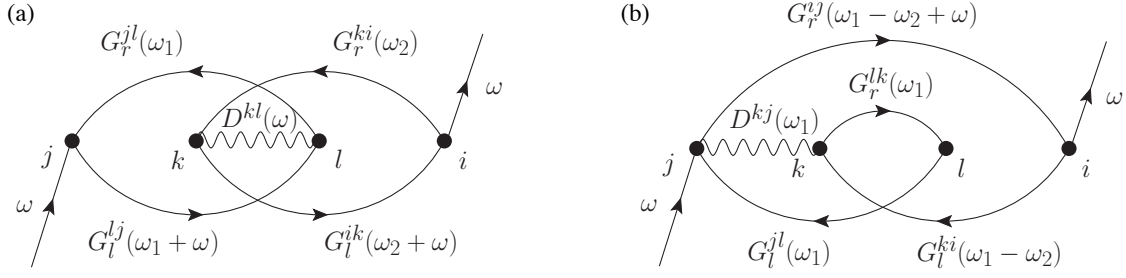
Figure 3.3: Examples of diagrams containing one oscillator correlation function D. In (a) a bubble diagram is depicted where the oscillator line is independent of an internal frequency. In (b) we show a closed loop diagram where the oscillator line always appears under integration of an internal frequency.

contributions $\sim t_0^2 t_1^2$ and $\sim t_1^4$ which are the only finite contributions in the stationary case. This allows us to write the current noise $S^{(4)}(\tau_3, \tau_4)$ for the further analysis as

$$S^{(4)}(\tau_3, \tau_4) = \hat{S}_D^{(4)}(\tau_3, \tau_4) + \check{S}_D^{(4)}(\tau_3, \tau_4) + \hat{S}_{DD}^{(4)}(\tau_3, \tau_4) + \check{S}_{DD}^{(4)}(\tau_3, \tau_4),$$

where $\hat{S}$ includes the bubble diagrams, $\check{S}$ includes closed loop diagrams and D indicates the number of oscillator lines in the diagrams. The final result we obtain is valid for an arbitrary relative phase η which goes beyond the result obtained by Wabnig et al. in Ref. [Wabnig07]. This fact allows us to study the p-detector in fourth order perturbation theory.

Results for $\hat{S}_D^{(4)}(\tau_3, \tau_4)$, $\check{S}_D^{(4)}(\tau_3, \tau_4)$, $\hat{S}_{DD}^{(4)}(\tau_3, \tau_4)$, and $\check{S}_{DD}^{(4)}(\tau_3, \tau_4)$

In the following, we sum up the different types of diagrams, bubble type diagrams as well as closed loop diagrams, both then can be integrated exactly.

First we consider all diagrams containing only one oscillator line, these diagrams are all proportional to $t_0^2 t_1^2$ and depend on η. We find for the symmetrized frequency-dependent current noise

$$\hat{S}_{\text{sym},D}^{(4)}(\omega) = 4\pi^2 e^2 \rho_0^4 \, t_0^2 t_1^2 \left\{ \vphantom{\frac{Q}{S}} \right.$$

$$\cos(\eta)^2 \left[4e^2V^2 - 4eV\sigma^-(\omega, V) \frac{Q(\omega)}{S_x(\omega)} \right] S_x(\omega) + \sin(\eta)^2 \left[\omega^2 - 2\omega\sigma^+(\omega, V) \frac{Q(\omega)}{S_x(\omega)} \right] S_x(\omega)$$

$$+ \frac{1}{2} \left[D^R(\omega) + D^A(\omega) \right] \cos(\eta)\sin(\eta) \left[4eV\sigma^+(\omega, V) - 2\omega\sigma^-(\omega, V) \right] \right\}, \tag{3.21}$$

which is one of the main results of this section.

In the case of the closed loop diagrams containing one oscillator line, it is also possible to sum up all diagrams and integrate them exactly. Since the expression for $\check{S}_{\text{sym},D}^{(4)}(\omega)$ is rather lengthy, we do not present it here.

We find that the current noise signature of $\check{S}_{\text{sym},D}^{(4)}(\omega)$ is of the kink-like structure similar to $S_{\text{sym},D}^{(2)}(\omega)$. In addition to the kinks at $|\omega| = |V \pm \Omega|$ coming from $S_{\text{sym},D}^{(2)}(\omega)$, $\check{S}_{\text{sym},D}^{(4)}(\omega)$ gives rise to extra kinks at $|\omega| = |V|$ and $|\omega| = |\Omega|$. However, these contributions are only minor modifications to the current noise floor $S_{\text{sym},D}^{(2)}(\omega)$. Experiments as in Ref. [Flowers-Jacobs07] focus on the current noise near the resonance frequency $\omega \approx \Omega$ for which $\hat{S}_{\text{sym},D}^{(4)}(\omega)$ is the most important contribution. Therefore, the discussion of our result will focus on the contributions stemming from $\hat{S}_{\text{sym},D}^{(4)}(\omega)$. These contributions posses a peaked structure, since the oscillator correlation functions $D^{R/A}(\omega)$ and the spectrum $S_x(\omega)$ are peaked around $\omega = \pm\Omega$.

The other contributions to the current noise stem from diagrams containing two oscillator lines $D(t, t')$. These diagrams are all proportional to $\beta_1\beta_1^*\beta_1\beta_1^* = t_1^4$ and therefore independent of the relative phase η between t_0 and t_1. Moreover, these current noise contributions are small compared to the ones containing only one oscillator line since $t_1^4 \ll t_0^2 t_1^2$. We however are mainly interested in the possibility to detect the oscillator's momentum which depends on η, for this reasons and the fact that they are small compared to $\hat{S}_{\text{sym},D}^{(4)}(\omega)$ we do not include them in our discussion. Nevertheless, we state our result which we obtain after summing up the diagrams

$$
\begin{aligned}
\hat{S}_{DD}^{(4)ij}(\omega) = &-\frac{e^2}{2\pi} \int d\omega_1 \sum_{k,l=\pm} (kl) \Big\{ \\
&D^{kl}(\omega_1)\, D^{ij}(\omega_1 + \omega)\, \bar{\mathcal{G}}_{11}^{kj}(-\omega_1)\, \bar{\mathcal{G}}_{11}^{li}(\omega_1) \\
&+ D^{ki}(\omega_1)\, D^{lj}(\omega_1 + \omega)\, \bar{\mathcal{G}}_{11}^{kj}(-\omega_1)\, \bar{\mathcal{G}}_{11}^{li}(-\omega_1 - \omega) \\
&- D^{ki}(\omega_1)\, D^{lj}(-\omega_1)\, \mathcal{G}_{11}^{kl}(-\omega_1)\, \mathcal{G}_{11}^{ij}(\omega_1 + \omega) \Big\}.
\end{aligned}
\tag{3.22}
$$

The last integration in Eq. (3.22) can be easily done since the oscillator correlation functions are peaked at $\pm\Omega$. Our result is then in accordance with the one obtained by Wabnig et al. [Wabnig07], where it is has been shown that these contributions to the current noise are peaked at $\omega = -2\Omega, 0, 2\Omega$ in contrast to the contributions arising from Eq. (3.21). Similar to $\check{S}_D^{(4)}(\omega)$, $\check{S}_{DD}^{(4)}(\omega)$ is of the kink-like structure and therefore only modifying the current noise floor.

Current noise in the Markovian and non-Markovian regime for arbitrary η

We now address the current noise stemming from $\hat{S}_{\text{sym},D}^{(4)}(\omega)$ for arbitrary η and also arbitrary system parameters. In order to compare our result for the momentum detector with

Ref. [Doiron08], we investigate $\hat{S}^{(4)}_{\mathrm{sym},D}(\omega)$ near the resonance ($\omega \approx \Omega$). We find

$$
\begin{aligned}
\hat{S}^{(4)}_{\mathrm{sym},D}(\omega) \approx 4\pi^2 e^2 \rho_0^4 \, t_0^2 t_1^2 \Bigg\{ & \\
4e^2 V^2 \cos(\eta)^2 & \left[1 - \frac{\sigma^-(\Omega,V)}{4eVm\Omega \langle \bar{x}^2 \rangle} \sqrt{1 - \left(\frac{\gamma_{\mathrm{tot}}}{\Omega} \right)^2} \right] S_x(\omega) \\
+ \frac{1}{m^2} \sin(\eta)^2 & \left[1 - \frac{2\sigma^+(\Omega,V)m}{\langle \bar{p}^2 \rangle} \sqrt{1 - \left(\frac{\gamma_{\mathrm{tot}}}{\Omega} \right)^2} \right] S_p(\omega) \\
+ \cos(\eta) \sin(\eta) \frac{1}{m} & \frac{\omega^2 - \Omega^2}{4\gamma_{\mathrm{tot}}^2 \Omega^2 + (\omega^2 - \Omega^2)^2} \left[4eV\sigma^+(\Omega,V) - 2\Omega\sigma^-(\Omega,V) \right] \Bigg\},
\end{aligned}
\tag{3.23}
$$

where $\sigma^{\pm}(\xi,V)$ is given in Eq. (3.6) and $S_x(\omega)$ and $S_p(\omega)$ near resonance are given by

$$
S_X(\omega) = \frac{2\gamma_{\mathrm{tot}}^2 \Omega^2 \left\langle \bar{X}^2 \right\rangle}{4\gamma_{\mathrm{tot}}^2 \Omega^2 + (\omega^2 - \Omega^2)^2} \, ,
$$

with $X = x, p$. The above expression is valid for the Markovian as well as for the non-Markovian regime. The relevant information about the oscillator can now be gained form the current noise spectrum.

We take two different ways of evaluating the expectation values $\langle \bar{x}^2 \rangle$ and $\langle \bar{p}^2 \rangle$. In the first one we use number-states which lead to expectation values $\langle \bar{x}^2 \rangle_n = (2n + 1)/m\Omega$ and $\langle \bar{p}^2 \rangle_n = (2n + 1) \, m\Omega$, where n denotes the oscillator's number of quanta.

Since we also could imagine, as already explained in Sec. 3.1, two equilibrium bathes to which the oscillator couples, the tunnel junction and an external heat bath, we can assign an effective temperature T_{eff} to the oscillator which obeys $\gamma_{\mathrm{tot}} T_{\mathrm{eff}} = \gamma_0 T_{\mathrm{env}} + \gamma_+ T_{\mathrm{junc}}$, where $\gamma_{\mathrm{tot}} = \gamma_0 + \gamma_+$ is the total damping due to coupling to the junction (γ_+) and an external heat bath (γ_0). The external heat bath is at temperature T_{env} and the junction's temperature is given by $T_{\mathrm{junc}} = eV/2k_B$. The oscillator's expectation values in this thermal regime are then given by $\langle \bar{x}^2 \rangle = 2 \, k_B \, T_{\mathrm{eff}}/m \, \Omega^2$ and $\langle \bar{p}^2 \rangle = 2 \, m \, k_B \, T_{\mathrm{eff}}$.

For both cases, the thermal case and the number-state one, it is convenient scaling the current noise $\hat{S}^{(4)}_{\mathrm{sym},D}(\omega)$ with $eI_0 = 2\pi\rho_0^2 e^2 t_0^2 \sigma^+(\Omega,V)$. We furthermore introduce dimensionless parameters f_1, f_2, f_3, f_4 which are defined in the following way

$$
\begin{aligned}
\gamma_{\mathrm{tot}} &= \frac{\Omega}{f_1} \, , \\
\gamma_+ &= \frac{\gamma_{\mathrm{tot}}}{f_2} = \frac{\Omega}{f_1 f_2} \, , \\
eV &= f_3 \, \Omega \, , \\
T_{\mathrm{env}} &= f_4 \frac{eV}{k_B} \, .
\end{aligned}
$$

f_1 can be interpreted as an overall quality-factor. The ratio $\gamma_0/\gamma_+ = (f_2 - 1)$ leads for

$f_2 \in]1,2[$ to a stronger coupling to the tunnel junction and for $f_2 > 2$ to a stronger coupling to the external heat bath. The parameter f_3 distinguishes the non-Markovian ($f_3 \in]0,1]$) from the Markovian regime ($f_3 \gg 1$). The last parameter f_4 quantifies the temperature T_{env} of the external bath with respect to the applied bias V.

We now compare the signal of the position detector

$$S^{(4)}_{\text{x-det}}(\omega) = \hat{S}^{(4)}_{\text{sym},D}(\omega; \eta = 0) \,,$$

to the signal of the momentum detector

$$S^{(4)}_{\text{p-det}}(\omega) = \hat{S}^{(4)}_{\text{sym},D}(\omega; \eta = \pi/2) \,,$$

and later their dependencies on the parameters f_i at resonance $\omega \approx \Omega$. Assuming a high quality resonator we take $\sqrt{1 - \gamma^2_{\text{tot}}/\Omega^2} \approx 1$ in Eq. (3.23). We call $\mathcal{Q}_x = \sigma^-(\Omega, V)/(4eVm\Omega \langle \bar{x}^2 \rangle)$ quantum corrections to the x-detector current noise, arising from the non-vanishing commutator $[\hat{x}, \hat{p}]$. Similarly we call $\mathcal{Q}_p = (2m\sigma^+(\Omega, V))/\langle \bar{p}^2 \rangle$ quantum corrections to the p-detector current noise. We then find

$$S^{(4)}_{\text{x-det}} = 4 \, f_3^2 \, \frac{[1 - \mathcal{Q}_x]}{[1 - \mathcal{Q}_p]} \, S^{(4)}_{\text{p-det}}$$

and conclude that in the Markovian regime where $f_3 \gg 1$ the signal of the position detector is always larger than the signal of the momentum detector. Whereas in the non-Markovian regime we have a stronger signature of the noise part showing the momentum signature of the oscillator. In the following, we investigate in more detail the current noise of the x- and p-detector.
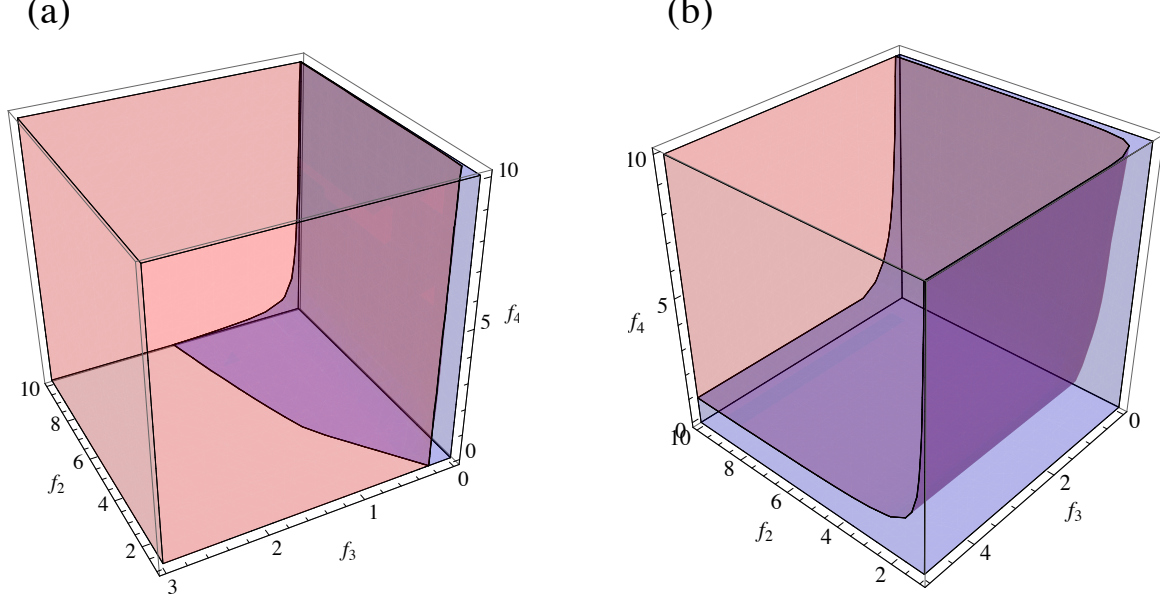
The x-detector

From Eq. (3.23) one can see that for $\eta = 0 \mod \pi$ we recover the position detector results of Refs. [Doiron07, Clerk04b, Wabnig07] with peaks in the current noise spectrum at $\omega = \pm\Omega$. Since we calculate the symmetrized current-current correlator, the current noise is symmetric in ω. The sign of the signal is given by the sign of $[1 - \mathcal{Q}_x]$ which for an oscillator in the thermal regime depends on f_2, f_3 and f_4, while for an oscillator in number-state n it depends on n and f_3 only. We stick to a thermal resonator, noting that as in Ref. [Doiron08] for the p-detector, here the quantum corrections $\mathcal{Q}_x \sim 1/f_3$ can become large (compared to 1) in the non-Markovian regime where $f_3 < 1$, leading to a sign change. The parameter regimes for a negative/positive peak in the current noise are depicted in Fig. 3.4(a) as blue/red regions.

The change of sign in the signal, depends on the environment temperature $f_4 \sim T_{\text{env}}$, the coupling to the environments f_2 and heavily on the bias voltage and therefore f_3. Deep in the Markovian regime, the sign change is hard to achieve, only if f_2 is very large and the bath temperature T_{env} is very low, meaning that heating of the oscillator can be compensated by strongly coupling to a cold environment. In the non-Markovian regime, the quantum corrections $\mathcal{Q}_x$ can become large more easily and due to the lower signal in the non-Markovian regime for the x-detector, the sign change is more pronounced.

Figures 3.5(a) and 3.5(b) show the current noise spectrum around $\omega \approx \Omega$ in the Markovian

and the non-Markovian regime for different couplings and environment temperatures.

(a)

(b)

Figure 3.4: The sign of the current noise peak at $\omega \approx \Omega$ for the x-detector (a) and of the p-detector (b) as a function of f_2, f_3, f_4, where we took $f_1 \to \infty$. Compared to the x-detector the sign change is possible for a wider range of parameters f_2, f_3, f_4. Here, blue/red denotes a negative/positive peak in the current noise.

(a)

(b)
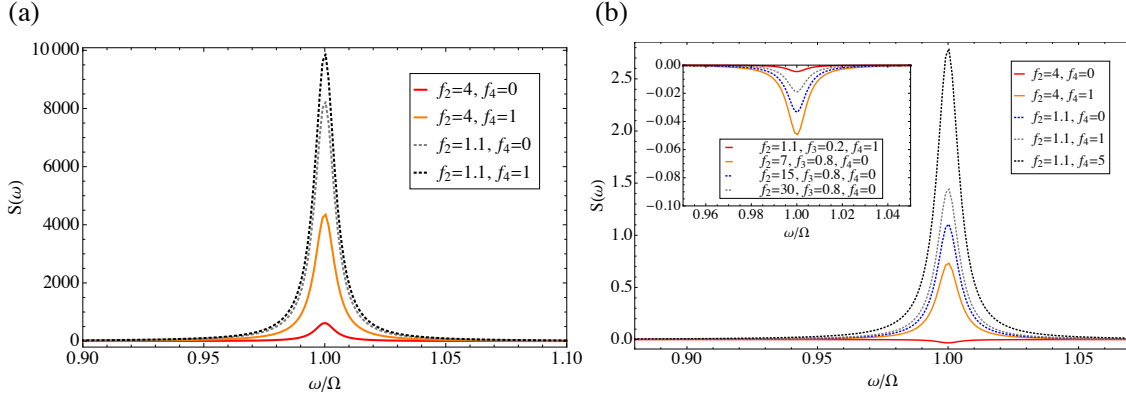
Figure 3.5: Current noise signal at $\omega = \Omega$ in the Markovian regime (a) for different values of f_2 and f_4 with $f_1 = 200$ and $f_3 = 50$. The current noise shows a peak due to the presence of the oscillator. In (b), the x-detector current noise signal in the non-Markovian regime for different values of f_2 and f_4 with $f_1 = 200$ and $f_3 = 0.8$ is shown. We note that here the signal is weaker than in the Markovian regime (a). In (b) however, it is possible to see a change of sign of the signal, depending on the parameters f_2, f_4. The inset in (b) illustrates this sign change. The noise is scaled by $2\pi\rho_0^2 e^2 t_0^2 \sigma^+(\Omega, V)$.

The p-detector

For the cases $\eta = \pi/2 \mod \pi$ in Eq. (3.23), the results of the momentum detector as stated in Ref. [Doiron08] are extended to the non-Markovian regime. Due to the fact that the quantum corrections $\mathcal{Q}_p$ are in the first place larger than $\mathcal{Q}_x$, the peak in the current noise spectrum stemming from the oscillator has a negative sign for $\eta = \pi/2$. However, it is also possible to change the sign by adjusting the parameters f_2, f_3, f_4 on which $\mathcal{Q}_p$ depends. In Fig. 3.4(b) we depict the regions with a negative sign blue and the ones with a positive sign red. Changing the sign of the current noise signal in the p-detector case is easier to achieve over a wide range of parameters, as compared to the x-detector, even deep in the Markovian regime ($f_3 \gg 1$). Figure 3.6 shows a summary of the p-detector current noise in the Markovian and non-Markovian regime for different parameters f_2, f_4, respectively.
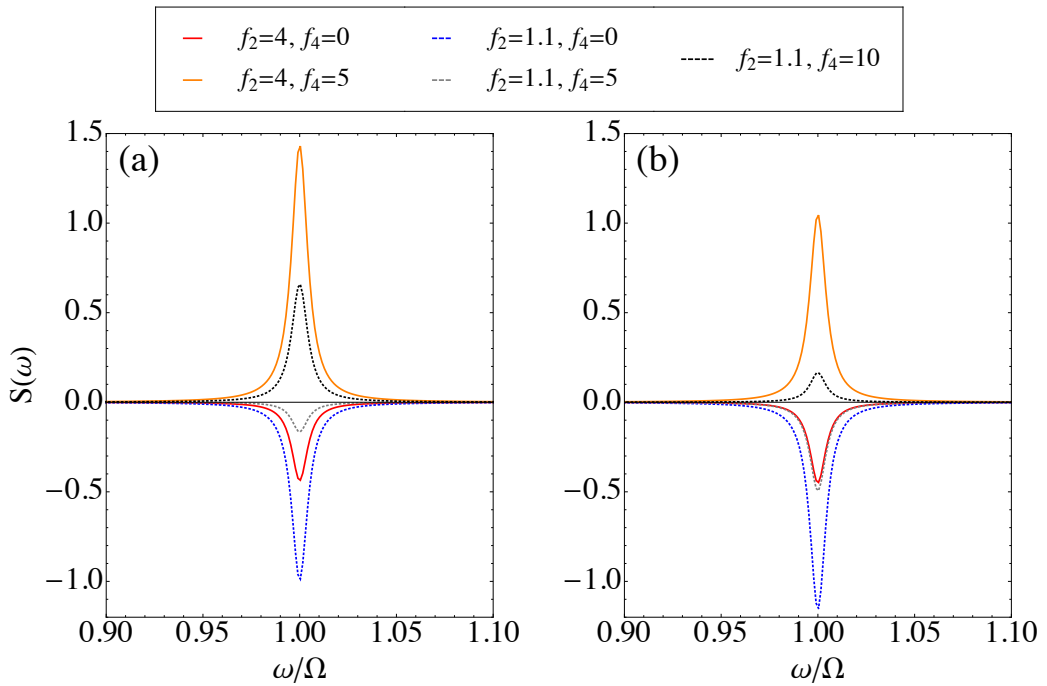
Figure 3.6: (a) p-detector current noise in the Markovian regime ($f_3 = 50$) for various parameters f_2, f_4 and $f_1 = 200$. (b) Current noise in the non-Markovian regime ($f_3 = 0.8$) for various parameters f_2, f_4. In both cases we can easily achieve a sign change in the signal. The noise is scaled by $2\pi \rho_0^2 e^2 t_0^2 \sigma^+(\Omega, V)$.

Detection of number states

With the expression for the current noise and definitions above it is possible to determine the occupation number of the oscillator, in a similar fashion to Ref. [Wabnig07]. Equation (3.23) for the current noise contains position and momentum expectation values of the oscillator which can be evaluated using (i) number states and (ii) a thermal state. In the case of number states the gained expression depends on n, the average number of quanta on the oscillator whereas in the case of a thermal state, it depends on the experimentally adjustable

parameters f_i. Arguing that the current noise signal is the same if $\langle X \rangle_n = \langle X \rangle_{th}$, leads to the following dependance of n on the parameters f_i

$$n = \frac{2f_2|f_3|f_4 - 2|f_3|f_4 - f_2 + |f_3|}{2f_2} \, . \tag{3.24}$$

The dependence of n on the adjustable parameters is depicted in Fig. 3.7, where for specific values of f_3 and f_4, which can be experimentally adjusted, and fixed values of f_1 and f_2, the contour lines show the corresponding number state. In principle, this can serve as a guidance for experimentalist to put the oscillator in a given state with a mean phonon occupation number n. By a later noise measurement it could be verified whether the data is consistent with this specific number state. Moreover, we can in principle fully determine the state of
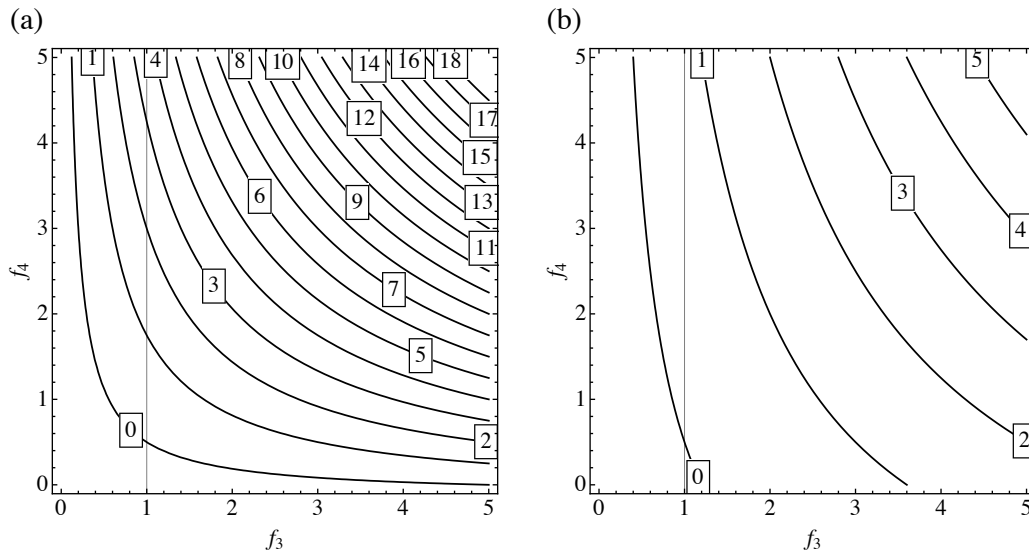
Figure 3.7: Number of quanta n on the oscillator in dependence of experimentally adjustable parameters, for dominant coupling to the external heat bath (a) with $f_2 = 5$ and dominant coupling to the tunnel junction (b) with $f_2 = 1.2$.

the oscillator via its covariance matrix σ by two noise measurements (one with $\eta = 0$ and one where $\eta = \pi/2$) which adds a second possibility to verify whether Eg. (3.24) serves as a good guide. Figure 3.7 shows that in the Markovian regime the oscillator is only in its ground state for low environmental temperatures, since the applied bias voltage is heating the oscillator. In the non-Markovian regime, we can have a higher environmental temperature for the oscillator being in its ground state.

3.3 Concluding remarks

We have studied the finite frequency current noise of a tunnel junction coupled to a harmonic oscillator. Here, we go beyond the Born approximation (because we calculate the noise up to fourth order in the tunneling amplitude) and beyond the Markov approximation (because we do not restrict ourselves to the regime $eV/\hbar\Omega \gg 1$). For a non-stationary oscillator, we have

shown that the finite frequency current noise of the detector can be complex. This complex current noise can be used to obtain information about expectation values depending on $\hat{x}$ as well as expectation values depending on $\hat{p}$. The former we call x-detector signal and the latter p-detector signal.

For the stationary oscillator, the finite frequency current noise is always real. Then, it is more complicated to get momentum information using a tunnel junction detector. An Aharonov-Bohm-loop setup is needed for this task. We analyze such a setup in the non-Markovian regime and thereby show how the x- and the p-signal can be used to determine the quantum state of the oscillator.

Our analysis is an essential prerequisite to study how the quantum entanglement of NEMS [Eisert04] can be measured on the basis of tunnel junction detectors.

Chapter 4

Nanomechanics and new states of matter

In this chapter of the thesis, we will focus on the aspect of nanomechanical systems being exceptional detection devices. Our aim is to propose a realistic setup which can be used as a detection scheme for new states of matter, namely Majorana bound states. Majorana fermions are among the most intriguing features of topological states of matter with prospect applications for topological quantum computation. However, they are also interesting on their own right because these particles behave as being their own antiparticle. We propose a nanomechanical detection scheme for Majorana bound states which have been predicted to exist at the edges of a one-dimensional topological superconductor. Before we start discussing the actual setup, we introduce the reader to some basic properties of Majorana fermions and their emergence in condensed matter systems on a very fundamental and easy to grasp level.

## 4.1 Basics on Majorana fermions and their potential use for quantum computation

Majorana fermions

In this section, we want to introduce the Majorana fermion by characterizing it in a more informal way. In the following section, we want to give a more formal introduction by briefly reviewing what is called Kitaev's one-dimensional toy model of a spinless p-wave superconductor where we see without much mathematics the emergence of Majorana states.

The relativistic description of quantum mechanics for spin-$1/2$ particles was introduced in 1928 by Paul Dirac [Dirac28]. The solutions to the Dirac equation are complex fermions where, for instance, c corresponds to the particle solution and $c^\dagger$ to the antiparticle solution. The particle and antiparticle solution obey fermionic statistics, i.e., we get a sign change when interchanging two fermions which manifests itself in the anticommutation relation $\{c_i, c_j^\dagger\} = \delta_{ij}$. In 1937, Ettore Majorana found a solution to the Dirac equation which is real [Majorana37], i.e., the particle solution equals the antiparticle solution $\gamma = \gamma^\dagger$, in contrast to the solutions of the Dirac equation where $c \neq c^\dagger$. The Majorana fermion has the anticommutation relation $\{\gamma_i, \gamma_j^\dagger\} = 2\delta_{ij}$ and in contrast to a Dirac fermion which obeys $c^2 = 0$ (due to the Pauli exclusion principle) fulfills $\gamma^2 = 1$. Due to these facts, a Majorana fermion does not have the usual fermionic statistics but it follows non-Abelian statistics which makes the Majorana fermion particularly interesting in the field of topological quantum computation [Nayak08].

Engineering Majorana bound states in a condensed matter setting

The question now is where can physicist find the Majorana fermion in nature. What particle manifests itself as its own antiparticle? Already in the early days after Majorana came up with his solution to the Dirac equation, particle physicists had the neutrino as a candidate for being a Majorana fermion, but up to date no clear evidence has been found in that direction. Other than in particle physics where the Majorana fermion would manifest itself as an elementary particle, things are different in a condensed matter setting. The only physical particles in condensed matter physics are electrons, atoms, ions, etc. In condensed matter systems, the Majorana fermion could therefore only manifest itself as an emergent quasiparticle excitation. In a condensed matter setting, a superconductor would be a natural candidate system hosting Majorana fermions because there, electrons and holes form an almost equal superposition. However, in ordinary *s*-wave superconductors, the spin degree of freedom prevents the Bogoliubov quasiparticle from being its own antiparticle. Therefore, we are looking for a superconductor where we get rid of the spin degree of freedom. In 2001, Kitaev [Kitaev01] introduce a toy model for a one-dimensional spinless *p*-wave superconductor, which can host a Majorana state. We will briefly, without too much mathematics revisit this
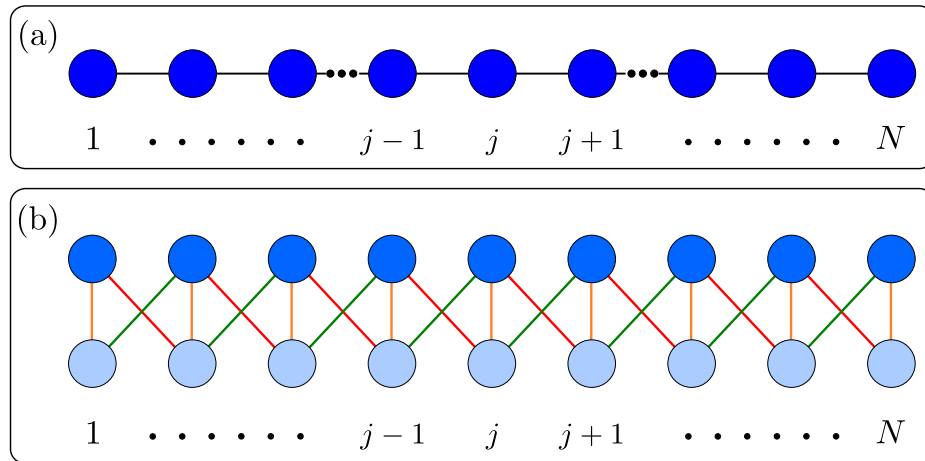
Figure 4.1: (a) Kitaev's toy model of a spinless *p*-wave superconductor. For each site j there is a fermionic annihilation (creation) operator c ($c^\dagger$). (b) Schematics of the one-dimensional chain when we apply a basis transformation using Majorana operators. Each physical site j is then represented by two Majorana operators γ_j^A (dark blue) and γ_j^B (light blue).

toy model. In Fig. 4.1(a) we show a one-dimensional chain of N sites which is governed by the Hamiltonian introduced by Kitaev

$$H = -\sum_{j=1}^{N} \mu \left[c_j^\dagger c_j - \frac{1}{2} \right] + \sum_{j=1}^{N-1} t \left[c_j^\dagger c_{j+1} + c_{j+1}^\dagger c_j \right] + \Delta \left[c_j c_{j+1} + c_{j+1}^\dagger c_j^\dagger \right],$$

where μ is the chemical potential, t is a nearest neighbor hopping parameter and Δ is the strength of the *p*-wave pairing described by the last term. For simplicity we assume t and Δ to be real and the same for each site. The operators c_j are annihilation operators for spinless electrons on site j. The main aspects of this toy model are best described by a change of

basis which is accomplished by introducing two Majorana operators on each site j

$$\gamma_j^A = c_j + c_j^\dagger,$$
$$\gamma_j^B = i(c_j - c_j^\dagger).$$

They obey the anticommutation relation $\{\gamma_i^s, \gamma_j^{s'}\} = 2\delta_{ij}\delta_{ss'}$ and we have $[\gamma_i^s]^\dagger = \gamma_i^s$. In this basis, the Hamiltonian becomes

$$H = \sum_{j=1}^{N} i\mu\gamma_j^A\gamma_j^B + \sum_{j=1}^{N-1} i(t-\Delta)\gamma_j^B\gamma_{j+1}^A - i(t+\Delta)\gamma_j^A\gamma_{j+1}^B. \tag{4.1}$$

We show in Fig. 4.1(b) a schematics of the transformed Hamiltonian, where the dark and light blue dots denote the species A and B, respectively. The colored lines in Fig. 4.1(b) match the three differently colored coupling terms in the transformed Hamiltonian Eq. (4.1). The parameters μ, t, and Δ can now be adjusted such that we will see the emergence of two separated Majorana states at each end of the one-dimensional chain. There are two limiting cases for the values of the parameters μ, t and Δ which yield us a trivial solution to the problem described by the Hamiltonian Eq. (4.1).

The first case we consider is the case $\Delta = t = 0$. In this case the green and red terms in Eq. (4.1) vanish and we see that only Majorana states at the same site j, γ_j^A and γ_j^B, pair with each other. This corresponds to a unique ground state of the problem which corresponds to the vacuum of the Dirac fermions c_j. This phase is schematically shown in Fig. 4.2(a).

For the case $\mu = 0$ and $\Delta = -t$, depicted in Fig. 4.2(b), subspecies B on site j pairs with subspecies A on site $j+1$. In this scenario we are left with two separated operators (empty dots in Fig. 4.2(b)) at the ends of the chain at site $j=1$ (subspecies A) and $j=N$ (subspecies B) which no longer appear in the Hamiltonian

$$H = 2it \sum_{j=1}^{N-1} \gamma_j^B\gamma_{j+1}^A. \tag{4.2}$$

The states γ_1^A and γ_N^B are exactly the Majorana operators we are looking for. Kitaev showed
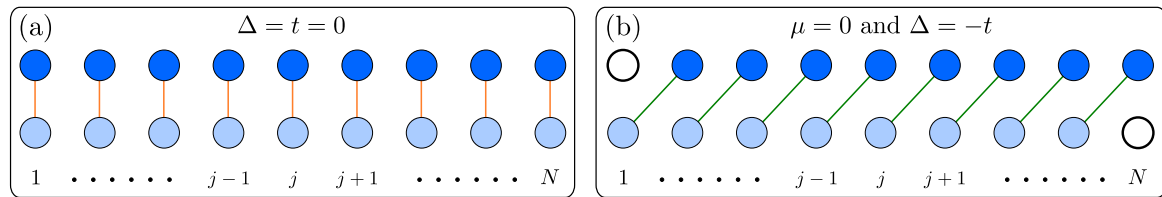
Figure 4.2: Two distinct phases of Kitaev's model where the Majorana physics becomes obvious. (a) The Majorana operators on site j pair together forming a ground state with occupation number zero. (b) Two Majorana operators each at one end of the chain (empty dots) are left unpaired.

that these end states appear as long as $|\mu| < 2t$. The two Majorana operators $\gamma_1^A \equiv \gamma_L$ and $\gamma_N^B \equiv \gamma_R$ which are absent from the Hamiltonian Eq. (4.2) can be combined to a single highly

nonlocal fermionic state f

$$f = \frac{1}{2}\left(\gamma_R - i\gamma_L\right) , \tag{4.3}$$

with $f|0\rangle = 0$ and $f^\dagger|0\rangle = |1\rangle$. With the two modes γ_L and γ_R being absent from the Hamiltonian in Eq. (4.2), zero energy is needed to occupy the nontrivial fermionic state f formed by these end states. This nonlocal fermion costs no energy and therefore it produces a two-fold degenerate ground state. It is important to note that for a general choice of parameters, i.e., $\mu \neq 0$ and $\Delta \neq t$ but still being in the phase where two unpaired Majorana states appear at each end of the chain, there is a finite overlap of the modes γ_L and γ_R. This means that the states γ_L and γ_R are no longer just described by the operators γ_1^A and γ_N^B, respectively, but they exponentially decay into the bulk of the chain. Additionally, this leads to a splitting of the degeneracy of the states $|0\rangle$ and $|1\rangle$ and the Majorana modes at the ends of the chain are no longer exact zero modes. The splitting depends on the length of the wire and is approximately given by e^{-L/ξ_0}, where L is the length of the wire and ξ_0 the coherence length of the superconductor which is a typical localization length of the Majorana bound states.

We learn from Kitaev's toy model that when we aim to search for Majorana states in superconductors, we need to get rid of the spin degree of freedom, i.e., ordinary *s*-wave superconductivity is not suitable but what we need is *p*-wave pairing which does not come about naturally in known systems. Such triplet pairing has been predicted for Sr_2RuO_4 [Murakawa04, Xia06] but has never been observed in experiments. The $\nu = 5/2$ quantum Hall state was also predicted to host Majorana quasiparticle excitations [Read00] but again no experimental evidence of their existence has been found.

In addition to that, various proposals have recently been made on how to generate Majorana states in a condensed matter setting. Fu and Kane showed that a topological insulator/*s*-wave superconductor heterostructure can induce effective *p*-wave pairing for the surface states of the topological superconductor [Fu08, Fu09b]. In such a realization, the Majorana states are bound to the vortices of the superconducting system.

A different and more promising approach was put forward by Lutchyn et. al [Lutchyn10] and Oreg et. al [Oreg10] which is crudely speaking a realization of Kitaev's one-dimensional toy model. The main ingredients to these proposal are a one-dimensional semiconducting wire with strong spin orbit coupling and an ordinary *s*-wave superconductor on which the one-dimensional wire is placed and thereby inherits superconductivity via the proximity effect. Finally, an external magnetic field has to be applied which can drive the topological superconductor into a phase where Majorana bound states emerge at each end of the wire.

Signatures of Majorana bound states

Proposed detection schemes for Majorana bound states in condensed matter systems are based on tunnel setups [Bolech07, Nilsson08, Law09, Flensberg10, Leijnse11b, Liu11b, Golub11b, Golub11a], interferometer setups [Akhmerov09, Fu09b, Fu10, Liu11a, Strübi11, Béri12], and the Josephson effect [Fu08, Fu09a, Lutchyn10, vanHeck11].

A measurement of the differential conductance through a topological superconductor should ideally yield a zero bias peak that is quantized to the value of $2e^2/h$, the robustness

of this peak can be tested against the external magnetic field which can drive the topological superconductor into a phase where the Majorana bound states are present or it can drive the topological superconductor out of this phase.

The Josephson effect in the presence of Majorana bound states would have a 4π-periodicity instead of a 2π-periodicity. For more details on the various signatures we refer the reader to reviews in Refs. [Beenakker11, Alicea12].

The signatures discussed above would just indirectly probe this quasiparticle state that merely has any properties. Beyond that the striking evidence of the presence of the Majorana bound states would of course be the verification of their non-Abelian statistics which is an intrinsic property these states carry.

Experimental evidence

Very recently, several experimental groups which were participating in the hunt for the Majorana fermion seemed to be successful and claim to have experimental evidence of the presence of Majorana bound states [Mourik12, Williams12, Deng12, Rokhinson12, Das12]. The majority of these groups reported an emergence of a zero bias peak when the parameters are such that the topological superconductor is in the phase where Majorana bound states are predicted to exist. In Ref. [Rokhinson12] the fractional Josephson effect was used as indicator for Majorana bound states. Although the experiments are a first step towards the detection of Majorana bound states, it has also been discussed lately, that the zero bias peak signature is far from being the smoking gun signature. As argued in Refs. [Bagrets12, Liu12], the emerging zero bias peak, which was used as an indicator for the Majorana bound states in most of the performed experiments, could also be due to other (disorder-induced) effects. To sum up, we can say that true qualitative experimental signatures of Majorana fermions that persist in realistic systems are rather difficult to predict and detect.

Protected Majorana bound states and topological quantum computation

Before we turn to the main subject of this chapter – the detection of Majorana bound states using a nanomechanical oscillator – we will briefly discuss the issue of topological protected quantum computation using Majorana bound states. Qubit realizations based on Majorana bound states have been considered promising candidates for quantum information processing which is inherently inert to decoherence. It is this statement that we will revisit with an open quantum system approach. [1]

Recently, proposals for topological quantum computing (TQC) with qubits based on Majorana bound states (MBS) as realized in one-dimensional (1D) topological superconductors (TSC) have attracted a lot of interest [Kitaev01, Oreg10, Alicea10, Lutchyn10, Sau10, Alicea11, Hassler10, Hassler11, Leijnse11a, Flensberg11, Martin12]. As we showed above when discussing Kitaev's model, these 1D TSC have a bulk superconducting gap and support a single subgap fermionic state f which is formed by a single delocalized pair of MBS, cf. Eq. (4.3). The two Majoranas at each end of the TSC (γ_L and γ_R) can combine to the

---

[1]This section of the thesis is built upon the published article in Ref. [Budich12].

nontrivial fermionic state f

$$\gamma_R = f^\dagger + f \,,$$
$$\gamma_L = -i \left(f^\dagger - f \right) \,.$$

This class of systems has originally been proposed and topologically classified by Kitaev [Kitaev01, Kitaev09]. The protected existence of the single pair of MBS is due to a nontrivial value of the $\mathbb{Z}_2$ invariant classifying a 1D bandstructure in the presence of particle hole symmetry [Kitaev09]. The qubit formed by the two occupation number eigenstates of the single subgap fermion f has been recently proposed as a candidate for TQC [Alicea11]. We show that while the existence of a single pair of MBS in a 1D TSC is protected, the coherence of the associated qubit is as vulnerable as that of an ordinary local fermionic subgap bound state. We first review the two general remarks in Ref. [Kitaev01] supporting the protection of this qubit against any local perturbation, a crucial prerequisite for TQC:

- Remark (*i*):
  The qubit is delocalized into the two MBS γ_L and γ_R which are spatially separated by the system length L. Since the overlap of the bound state wave function decays exponentially with the system length, direct coupling between the two MBS can be suppressed to exponential accuracy.

- Remark (*ii*):
  Fermion parity, i.e., particle number conservation modulo 2, is a good quantum number in the superconducting system. Thus, any perturbation containing a single Majorana operator is forbidden as its action would change the fermion parity of the TSC.

Now, we want to investigate whether these key observations for a closed, non-interacting TSC still hold in an open quantum system scenario which is the only realistic approach to describe an actual experimental setup for quantum information processing.

Discussion of Remark (*i*)

For a system consisting of two entangled spatially separated subsystems, the existence of states where information about the composite system can be inferred by locally coupling to one subsystem due to the mutual information of the entangled constituents, has been known for many decades. Furthermore, ground state entanglement and topological order are in close correspondence [Levin06, Kitaev06, Chen11b, Fidkowski11]. Several recent proposals [Semenoff07, Tewari08, Fu10, Bose11] related to teleportation between the two MBS could demonstrate how a local operation on one side of the system changes the system state nonlocally even in the limit $L \to \infty$ [Semenoff07, Bose11], where the direct overlap and with that the direct coupling between the end states vanishes. In this sense a vanishing direct coupling between the two MBS does not imply that the information of the qubit is split into two independent halves.

Discussion of Remark (*ii*)

The susceptibility to decoherence of any candidate system has to be investigated from an open quantum system point of view since decoherence is the elusion of coherence to a larger Hilbert space of the combined qubit-environment system. Considering only the isolated qubit system the absence of decoherence would be a trivial corollary from the unitarity of its time evolution. From this point of view the practical relevance of remark (*ii*) is not very convincing as it only pertains to the TSC representing the qubit as an isolated system. In presence of an environment which is particle number conserving or at least fermion parity conserving, the only constraint on the dynamics of the total system is the conservation of the total fermion parity. Operations like particle tunneling conserve the total fermion parity but change the parity of each subsystem, the TSC and the environment. Hence, it is not surprising that several proposals [Bolech07, Tewari08, Law09, Flensberg10, Shivamoggi10, Fu10, Golub11a, Leijnse11b, Zazunov11, Liu11b, Stanescu11, Walter11a, Bose11] use such couplings to probe the properties of MBS by tunneling based transport experiments. In the limit of a large superconducting gap, the only low energy degrees of freedom are the two degenerate ground states $|0\rangle$, $|1\rangle = f^\dagger |0\rangle$ of the wire forming the qubit. Tunneling between an electron from the environment and this subgap fermion will thus inevitably flip the information stored in the parity qubit, i.e., lead to σ_x errors. Unless any fundamental reason beyond the parity argument by Kitaev can be found that such couplings are weaker than sources of decoherence in any alternative realization of a qubit, there is no topological protection against decoherence in the MBS paradigm of a qubit to speak of. Considering these rather general arguments it is again not surprising, that recently the vulnerability of the MBS qubit to several concrete mechanisms of decoherence has been demonstrated [Goldstein11]. In addition to this the decoherence of the Majorana qubit has been put to test considering quasiparticle poisoning [Rainis12] and noisy gates [Schmidt12].

We now illustrate the fragility of the parity qubit with the help of two minimal toy models for imperfections which will be present in any realistic experimental setup for topological quantum computing with qubits based on MBS in 1D TSC. Both toy models are described by a similar Hamiltonian $H = H_{\text{env}} + H_{\text{MBS}} + H_{\text{tun}}$, with H_{env} being the Hamiltonian of the environment and $H_{\text{MBS}} = i\xi\gamma_L\gamma_R/2 = \xi f^\dagger f$ describing the overlap between MBS at the left and right edge of the 1D TSC. H_{tun} is a tunnel Hamiltonian coupling the MBS and the environment and will be specified for each toy model. Note that no orthogonality catastrophe forces H_{tun} to have a vanishing tunneling matrix element in the thermodynamic limit. This can be seen by an explicit derivation of the tunneling Hamiltonian as, for instance, done in Ref. [Flensberg10]. The toy models resemble typical physical situations which are present in the 1D TSC wire (e.g., adatoms or trapped charges nearby the MBS) or are induced from the outside to the wire (biased gates near the MBS to manipulate the MBS as, e.g., in Ref. [Alicea11]).

The first toy model schematically shown in Fig. 4.3 is a single level quantum dot tunnel coupled to the parity qubit, see also Ref. [Leijnse11b], here without the spin degree of freedom for simplicity. Such a two level system describes, e.g., a minimal model for trapped charges nearby the MBS in the wire which is allowed by symmetry, where $H_{\text{env}} = \varepsilon d^\dagger d$ and the dot

only couples to γ_R via the following tunnel Hamiltonian

$$H_{\text{tun}} = \lambda \left[d^\dagger - d \right] \gamma_R \tag{4.4}$$

with $\lambda \in \mathbb{R}$. The low energy Hamiltonian H can be conveniently written as a matrix choosing the basis $\{|00\rangle, |10\rangle, |01\rangle, |11\rangle\}$

$$H = \begin{pmatrix} 0 & 0 & 0 & \lambda \\ 0 & \varepsilon & \lambda & 0 \\ 0 & \lambda & \xi & 0 \\ \lambda & 0 & 0 & \varepsilon + \xi \end{pmatrix}$$

with $|n_{\text{dot}} \, n_f\rangle$ and $n_{\text{dot},f} \in \{0,1\}$ being the occupation number of the single dot level and the MBS qubit, respectively. In order to investigate decoherence of the parity qubit, we study the time evolution of the reduced density matrix for the MBS qubit $\rho_f(t) = \text{Tr}_{\text{dot}}[\rho(t)]$ which can readily be solved exactly. The time evolution of the density matrix of the full system reads $\rho(t) = e^{-iHt}\rho(0)e^{iHt}$, where we have set $\hbar = 1$. As an example, we consider the time evolution of the parity qubit's occupation number n_f for an initially occupied dot and an empty subgap fermion state for $\varepsilon = \xi = 0$. The MBS qubit performs Rabi oscillations of full amplitude and is thus totally unstable on the time scale given by the coupling strength λ. The revivals of the initial state are of course due to the finite number of environmental degrees of freedom. However, since the precise number of imperfections, coupling parameters etc. are not experimentally accessible, the reduced state of the qubit to be finally read out will become totally unpredictable due to this kind of environmental coupling. Furthermore, the coupling between a trapped charge and the TSC can change
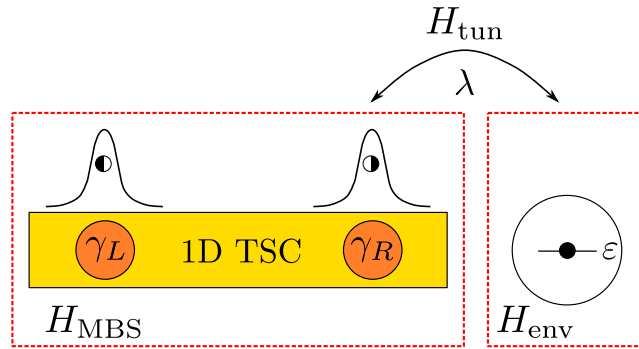
Figure 4.3: TSC tunnel coupled to its environment here represented by a single level dot as toy model for a surface adatom.

during a braiding operation, and thus lead to unwanted errors. Look, for instance, at the operations proposed in Ref. [Alicea11]. A trapped charge might be close to one of the arms of the wire network. If the MBS is located (during an operational step) in that arm it is coupled to the trapped charge via electron tunneling and if not it does not feel its presence. Hence, during a braiding operation, the tunnel coupling could be unintentionally turned on and off. It needs to be analyzed how this kind of error may affect the success of braiding operations.

The second model we investigate consists of a 1D TSC tunnel coupled on one end to a metallic lead which might be realized by a gate or a tip used to implement operations on the qubit. We assume a very long 1D TSC and therefore concentrate on the MBS at the right edge. The lead Hamiltonian $H_{\text{env}} = \sum_k \varepsilon(k)\psi_{k,R}^{\dagger}\psi_{k,R}$ and the coupling is given by

$$H_{\text{tun}} = \lambda_R \left[\psi_R^{\dagger}(x=0) - \psi_R(x=0)\right]\gamma_R, \tag{4.5}$$

where $\lambda_R \in \mathbb{R}$ and we assume a linear dispersion $\varepsilon(k)$ for simplicity. In the following, we study the spectral function of the MBS at the right edge $A(\omega) = -2\text{Im}\left[G_{\gamma_R\gamma_R}^{R}(\omega)\right]$, where the retarded Green's function of the MBS is calculated solving the full non-equilibrium Dyson equation on the Keldysh contour. For the sake of brevity, and just to make the important point, we do not go into detail of the calculation. Later in this chapter some more details on a similar Hamiltonian and the corresponding Green's functions are given. After Fourier transforming back to the time domain, we obtain

$$A(t > 0) = e^{-4\pi\rho_0\lambda_R^2 t},$$

where ρ_0 is the constant density of states in the metallic lead. The lifetime of the Majorana bound state is thus determined by the tunnel coupling and the density of states offered for tunneling by the environment, similarly to any local qubit exposed to tunnel coupling. In particular, an ordinary local fermionic subgap bound state would behave very similar when tunnel coupled to its environment. Of course, the spectral weight of our MBS based state f is delocalized over the two ends of the TSC, but this would only lead to a reduction of the tunnel coupling by a factor of $1/\sqrt{2}$ as compared to a local bound state.

Although the Majorana qubit is defined as a nonlocal object, local coupling to a MBS via a tunnel Hamiltonian as in Eqs. (4.4) and (4.5) is extensively studied in the literature [Bolech07, Tewari08, Law09, Flensberg10, Shivamoggi10, Fu10, Golub11a, Leijnse11b, Zazunov11, Liu11b, Stanescu11, Walter11a, Bose11], particularly as a way to detect the MBS. We would like to point out that such a coupling already contradicts the fundamental conjecture (*ii*) which is crucial for TQC in MBS based systems. While the presence of subgap MBS is topologically protected by particle hole symmetry [Kitaev01, Kitaev09], TQC tasks with MBS as proposed, for instance, in [Hassler10, Alicea11, Flensberg11, Leijnse11a] are not protected against decoherence by any fundamental symmetry, in particular not by a topological one.

To sum up, as far as MBS based qubits are concerned we gave two general reasons why the protection against decoherence will fail for quite mundane coupling mechanisms. In particular, there is no fundamental difference in the stability of the fermion parity for a MBS pair and a local fermionic bound state which is separated from bulk excitations by a superconducting gap. The topological protection in a 1D TSC thus pertains to the presence of the single pair of MBS and not to the coherence of the associated qubit. Furthermore, since braiding operations are in a closed system independent of the local details of the path traversed by the quasiparticles, the precision of these operations is not sensitive to the mechanical fine tuning of the control ports of the setup. This feature is of course not related to the coherence properties of a candidate system for TQC. The usefulness of MBS based quantum computers will thus be decided by practical aspects of material science rather than

by fundamental arguments related to nonlocal storing of information: Can particle exchange be suppressed much more efficiently than other mechanisms leading to decoherence of say the spin of a trapped ion or a quantum dot or the phase of a flux qubit? Comparing different approaches on this rather applied level a strong argument supporting many alternative approaches to quantum computing, see e.g., Refs. [Cirac95, Loss98, Wallraff04], is that their basic constituents are readily experimentally accessible.

4.2 Overview of the proposed detection setup for Majorana bound states

We now turn to the main topic of this chapter and introduce our proposal of a nanomechanical detection scheme for Majorana bound states [2]. Our detection scheme aims to reveal the presence of Majorana bound states hosted in one-dimensional topological superconductors. The detector makes use of an oscillating electrode, which can be realized using a doubly clamped metallic beam, tunnel coupled to one edge of the topological superconductor. The detection scheme we propose is schematically depicted in Fig. 4.4. The left and right edges of the topological superconductor host two MBS which we call γ_L and γ_R. With a Majorana fermion having half the degrees of freedom of a Dirac fermion, we can expressing two Majorana fermions $\gamma_{L,R}$ as

$$
\begin{aligned}
\gamma_R &= c^\dagger + c\,, \\
\gamma_L &= -i(c^\dagger - c)\,,
\end{aligned}
$$

where c and $c^\dagger$ are the annihilation and creation operators, respectively, of a single Dirac fermion and satisfy $\{c^\dagger, c\} = 1$. The Majorana operators also satisfy $\gamma_{L/R} = \gamma_{L/R}^\dagger$, and the anticommutation relation $\{\gamma_i, \gamma_j\} = 2\,\delta_{ij}$. One of the edges of the topological superconductor, say the right one, is coupled by tunneling to a movable doubly clamped beam. While this setup can be technically challenging to realize, one should note that the fabrication of metallic doubly clamped nanoresonators with very high frequencies and quality factors has been recently reported [Flowers-Jacobs07, Li08]. The motion of the beam modulates the tunnel amplitude, such that it depends on the displacement $\hat{x}$ of the beam. The oscillating electrode is held at a bias voltage V and the topological superconductor is grounded. We approximate the tunnel amplitude as linear in the displacement of the beam, $t_0 - t_x\hat{x}$. This approximation is justified if the oscillation amplitude is small compared to the mean distance between the beam and the edge of the topological superconductor. The Hamiltonian for the total setup then given by

$$
H = H_\mathrm{res} + H_\mathrm{osc} + H_\mathrm{MBS} + H_\mathrm{tun,0} + H_\mathrm{tun,x}\,,
$$

where

$$
H_\mathrm{res} = \sum_k \varepsilon(k)\,\psi_k^\dagger\,\psi_k
$$

---

[2]This section of the thesis is built upon the published article in Ref. [Walter11a].
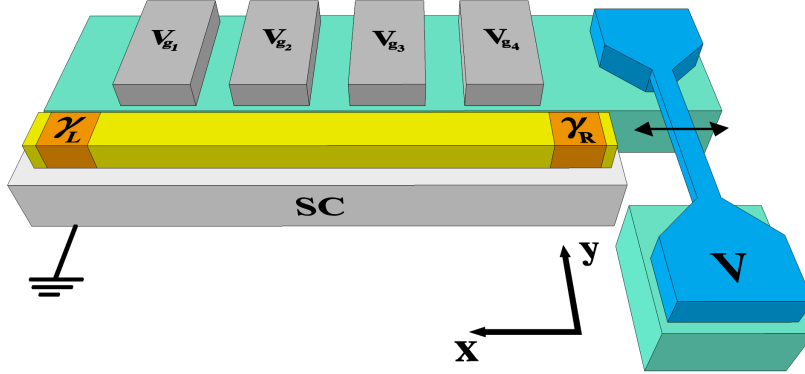
Figure 4.4: Schematic of the setup. A topological superconductor is assumed to be realized as a 1D semiconducting wire on top of a grounded *s*-wave superconductor. The wire can host MBS at its left (γ_L) and right (γ_R) edges. We assume that one of the edges is tunnel coupled to a movable, doubly clamped beam (at bias voltage V). The gate electrodes (V_{g_1}–V_{g_4}) can be used to increase or decrease the overlap ξ of the MBS by changing the effective length L of the topological superconductor.

describes a spinless electron reservoir in the metallic oscillating electrode. Here, we restrict ourselves to one spin channel only. This is appropriate since the one-dimensional semiconducting wire on top of an *s*-wave superconductor in the presence of a magnetic field has the same degrees of freedom as a spinless $p_x + ip_y$ superconductor [Fu08, Oreg10]. In reality, both spins will participate and their signal will add up to the one we calculate below. Furthermore, we assume a linear dispersion $\varepsilon(k)$. Next,

$$H_{\text{osc}} = \frac{\hat{p}^2}{2m} + \frac{1}{2}m\Omega^2\hat{x}^2$$

is the usual harmonic oscillator Hamiltonian describing the motion of the beam with an effective mass m and resonance frequency Ω. The third term

$$H_{\text{MBS}} = \frac{i}{2}\xi\gamma_L\gamma_R$$

characterizes the overlap between the MBS on the left edge and the right edge of the topological superconductor [Semenoff07]. Describing these two Majorana fermions as one Dirac fermion, we can rewrite

$$H_{\text{MBS}} = \xi c^\dagger c \ . \tag{4.6}$$

We recognize that the Hamiltonian H_{MBS} is formally identical to that of a single resonant level (RL) at energy ξ. However, due to the nonlocal nature of the MBS, the overlap ξ depends exponentially on the effective length L of the topological superconductor, cf. the discussion on Kitaev's toy model above. This distinguishes the MBS Hamiltonian from a RL. In order to probe the length dependence of ξ, gate electrodes can be installed in proximity to the topological superconductor [Hassler10, Alicea11], schematically shown in Fig. 4.4. Then, by applying gate voltages, the effective length L, and thus ξ, can be tuned.

The bare tunnel Hamiltonian $H_{\text{tun,0}}$ has been introduced for a related setup in [Bolech07] and the x-dependent term $H_{\text{tun,x}}$ is new and due to the oscillating electrode. Assuming that the tunneling takes place locally at $y = 0$, both are given by

$$H_{\text{tun,0}} = t_0[\psi^\dagger(y = 0) - \psi(y = 0)]\gamma_R \tag{4.7}$$

$$H_{\text{tun,x}} = -t_{\text{x}}\hat{x}[\psi^\dagger(y = 0) - \psi(y = 0)]\gamma_R \,. \tag{4.8}$$

Note that, due to the form of $H_{\text{tun,0}}$ and $H_{\text{tun,x}}$, the Majorana fermion couples to lead electrons as well as lead holes. We cast Eq. (4.7) and (4.8) into a form containing Dirac fermions:

$$H_{\text{tun,0}} = t_0 \left\{ \left[c^\dagger\psi(0) + \psi^\dagger(0)c \right] + \left[\psi^\dagger(0)c^\dagger + c\psi(0) \right] \right\} \,,$$

$$H_{\text{tun,x}} = -t_{\text{x}}\hat{x} \left\{ \left[c^\dagger\psi(0) + \psi^\dagger(0)c \right] + \left[\psi^\dagger(0)c^\dagger + c\psi(0) \right] \right\} \,.$$

We assume that the lead electrons only couple to γ_R in $H_{\text{tun,0}}$ and $H_{\text{tun,x}}$, which is justified if the wire is much longer than the superconducting coherence length ξ_{SC} of the s-wave superconductor, the characteristic localization length of the MBS [Fu08]. Since MBS are subgap states, we investigate the regime of a large superconducting gap Δ_{SC}, i.e., $\rho_0 t_0^2, \xi, eV \ll \Delta_{\text{SC}}$, where ρ_0 is the density of states of the metallic lead. If the electrode does not oscillate, the system is described by the quadratic Hamiltonian $H_0 = H_{\text{res}} + H_{\text{osc}} + H_{\text{MBS}} + H_{\text{tun,0}}$. In this case, all Green's functions involving ψ and c operators are known exactly. Since H_0 does not conserve fermion numbers, the anomalous Green's functions do not vanish, e.g., $\langle c(t)c(0)\rangle_0 \neq 0$. Then, non-equilibrium transport properties like the average current or the current noise can be determined exactly [Bolech07].

4.3 Current calculation

We shall treat the x-dependence of the tunneling amplitude as a perturbation to the Hamiltonian H_0. This requires that $t_{\text{x}}x_{\text{zpf}}\sqrt{2\langle n\rangle + 1} \ll t_0$, where $x_{\text{zpf}} = 1/\sqrt{2m\Omega}$ is the amplitude of the zero point fluctuations and $\langle n\rangle$ the mean phonon number of the resonator. We restrict ourselves to second order perturbation theory in $H_{\text{tun,x}}$. Our main focus is the calculation of the average current and the differential conductance $d\langle I\rangle/dV$. Putting $\hbar = 1$, the current operator is given by $I = -e\,\partial_t N = -ie[H, N]$, where $N = \int dy\,\psi^\dagger(y)\psi(y)$ denotes the number of fermions in the lead. Using the vector notation $\vec{\Psi} = \left(c, c^\dagger, \psi(0), \psi^\dagger(0) \right)$, we find $I = I_0 + I_{\text{x}}$, where

$$I_0 = -iet_0\vec{\Psi}^T\mathbf{B}\vec{\Psi} \,,$$

$$I_{\text{x}} = iet_{\text{x}}\hat{x}\vec{\Psi}^T\mathbf{B}\vec{\Psi} \,.$$

Here, $\mathbf{B}$ is a real 4×4 matrix

$$\mathbf{B} = \begin{pmatrix} 0 & 0 & 1 & 0 \\ 0 & 0 & 1 & 0 \\ 0 & 0 & 0 & 0 \\ -1 & -1 & 0 & 0 \end{pmatrix}.$$

We introduce the fermion Green's functions on the Keldysh contour

$$G_{\Psi_j \Psi_k}(t,t') \equiv G_{jk}(t,t') = -i \left\langle T_c \, \Psi_j(t) \Psi_k(t') \right\rangle_0$$

where $j,k \in \{1,2,3,4\}$ and T_c denotes the time-ordering operator on the Keldysh contour. Later we will introduce Keldysh indices $\{-,+\}$ referring to the lower (time-ordered) and upper (anti-time-ordered) branch of the Keldysh contour, respectively, cf. Fig. 1.2. The average is taken with respect to the ground state of the unperturbed Hamiltonian H_0. For $t_\mathrm{x} = 0$, the time-independent average current can be written as

$$\langle I_0 \rangle = -\frac{et_0}{2} \int \frac{d\omega}{2\pi} \left\{ [G^K_{\psi c^\dagger}(\omega) - G^K_{c\psi^\dagger}(\omega)] + [G^K_{\psi^\dagger c^\dagger}(\omega) - G^K_{\psi c}(\omega)] \right\}, \tag{4.9}$$

where

$$G^K_{\Psi_j \Psi_k}(t,t') = -i \left\langle [\Psi_j(t), \Psi_k(t')] \right\rangle_0$$

is the Keldysh Green's function, for which in general we have $G^K(t,t') = G^{-+}(t,t') + G^{+-}(t,t')$.

Next, we consider the corrections to this current for small t_x. Using a similar matrix notation allows us to write

$$H_\mathrm{tun,x} = -t_\mathrm{x} \hat{x} \vec{\Psi}^T \mathbf{A} \vec{\Psi},$$

with

$$\mathbf{A} = \begin{pmatrix} 0 & 0 & 1 & 0 \\ 0 & 0 & 1 & 0 \\ 0 & 0 & 0 & 0 \\ 1 & 1 & 0 & 0 \end{pmatrix}.$$

Introducing the unperturbed oscillator Green's function on the Keldysh contour

$$D(t,t') = -i \left\langle T_c \, \hat{x}(t) \hat{x}(t') \right\rangle_0,$$

the first order correction to the fermion Green's function can be expressed as (for $j,k \in \{1,2,3,4\}$)

$$iG^{(1)\alpha\beta}_{jk}(t,t') = t_\mathrm{x} \int_{-\infty}^{\infty} d\tau_1 \sum_{\gamma = \pm} (-\gamma) \sum_{m,n=1}^{4} \tilde{A}_{mn} \, D^{\alpha\gamma}(t,\tau_1) \, G^{\alpha\gamma}_{jm}(t,\tau_1) \, G^{\gamma\beta}_{nk}(\tau_1,t'),$$

where $\tilde{\mathbf{A}} = \mathbf{A} - \mathbf{A}^{\mathrm{T}}$ and $\alpha, \beta, \gamma \in \{-, +\}$ denote the branches of the Keldysh contour.

We express the second-order correction to the Green's functions matrix in terms of the advanced, retarded, and Keldysh components as

$$\tilde{\mathbf{G}}_{jk}(t, t') = \mathbf{U}\, \mathbf{G}_{jk}(t, t')\, \mathbf{U}^\dagger = \left(\begin{array}{cc} 0 & G_{jk}^A \\ G_{jk}^R & G_{jk}^K \end{array} \right) (t, t')\,,$$

where the transformation is given by

$$\mathbf{U} = \frac{1}{\sqrt{2}} \left(\begin{array}{cc} 1 & -1 \\ 1 & 1 \end{array} \right)\,.$$

This leads to the following compact form of the second-order correction to the Green's functions in the rotated Keldysh space

$$i\tilde{\mathbf{G}}_{jk}^{(2)}(t, t') = -t_{\mathrm{x}}^2 \int_{-\infty}^{\infty} d\tau_1\, d\tau_2 \left[\tilde{\mathbf{G}}(t, \tau_1) \tilde{\mathbf{A}} \tilde{\mathbf{\Sigma}}(\tau_1, \tau_2) \tilde{\mathbf{A}} \tilde{\mathbf{G}}(\tau_2, t') \right]_{jk}\,,$$

where the effects of the oscillator are contained in the self-energy

$$\tilde{\mathbf{\Sigma}}_{jk}(t, t') = \mathbf{U}\mathbf{\Sigma}_{jk}(t, t')\mathbf{U}^\dagger = \frac{1}{2} \left(\begin{array}{cc} D^A G_{jk}^A + D^R G_{jk}^R + D^K G_{jk}^K & D^R G_{jk}^K + D^K G_{jk}^R \\ D^K G_{jk}^A + D^A G_{jk}^K & 0 \end{array} \right) (t, t')\,.$$

We will assume that the mechanical oscillator has a very high quality factor, such that the linewidth of the uncoupled oscillator is small compared to the effective linewidth of the fermionic level at ξ. With these assumptions, we can use the following advanced, retarded and Keldysh Green's functions in Fourier space

$$D^R(\omega) = i\pi[\delta(\omega + \Omega) - \delta(\omega - \Omega)]/[2m\Omega]\,,$$
$$D^K(\omega) = -i\pi \left\langle \bar{x}^2 \right\rangle [\delta(\omega - \Omega) + \delta(\omega + \Omega)]\,,$$
$$D^A(\omega) = [D^R(\omega)]^*$$

with $\bar{x}^2 = \hat{x}^2 + \hat{p}^2/(m^2\Omega^2)$. Finally, the average current including the oscillator can be written as $\langle I \rangle = \langle I_0 \rangle + \langle I_{\mathrm{x},1} \rangle + \langle I_{\mathrm{x},2} \rangle$, where $\langle I_0 \rangle$ is given in Eq. (4.9) and the two remaining terms are ($j \in \{1, 2\}$)

$$\langle I_{\mathrm{x},j} \rangle = \frac{e}{2}(-t_0\delta_{2j} + t_{\mathrm{x}}\delta_{1j}) \int \frac{d\omega}{2\pi} \Big\{ [G_{\psi c^\dagger}^{(j)K}(\omega) - G_{c\psi^\dagger}^{(j)K}(\omega)] + [G_{\psi^\dagger c^\dagger}^{(j)K}(\omega) - G_{\psi c}^{(j)K}(\omega)] \Big\}\,.$$

The analytic result for $\langle I \rangle$ is too long to be displayed here. We demonstrate in the following that the average current contains unique information about the MBS which can be most easily identified in the nonlinear differential conductance $d\langle I \rangle/dV$.

4.4 Results

Compared to earlier proposals [Bolech07], we have two additional energy scales involved in the detection scheme: the resonance frequency Ω of the oscillator and its effective temperature T_{eff}. Both are to some extent experimentally tunable. Assuming that the oscillator is in a thermal state, one has $\langle \bar{x}^2 \rangle_{th} = 2 x_{\text{zpf}}^2 (2\langle n \rangle + 1)$ where $\langle n \rangle = 1/\left[\exp(\Omega/T_{\text{eff}}) - 1\right]$ is the mean phonon number of the oscillator and where we set $k_{\text{B}} = 1$. In the following, we will discuss the regime where $\langle n \rangle$ is small, i.e., comparable to 1. This is challenging to realize experimentally. Note, however, that for the highest resonance frequencies of the doubly clamped beams in Ref. [Li08] ($\sim 500\,\text{MHz}$), the thermal occupation number could actually become less than 1 at typical dilution refrigerator temperatures. At higher temperatures or lower frequencies, one would have to implement additional cooling schemes to bring the oscillator to the quantum regime.

In our model, we make the assumption that the electronic system is at zero temperature, $T_{el} = 0$. The side peaks in the differential conductance which are due to the oscillator can be resolved as long as $T_{el} \ll \Omega$. If the electronic system and the oscillator are in equilibrium with the same heat bath, this translates to the requirement $\langle n \rangle \ll 1$. However, $T_{el} \ll \Omega$ can also be fulfilled for larger $\langle n \rangle$ if the oscillator is put into an excited state using experimental techniques as, for instance, done in Ref. [O'Connell10].

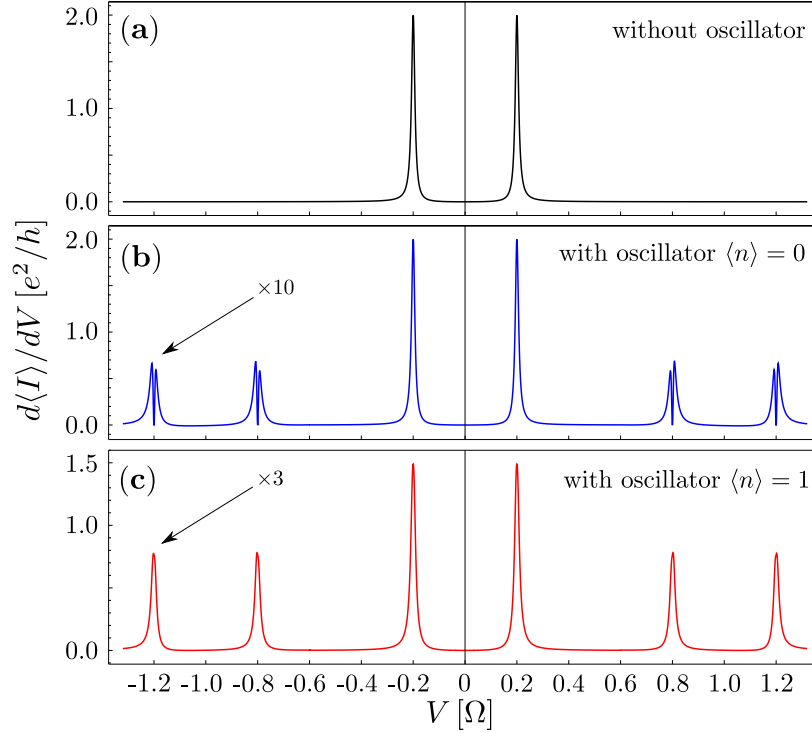### 4.4.1 Differential conductance without the resonator

For clarity, let us start with the case without the oscillator ($t_{\text{x}} = 0$) and briefly discuss the dependence of the differential conductance on the length of the topological superconductor and thus its dependence on ξ. In the case of a finite overlap of the two MBS, the differential conductance shows two peaks at $eV = \pm|\xi|$ which can be seen in Fig. 4.5(a) (see also Ref. [Stanescu11] for comparison). Both of the peaks have the height $2e^2/h$ [3]. Importantly, for any finite ξ, $d\langle I \rangle/dV$ at $V = 0$ vanishes in our model. This is in stark contrast to the differential conductance in quantum dots coupled to one superconducting and one normal metal lead [Domański08]. Hence, it is rather straightforward to distinguish this situation from the MBS case.

As mentioned above, the Hamiltonian H_{MBS} is formally equivalent to one describing a spinless resonant level at energy ξ. Therefore, a comparison to a resonant level case is of pedagogical value. Two resonant levels with energies $\pm|\xi|$ might lead to a similar signal in the differential conductance as in the MBS case. This could, for instance, happen if the magnetic field destroys the superconductivity in an experimental realization of our proposal. Increasing the effective length of the wire using the gate electrodes, one can tune ξ close to zero, which would yield a single peak at $V = 0$ (not shown in Fig. 4.5). However, this feature in the differential conductance could also be due to a single RL with energy $\xi = 0$ and consequently an ordinary bound state might mistakenly be identified as a MBS.

We conclude that tunneling into resonant levels could be hard to distinguish from tunneling into MBS. However, it is fair to say that a measurement of $d\langle I \rangle/dV$ as a function of the variation of the length of the topological superconductor could yield a strong signature of MBS, even in the case of static leads. Furthermore, $d\langle I \rangle/dV = 2e^2/h$ on resonance in the

---

[3]Their height will decrease if we couple the lead electrons not only to γ_R but also to γ_L.

MBS case, which might not be the case for tunneling into a RL. Interestingly, we show below that the oscillating electrode exhibits additional features in the differential conductance, allowing for an unambiguous identification of MBS.

Figure 4.5: Differential conductance for $\xi/\Omega = 0.2$ in the presence of MBS for the case $t_\mathrm{x} = 0$ (without oscillator) as well as for the case $t_\mathrm{x} \neq 0$ for different values of $\langle n \rangle$. The satellite peaks have been enlarged for better visibility.

4.4.2 Differential conductance with the resonator

The differential conductance in the presence of the oscillator and its dependence on the oscillator's temperature is shown in Figs. 4.5(b) and 4.5(c) for two temperatures corresponding to $\langle n \rangle = 0$ and 1, respectively. Due to the presence of the oscillator, satellite peaks emerge at $eV = \pm|\xi \pm \Omega|$.

In Fig. 4.6, we depict the energetically allowed tunnel processes for $\langle n \rangle = 0$, which explain the emerging satellite peaks in Fig. 4.5. (Note that for $\langle n \rangle = 1$ more processes are possible corresponding to the emission of a phonon by the oscillator. These are not shown in Fig. 4.6.) Evidently, for the conventional processes in Figs. 4.6(a), 4.6(c), and 4.6(e), the superconducting condensate does not play any role. Hence, these processes also matter for tunneling into a RL where the condensate in Fig. 4.6 would be replaced by a second lead. The processes in Figs. 4.6(b), 4.6(d), and 4.6(f), on the other hand, rely on the presence of the superconducting condensate. Importantly, all processes in Figs. 4.6(a) to 4.6(f) contribute together to the rich structure in the $d \langle I \rangle /dV$ shown in Fig. 4.5. Increasing the oscillator's temperature leads to an increase in the heights of the satellite peaks and

smoothly transforms a dip at $eV = \pm|\xi \pm \Omega|$ into a peak. This will be further discussed in Fig. 4.7.
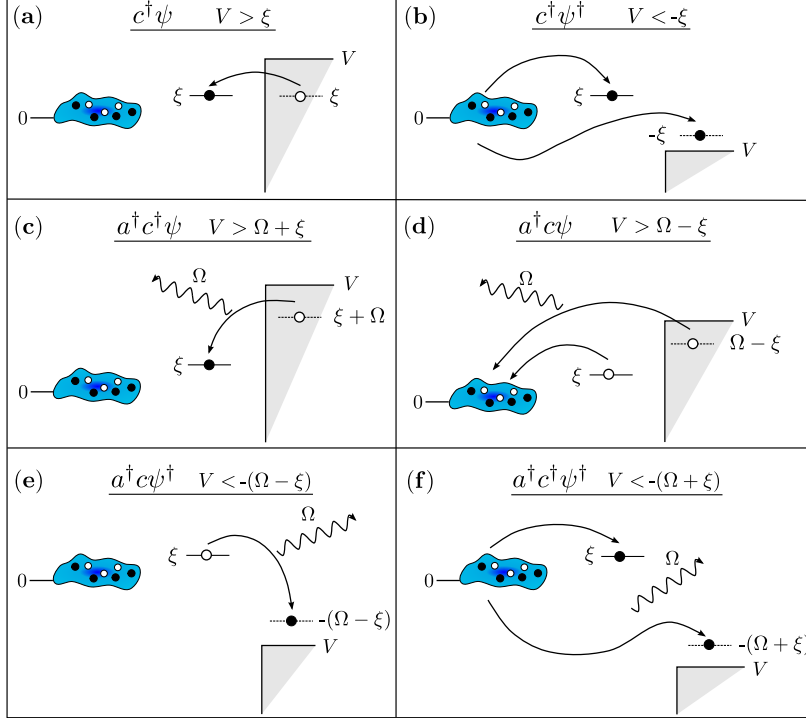
Figure 4.6: Schematic of energetically allowed tunnel processes for an oscillator in the ground state. Panels (a)-(f) depict the processes stemming from the tunnel terms $c^\dagger\psi$, $c^\dagger\psi^\dagger$, $a^\dagger c^\dagger\psi$, $a^\dagger c\psi$, $a^\dagger c\psi^\dagger$, and $a^\dagger c^\dagger\psi^\dagger$, respectively, where $\hat{x} = a^\dagger + a$. Black dots (circles) represent electrons (holes) and the superconducting condensate is depicted as the blue bubble.

As mentioned above, one can argue that in a single RL scenario with level energy $\xi = 0$, the signal in the differential conductance could not be clearly distinguished from the one stemming from MBS. Including the oscillator permits us to unambiguously distinguish the two cases. Figure 4.7 shows our key result. In that figure, we compare the RL case to the MBS case, both in the presence of an oscillating tunnel contact. For clarity, we focus on a region around the resonant frequency Ω of the oscillator and positive bias voltage V. Importantly, an oscillator in its ground state ($\langle n \rangle = 0$) can only absorb a phonon. In the case of the single RL, the crucial tunnel process near the resonance at $eV = \Omega$ (for an oscillator with $\langle n \rangle = 0$) is depicted in the right inset of Fig. 4.7. We see that this process only sets in for voltages $eV > \Omega$ (at zero temperature) since the state in the right lead has to be occupied in order to transfer the energy Ω to the oscillator. As a consequence, the differential conductance is only positive for $eV > \Omega$ (shown as a solid black line in Fig. 4.7). The situation is very different for the MBS case. Here, we have a second crucial tunnel process depicted in the left inset of Fig. 4.7. Then, the dashed-dotted blue line in Fig. 4.7 illustrates that, for the oscillator in its ground state and MBS present, the $d\langle I \rangle / dV$ is positive for $eV < \Omega$ and $eV > \Omega$. This feature is only due to tunneling through the MBS and clearly separates the RL from the MBS scenario. If we gradually increase $\langle n \rangle$ from zero

to one (where only the two extremes are shown in Fig. 4.7), the dip for $\langle n \rangle = 0$ in the MBS case transforms smoothly into a peak due to additional processes where the oscillator emits a phonon.
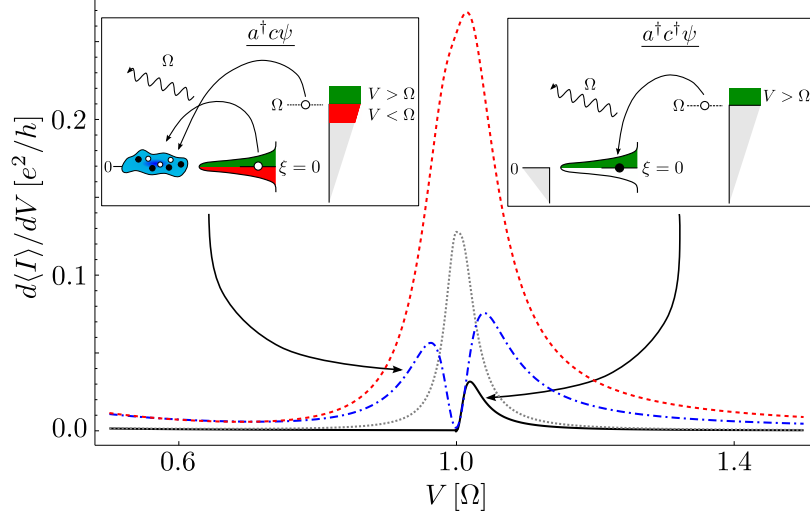
Figure 4.7: Differential conductance for $\xi \simeq 0$ at $eV \approx \Omega$ for a single RL coupled to an oscillator with $\langle n \rangle = 0$ (solid black line) and $\langle n \rangle = 1$ (dotted gray line). In the former case, the oscillator can enhance transport only for $eV > \Omega$. This is different in the presence of MBS. Then, an oscillator with $\langle n \rangle = 0$ gives rise to a positive $d \langle I \rangle / dV$ for $eV > \Omega$ and $eV < \Omega$ (dashed-dotted blue line). We also show in dashed red the $d \langle I \rangle / dV$ for $\langle n \rangle = 1$ in the MBS situation. The insets depict the decisive tunnel processes for the $\langle n \rangle = 0$ case.

The dip at $eV = \Omega$ is due to an interference effect between the two participating tunnel processes which can be understood on the basis of Fermi's golden rule. To illustrate this, we choose $\xi = 0$ and $\langle n \rangle = 0$ and write the system Hamiltonian as $H = \tilde{H}_0 + \tilde{H}_{\text{tun}}$ with

$$\tilde{H}_0 = H_{\text{res}} + H_{\text{osc}} \, ,$$
$$\tilde{H}_{\text{tun}} = H_{\text{tun},0} + H_{\text{tun,x}} \, .$$

In our initial state, the Fermi sea should be filled up to the chemical potential eV (measured from $\xi = 0$). Furthermore the fermionic subgap state c is empty and no phonons are present. The initial state can then be written as

$$|i\rangle = |0_\psi, 0_c, 0_a\rangle$$

with energy $E_i = E_F$, E_F being the energy of the filled Fermi sea.

To the lowest order in t_{x}, the leading contribution to $d \langle I \rangle / dV$ at $eV \approx \Omega$ is generated by a combination of the two tunneling processes $c^\dagger \psi$ and ψc, where one of them is accompanied by the creation of a phonon mode.

The current-carrying transport processes we focus on are mediated by the processes described by $c^\dagger \psi$ in combination with ψc (cf. insets in Fig. 4.7). For these transport processes the final state lacks two electrons in the Fermi sea (at momenta $|k|, |k'| < k_F$),

contains one phonon, and an unoccupied subgap state c, i.e., we have for the final state

$$|f\rangle = \psi_k \psi_{k'} |0_\psi, 0_c, 1_a\rangle$$

with energy

$$E_f = E_F - \varepsilon(k) - \varepsilon(k') + \Omega \,,$$

where $\varepsilon(k)$ is the single-particle electron energy and the phonon energy is Ω. As usual, the transition amplitude between the states $|i\rangle$ and $|f\rangle$, up to second order in $\tilde{H}_{\text{tun}}$ is given by

$$A_{fi} = \langle f | \tilde{H}_{\text{tun}} \frac{1}{E_i - \tilde{H}_0} \tilde{H}_{\text{tun}} | i \rangle \,,$$

and according to Fermi's golden rule, the transition rate Γ is given by summing over all final states respecting energy conservation

$$\Gamma = 2\pi \sum_{k,k'} |A_{fi}|^2 \delta(E_f - E_i) \,.$$

The transition rate Γ is proportional to the current, and therefore $d\Gamma/dV$ is proportional to the differential conductance. By evaluating the amplitude A_{fi} and the transition rate Γ, we find that for the above process, the amplitude A_{fi} vanishes for tunneling particles with energy close to $eV \approx \Omega$. This leads to the conclusion that for $eV \approx \Omega$ the differential conductance vanishes due to an interference effect between the two processes (of order $t_0 t_{\text{x}}$) generated by the terms $c^\dagger \psi (t_0 + t_{\text{x}} a^\dagger)$ and $\psi c (t_0 + t_{\text{x}} a^\dagger)$ in the tunneling Hamiltonian. This explains the dip in the differential conductance $d \langle I \rangle / dV$ in Fig. 4.7.

4.5 Concluding remarks

To conclude, we have presented a novel idea of coupling Majorana bound states to a sensitive nanoelectromechanical measurement device. We have shown that a setup where an oscillating, doubly clamped beam is tunnel coupled to a topological superconductor gives rise to unique transport signatures based on the interplay between the mechanical excitations and the Majorana bound state. Therefore, a measurement of the nonlinear differential conductance provides the necessary information to uniquely identify Majorana bound states. We find that in the presence of the resonator satellite peaks appear in the differential conductance. We identify the underlying transport processes giving rise to this rich structure in the differential conductance. A signature of Majorana bound states has been identified for an oscillator close to the quantum ground state which can be achieved by cooling a $500\,\text{MHz}$ resonator to $T \approx 20\,\text{mK}$. This energy scale is well below the large parameter of our model, i.e., the superconducting gap Δ_{SC}. When we, for instance, take an InAs wire proximity coupled to an Nb s-wave superconductor, the superconducting gap of Nb $\Delta_{\text{SC}}^{\text{Nb}} \sim 15\,\text{K}$ can induce a superconducting gap of $\Delta_{\text{SC}}^{\text{InAs}} \sim 1\,\text{K}$ in the wire [Lutchyn10]. Hence, our predictions are in principle observable at dilution refrigerator temperatures.

Chapter 5

Entanglement generation in nanoelectromechanical systems

Since the early days of quantum mechanics, entanglement has been one of its most fascinating key elements [Schrödinger35b]. The study of entanglement is not only concerned with fundamental questions but also with applications, for instance, entangled qubits being the building blocks for quantum computers. Two of the main questions when studying entanglement are: How can one generate entanglement in a multipartite system and what is a good measure for entangled states? For discrete variable multipartite systems with, for instance, qubits as representatives, the former two questions have been extensively studied theoretically as well as experimentally [Steane98, Horodecki09, Nielsen00].

Entanglement creation and verification of quantum systems, as for instance, atoms and photons is a theoretically well understood subject and routinely done experimentally in various labs [Aspect82, Edamatsu04, Stevenson06]. Entanglement of quantum systems with constituents being more than just one atom or photon, as for instance, collective spin ensembles and Josephson qubits, have also been studied recently [Steffen06, Neeley10]. These kinds of systems are often times discrete variable systems with a finite dimensional Hilbert space and true quantum systems in the sense that they do not have any classical counterpart. With the laws of quantum mechanics describing atomic and subatomic systems and the laws of classical Newtonian mechanics describing macroscopic objects, there must exist a boundary between the quantum and the classical world. This quantum to classical boundary is still subject in contemporary physics [Zurek03, Leggett05]. Emerging questions are: What causes the quantum to classical transition? Where is the limit that causes objects to behave quantum mechanically and not classically? How macroscopic can an object be to be still considered quantum? This chapter is motivated by exactly these questions.

The study of entanglement in nanomechanical systems can help to understand these questions. The generation of entanglement in nanomechanical systems has been a goal for many years. In the pioneering work [Eisert04], a route towards entanglement in NEMS was proposed making use of a global non-adiabatic change of the interaction strength in a one-dimensional chain of nanomechanical oscillators, leading to entanglement of two spatially well separated oscillators of the chain. This type of entanglement has, however, up to date not been realized in experiments. Subsequent proposals in (hybrid) nanooptomechanical systems have suggested to generate entanglement between a moveable mirror of a cavity and a collective spin ensemble of an atomic medium [Hammerer09], a Bose-Einstein condensate [Genes08, De Chiara11], the cavity field itself [Vitali07a], or another mirror [Mancini02, Pirandola06, Pinard07].

In this chapter, our aim is to investigate the quantum mechanical feature per se, entanglement, in a quantum harmonic oscillator that behaves as classically as it gets (in the sense of the Ehrenfest theorem). We like to study the challenge to generate entanglement between two nanomechanical oscillators, being representatives of two mesoscopic continuous variable systems. Before we introduce two fundamentally new schemes towards entanglement generation in NEMS, we briefly review some basics on entanglement.[1]

5.1 Entanglement basics

Still today, entanglement is one of the most counter intuitive, fascinating, intriguing, and frequently studied elements of quantum mechanics. In fact, there is no classical counterpart to entanglement. Entanglement can be defined as purely quantum mechanical correlations between two non-interacting systems. These systems can even be separated in space by quite some distance. The correlations are of the kind that neither of the participating parties can be assigned a pure reduced state itself. Rather than being a pure theoretical fact, A. Aspect et al. [Aspect81] proved with a pioneering experiment the entanglement between two photons by the violation of Bell's inequalities [Bell64]. We will only briefly introduce the notion of entanglement and refer the reader to Ref. [Horodecki09] for a modern and comprehensive review on entanglement.

We say that two quantum systems, described by a density matrix ρ, are separable if and only if ρ can be expressed as

$$\rho = \sum_i \rho_{i,A} \otimes \rho_{i,B} \tag{5.1}$$

with $\sum_i p_i = 1$, and where $\rho_{i,A}$ and $\rho_{i,B}$ are the density matrices of subsystems A and B, respectively. In order to test whether a quantum mechanical state is separable or inseparable, A. Peres [Peres96] introduced an inseparability criterion based on the partial transpose of the density matrix ρ. For example, partial transposition in the case of the separable state in Eq. (5.1) with respect to subsystem B means

$$\rho^{T_B} = \sum_i p_i \, \rho_{i,A} \otimes [\rho_{i,B}]^T \ .$$

Since ρ is positive semidefinite, ρ^{T_B} is also positive semidefinite which already shows the necessity of the positive partial transpose criterion. P. Horodecki [Horodecki97] showed that the proposed criterion is necessary and sufficient in the case of 2×2 and 2×3 dimensional quantum states and still necessary for higher dimensional quantum states. The degree of entanglement of the state ρ is then quantified by the logarithmic negativity $E_N = \log_2(||\rho^{T_B}||_1)$ where the trace-norm of an operator O is defined as $||O||_1 = \text{Tr}\,|O|$.

Since the systems under investigation in this thesis are continuous variable systems having an infinite Hilbert space, we will introduce in the following section the main ideas behind bipartite continuous variable entanglement and briefly review Gaussian states and a suitable inseparability criterion based on Peres' positive partial transpose criterion.

---

[1]This chapter of the thesis is built upon the pre-print [Walter12]

Bipartite continuous variable entanglement

Since two nanomechanical oscillators are two continuous variable systems, we will review entanglement in bipartite continuous variable system. We will focus on the study of multimode Gaussian states. A Gaussian state is a state with its Wigner function being a normalized Gaussian distribution. Some of the prominent quantum mechanical Gaussian states are the vacuum state, squeezed states, or two mode squeezed states. Multimode Gaussian states are fully characterized by their second moments or the so-called covariance matrix. Here, we will only treat two-mode Gaussian states, for which the covariance matrix is given by

$$\sigma_{ij} = \text{Tr}\left[\rho\left\{\xi_i, \xi_j\right\}/2\right]$$

with

$$\xi = (\hat{x}_1, \hat{p}_1, \hat{x}_2, \hat{p}_2)^T \,,$$

and ρ being the density matrix of the composite system. The quadrature operators in ξ satisfy the canonical commutation relations $(\hbar = 1)$

$$[\xi_i, \xi_j] = iJ_{ij} \,,$$

where J is the simplectic form

$$J = \left(\begin{array}{cccc} 0 & 1 & 0 & 0 \\ -1 & 0 & 0 & 0 \\ 0 & 0 & 0 & 1 \\ 0 & 0 & -1 & 0 \end{array} \right) \,.$$

A consequence of the commutation relations is the uncertainty relation for the covariance matrix [Simon00, Werner01]

$$\sigma + \frac{1}{2}iJ \geq 0 \,.$$

This uncertainty relation applies to any physical state, not only to Gaussian ones. Every two-mode Gaussian covariance matrix can be written in a compact form as

$$\sigma = \left(\begin{array}{cc} \alpha & \gamma \\ \gamma^T & \beta \end{array} \right)$$

with α and β being the correlation matrices of subsystem A and B, respectively, and γ containing correlations between the subsystems. In order to characterize the entanglement, we need the symplectic eigenvalues λ_i of σ, as well as the symplectic eigenvalues $\tilde{\lambda}_i$ of the partially transposed covariance matrix

$$\tilde{\sigma} = \sigma^{T_1} \,.$$

In short, partial transposition T_1 in the case of continuous variable systems described by quadrature operators $\hat{x}_i$ and $\hat{p}_i$, means multiplying -1 to all elements of σ that contain $\hat{p}_1$, see Refs. [Duan00, Simon00, Vidal02, Pirandola09]. The symplectic eigenvalues λ_i are easily obtained as the spectrum of the matrix $|iJ\sigma|$. In the case of a two-mode Gaussian state the symplectic eigenvalues of σ and $\tilde{\sigma}$ are calculated in the following way [Pirandola09]

$$\lambda_{\pm} = \sqrt{\frac{\Delta \pm \sqrt{\Delta^2 - 4\det\sigma}}{2}}\,,$$

$$\tilde{\lambda}_{\pm} = \sqrt{\frac{\tilde{\Delta} \pm \sqrt{\tilde{\Delta}^2 - 4\det\sigma}}{2}}$$

with

$$\Delta = \det\alpha + \det\beta + 2\det\gamma\,,$$

$$\tilde{\Delta} = \det\alpha + \det\beta - 2\det\gamma\,.$$

The positive partial transpose criterion yields that a state described by σ is separable if and only if

$$\tilde{\lambda}_- \geq 1/2\,.$$

In order to quantify the entanglement we can make use of the logarithmic negativity

$$E_N = \max\left\{0, -\log_2(2\tilde{\lambda}_-)\right\}$$

which is zero for separable states and nonzero for entangled states.

The criterion of positive partial transposition reviewed here, is applicable to Gaussian states only. An initially Gaussian state stays Gaussian, if the interaction is linear or at most bilinear in the operators of the two modes [Schumaker86, Olivares12] which is given for the types of interactions we consider later.

When we study the entanglement in a particular setup, we will employ an equation of motion approach for the reduced density matrix of the total system, $\rho_S(t)$. With the equation of motion for $\rho_S(t)$, we can then calculate the equations of motion for expectation values of arbitrary system operators X (or products of them) by solving

$$\frac{d}{dt}\langle X(t)\rangle = \text{Tr}_S\left[\dot{\rho}_S(t)X\right]\,,$$

i.e., we can calculate the time dependence of the covariance matrix $\sigma(t)$ and therefore the time dependence of the logarithmic negativity $E_N(t)$.

## 5.2 Brief outline of the two proposed setups

We will study entanglement between two nanomechanical oscillators for two different types of setups. They both have in common that the two oscillators are never directly coupled to

each other. The oscillators are part of a tunnel junction setup and the coupling between them is always mediated via common reservoirs. We take into account different types of reservoirs and therefore will give a brief overview of the proposed schemes.

Fermionic reservoir

The first setup we propose, Setup (A), is depicted in Fig. 5.1. It can be seen as a natural extension of the experimental realization of one oscillator coupled to a single atomic point contact [Flowers-Jacobs07]. Setup (A) consists of two nanoelectromechanical oscillators coupled to a common measurement device/reservoir. Importantly, the oscillators are not directly coupled to each other (as e.g., in Ref. [Ludwig10]), but only through the electron reservoirs which act as fermionic baths. The yellow tunnel junctions in Fig. 5.1 are sufficient to generate an entangled state of the two oscillators. This setup being rather academic serves us as a model and provides us with new insight into the situation where two nanomechanical oscillators are effectively coupled through two common fermionic baths. This is a less studied case compared to the more common situation of coupling two oscillators to a common bosonic bath, for instance, within a Caldeira-Leggett model [Liu07]. When we discuss this setup in
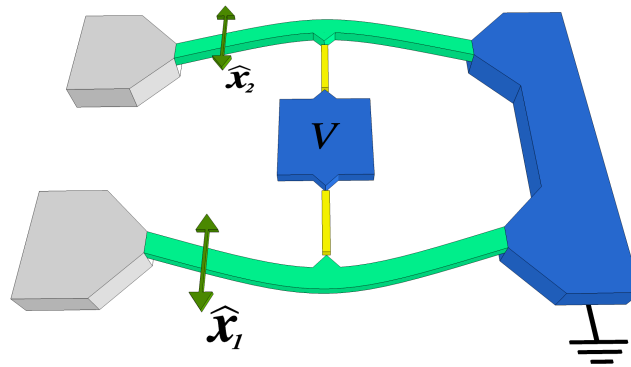

Figure 5.1: Schematic setup of a bipartite continuous variable quantum system, realized as two nanoelectromechanical oscillators (green) in a tunnel junction setup which share common fermionic reservoirs (blue). Yellow lines indicate tunnel junctions that are needed for the generation of entanglement.

Sec. 5.3 we will see that the reservoir needs to have a finite correlation time. This means, the reservoir correlation functions must not decay on a time scale that is small compared to the time scale of the system given by the resonance frequency of the oscillators. Therefore, we need to investigate the non-Markovian regime of this setup. For a more feasible version of Setup (A), we now introduce a different setup which relies on the working principle of the Andreev entangler introduced in Ref. [Recher01].

Andreev entangler

The major drawback of Setup (A) is the assumption that the which-path information of the tunneling electrons is lost because the common right reservoir cannot spatially distinguish the electrons. To circumvent this assumption, we now introduce an alternative realization based

on a superconducting reservoir in the center and two independent normal metal reservoirs which nonetheless is capable of generating entanglement. This realization, Setup (B), is of an Andreev entangler type. In its original sense, the Andreev entangler [Recher01] relies on the splitting of a Cooper-pair which is a spin-singlet. There, the split Cooper-pair from an *s*-wave superconductor can coherently tunnel via two different quantum dots into different leads. Throughout this process, the spin-singlet is preserved. Therefore, the Andreev entangler is capable of generating nonlocal spin-entangled electrons. In our context of nanomechanical systems, we use only charge properties of the split Cooper-pair as a mediator for an effective coupling between the oscillators. We show in Fig. 5.2 what such an Andreev entangler setup could look like. A superconducting island (orange) serves as a source of Cooper-pairs which can tunnel onto two different (conducting) nanomechanical oscillators. The process where the Cooper-pair is split and one electron tunnels to the lower oscillator and the other one tunnels to the upper oscillator gives rise to an effective coupling between them. With Setup (B) we bypass the common right reservoir of Setup (A) and the need for long coherence times. We will study the Andreev entangler in the non-Markovian regime up to second order in the coupling and in the Markovian regime, where it is possible to formulate a master equation for the density matrix of the oscillators which is of Lindblad form. We study Setup (B) in Sec. 5.4.
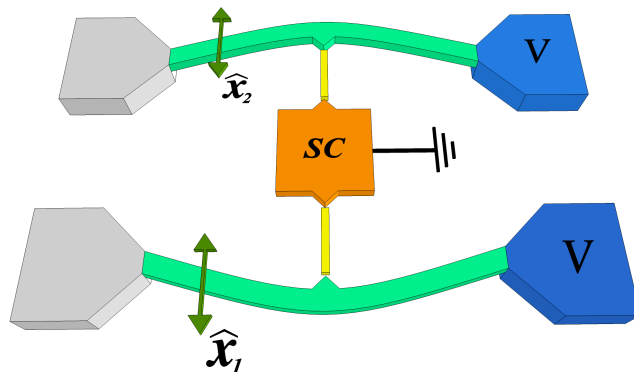
Figure 5.2: Two nanomechanical oscillators are effectively coupled in an Andreev entangler setup due to a Cooper-pair that is split. Each of the two electrons of the Cooper-pair is assumed to tunnel from the superconductor (orange) onto a different oscillator.

Master equation formalism

We will focus on the dynamics of the two oscillators from which we get enough information to characterize the state of the bipartite continuous variable system, cf. Sec. 5.1. Therefore, we treat the problem as an open quantum system, cf. Chap. 2. Before we start investigating each of the proposed scenarios, we will setup an equation of motion for the reduced system which is of general form in a very compact notation [Paz02]. The Hamiltonian of the problem is written in the usual system-bath language

$$H = H_B + H_S + H_{\mathrm{SB}}\,, \tag{5.2}$$

where H_S and H_B describe the system and bath degrees of freedom, respectively. We write the system-bath interaction in a general form

$$H_{SB} = \sum_n S_n E_n + S_n^\dagger E_n^\dagger. \tag{5.3}$$

Here, S_n and E_n denote arbitrary operators acting only on the Hilbert space of the system and bath, respectively. Up to second order in the system-bath coupling H_{SB}, we can then write for the reduced density matrix of the system $\rho_S(t) = \mathrm{Tr}_B[\rho_{\mathrm{tot}}(t)]$ [Paz02]

$$\dot{\rho_S}(t) = -i\left[H_S, \rho_S(t)\right] - \sum_{n,m} \int_0^t dt_1 K_{nm}^{(1)}(t, t_1) \left[S_n, \left[S_m^\dagger(t_1 - t), \rho_S(t)\right]\right] + \mathrm{H.c.}$$
$$- \sum_{n,m} \int_0^t dt_1 K_{nm}^{(2)}(t, t_1) \left[S_n, \left\{S_m^\dagger(t_1 - t), \rho_S(t)\right\}\right] + \mathrm{H.c.}. \tag{5.4}$$

The time-dependent kernels $K_{nm}^{(1/2)}(t, t')$ which dominate the time evolution of the system, are given by

$$K_{nm}^{(1)}(t, t_1) = \frac{1}{2}\left\langle \left\{E_n(t), E_m^\dagger(t_1)\right\}\right\rangle, \tag{5.5}$$

$$K_{nm}^{(2)}(t, t_1) = \frac{1}{2}\left\langle \left[E_n(t), E_m^\dagger(t_1)\right]\right\rangle. \tag{5.6}$$

Up to now, we neither specified the system nor the environment. We first specify the system and the system-bath coupling. The environment is introduced later when we discuss the actual setups (A) and (B). One major task for both setups will be the calculation of the kernels $K_{nm}^{(1/2)}(t, t')$ for the given environment. The system we want to study are two nanomechanical oscillators, described by the Hamiltonian

$$H_S = \sum_{n=1,2} \frac{\hat{p}_n^2}{2m_n} + \frac{1}{2} m_n \Omega_n^2 \hat{x}_n^2. \tag{5.7}$$

Concerning the system-bath coupling, we still use a very general form, only specifying that the system-bath coupling is mediated via tunneling which is approximated to depend linearly on the displacement of the oscillator, i.e., we write

$$H_{SB} = \sum_{n=1,2} S_n E_n + S_n^\dagger E_n^\dagger, \tag{5.8}$$

where

$$S_n = \gamma_{0n} + \gamma_{xn}\hat{x}_n.$$

With the above and assuming two identical oscillators and symmetric coupling, i.e., $\Omega_1 = \Omega_2 = \Omega$, $m_1 = m_2 = m$, we can write the equation of motion of the reduced density matrix,

Eq. (5.4), as

$$\dot{\rho}_S(t) = -i\left[H_S, \rho_S(t)\right] - \sum_{n,m} \int_0^t d\tau \Big\{ \left[K^{(1)}(\tau) + K^{(1)}(-\tau)\right] \gamma_{xn}\gamma_{xm} \left[\hat{x}_n, \left[\hat{x}_m(-\tau), \rho_S(t)\right]\right]$$
$$+ \left[K^{(2)}(\tau) - K^{(2)}(-\tau)\right] \gamma_{xn}\gamma_{xm} \left[\hat{x}_n, \{\hat{x}_m(-\tau), \rho_S(t)\}\right] \Big\}.$$

We can further simplify the equation of motion to

$$\begin{aligned}
\dot{\rho}_S(t) = -&i\left[H_S + i\mathcal{K}_-^{(2)}(t)(\hat{x}_1 + \hat{x}_2)^2, \rho_S(t)\right] \\
& -\mathcal{K}_+^{(1)}(t)\left[\hat{x}_1 + \hat{x}_2, \left[\hat{x}_1 + \hat{x}_2, \rho_S(t)\right]\right] \\
& +\tilde{\mathcal{K}}_+^{(1)}(t)\left[\hat{x}_1 + \hat{x}_2, \left[\hat{p}_1 + \hat{p}_2, \rho_S(t)\right]\right] \\
& +\tilde{\mathcal{K}}_-^{(2)}(t)\left[\hat{x}_1 + \hat{x}_2, \{\hat{p}_1 + \hat{p}_2, \rho_S(t)\}\right],
\end{aligned} \tag{5.9}$$

where in Eq. (5.9) we defined new time-dependent kernels

$$\mathcal{K}_+^{(1)}(t) = \int_0^t d\tau \left[K^{(1)}(\tau) + K^{(1)}(-\tau)\right] \tilde{\gamma} \cos(\Omega\tau), \tag{5.10}$$

$$\tilde{\mathcal{K}}_+^{(1)}(t) = \int_0^t d\tau \left[K^{(1)}(\tau) + K^{(1)}(-\tau)\right] \frac{\tilde{\gamma}}{m\Omega} \sin(\Omega\tau), \tag{5.11}$$

$$\mathcal{K}_-^{(2)}(t) = \int_0^t d\tau \left[K^{(2)}(\tau) - K^{(2)}(-\tau)\right] \tilde{\gamma} \cos(\Omega\tau), \tag{5.12}$$

$$\tilde{\mathcal{K}}_-^{(2)}(t) = \int_0^t d\tau \left[K^{(2)}(\tau) - K^{(2)}(-\tau)\right] \frac{\tilde{\gamma}}{m\Omega} \sin(\Omega\tau). \tag{5.13}$$

In Eqs. (5.10-5.13), $\tilde{\gamma}$ denotes the tunneling amplitude characterizing the system-bath coupling, which is different for setups (A) and (B). The equation of motion for $\rho_S(t)$ contains four different time-dependent damping and decoherence kernels which we can identify as:

- $\mathcal{K}_+^1(t)$
  a diffusion term, depending on the environment temperature

- $\mathcal{K}_-^2(t)$
  a term leading to a renormalization of the oscillator's frequency, which can be dropped, or compensated by an appropriate counter term in the equation of motion

- $\tilde{\mathcal{K}}_+^1(t)$
  a second diffusion term, depending on the environment temperature

- $\tilde{\mathcal{K}}_-^2(t)$
  a damping term, being independent of the environment temperature

With this general framework, we will now study both setups in more detail.

5.3 Coupling via a common fermionic reservoir – Setup (A)

In Setup (A) the two oscillators couple to common fermionic reservoirs with a long coherence time, cf. Fig. 5.1. Here, the reservoirs correspond to the two leads, described by the Hamiltonian

$$H_B = \sum_r \varepsilon_r \psi_r^\dagger \psi_r + \sum_l \varepsilon_l \psi_l^\dagger \psi_l \ .$$

The system-bath coupling is meditated via a tunneling Hamiltonian

$$H_{SB} = \sum_{l,r} \sum_{n=1,2} (\gamma_0 + \gamma_x \hat{x}_n) \psi_l^\dagger \psi_r + \text{H.c.} \,,$$

where for small oscillation amplitudes we approximate the tunneling matrix elements as linear in the oscillator displacement, and for the sake of simplicity assume all tunneling amplitudes to be real and take the coupling to be symmetric. From Eq. (5.8) we immediately see that we can identify the bath operators E_n as $E_n = \psi_l^\dagger \psi_r$ which allows us to calculate the kernels $K^{(1/2)}(t, t_1)$. From now on, we drop the subscript indices of the operators E_n because $\hat{x}_1$ and $\hat{x}_2$ couple to the same bath operator.

5.3.1 Calculation of the memory kernels

As we already mentioned, the time evolution of $\rho_S(t)$ is mainly governed by the memory kernels of the master equation. Therefore, we take some time to sketch how they are calculated. We will exemplify the calculation for kernel $K^{(1)}(t, t_1)$ and just state the results for kernel $K^{(2)}(t, t_1)$. We start by using the definition Eq. (5.5) for $K^{(1)}(t, t_1)$ and plug in the bath operators E

$$
\begin{aligned}
K^{(1)}(t, t_1) &= \frac{1}{2} \sum_{r,l,r',l'} \left\langle \psi_l^\dagger(t)\psi_r(t)\psi_{r'}^\dagger(t_1)\psi_{l'}(t_1) + \psi_{r'}^\dagger(t_1)\psi_{l'}(t_1)\psi_l^\dagger(t)\psi_r(t) \right\rangle \\
&= \frac{1}{2} \sum_{r,l,r',l'} e^{it(\varepsilon_l - \varepsilon_r)} e^{it_1(\varepsilon_{r'} - \varepsilon_{l'})} \left\langle \psi_l^\dagger \psi_r \psi_{r'}^\dagger \psi_{l'} + \psi_{r'}^\dagger \psi_{l'} \psi_l^\dagger \psi_r \right\rangle \\
&= \frac{1}{2} \sum_{r,l} e^{i(\varepsilon_l - \varepsilon_r)(t - t_1)} \left[n(\varepsilon_l)[1 - n(\varepsilon_r)] + n(\varepsilon_r)[1 - n(\varepsilon_l)] \right],
\end{aligned}
$$

where $n(\varepsilon_x) = [e^{\beta(\varepsilon_x - \mu_x)} + 1]^{-1}$ is the Fermi distribution function with $\beta = 1/k_B T$. We transform the sum over r and l into an integral $\sum_{r,l} \rightarrow \int d\varepsilon_l \int d\varepsilon_r \rho_l(\varepsilon_l) \rho_r(\varepsilon_r)$ with an energy-dependent density of states $\rho_\alpha(\varepsilon_\alpha)$. We can write for both kernels $K^{(m)}(t', t'') = K^{(m)}(t' - t'') \equiv K^{(m)}(t)$ with $m = 1, 2$

$$
\begin{aligned}
K^{(m)}(t) &= \frac{1}{2} \int d\varepsilon_l \int d\varepsilon_r \, \rho_l(\varepsilon_l)\rho_r(\varepsilon_r) \, e^{i(\varepsilon_l - \varepsilon_r)t} \left[n(\varepsilon_l)[1 - n(\varepsilon_r)] - (-1)^m n(\varepsilon_r)[1 - n(\varepsilon_l)] \right] \\
&= \frac{1}{2} \int d\varepsilon_l \int d\varepsilon_r \, J(\varepsilon_l, \varepsilon_r) \, e^{i(\varepsilon_l - \varepsilon_r)t} \left[n(\varepsilon_l)[1 - n(\varepsilon_r)] - (-1)^m n(\varepsilon_r)[1 - n(\varepsilon_l)] \right],
\end{aligned}
$$

$$(5.14)$$

where in the last step we introduced the spectral function

$$J(\varepsilon_l, \varepsilon_r) = \sum_k \sum_q \delta(\varepsilon_l - \varepsilon_k)\delta(\varepsilon_r - \varepsilon_q). \tag{5.15}$$

Due to the fact that the equation of motion for $\rho_S(t)$ is of second order in H_{SB}, the only possibility of including non-Markovian effects is by considering an energy-dependent density of states in the leads. Including non-Markovian effects leads to a finite correlation time in the leads and is a key ingredient for the entanglement. Non-Markovian effects in reservoirs and their influence on entanglement of two quantum systems haven been studied also in, for instance, Refs. [Liu07, Ying-Hua10, Xiao10, Bellomo10]. In order to include non-Markovian effects (without facing divergencies) we choose a spectral function that introduces a finite lifetime of quasiparticles in the reservoir. The reservoirs will therefore have a finite and not negligible correlation time. To account for this finite lifetime of quasiparticles in the leads, the δ-functions in Eq. (5.15) are smeared out and replaced by Lorentzians of width L_c

$$J(\varepsilon_l, \varepsilon_r) = \sum_k \sum_q \frac{L_c}{(\varepsilon_l - \varepsilon_k)^2 + L_c^2} \frac{L_c}{(\varepsilon_r - \varepsilon_q)^2 + L_c^2}. \tag{5.16}$$

The largest contribution of each of the independent sums in Eq. (5.16) will come from energies close to the Fermi level of each lead. We further restrict ourselves to the regime of low applied bias voltages $V < L_c$ with $V = \mu_l - \mu_r$. This is just a simplification in order to keep the number of parameters in the problem as low as possible. With these assumptions, the energy-dependent spectral function can be approximated as

$$J(\varepsilon_l, \varepsilon_r) = \frac{1}{(\varepsilon_l - \varepsilon_r)^2 + L_c^2}. \tag{5.17}$$

Physically, Eq. (5.17) means that an electron with energy ε_l in the left lead can tunnel into states of the right lead with energy ε_r, broadened by L_c [Wingreen94, Zhu05, Liu07, Lee08]. With the spectral function in Eq. (5.17), the time-dependent kernels $\mathcal{K}_{+/-}^{1/2}(t)$ and $\tilde{\mathcal{K}}_{+/-}^{1/2}(t)$ can now be calculated analytically. We continue from Eq. (5.14) using Eq. (5.17) and for $m = 1$ we arrive at (we introduce $\rho_{0r} = \rho_{0l} = 1/L_c$)

$$K^{(1)}(t) = \frac{1}{2} \int d\varepsilon_l \int d\varepsilon_r \rho_{0r}\rho_{0l} \frac{L_c^2}{(\varepsilon_l - \varepsilon_r)^2 + L_c^2} e^{i(\varepsilon_l - \varepsilon_r)t}[n(\varepsilon_l)[1 - n(\varepsilon_r)] + n(\varepsilon_r)[1 - n(\varepsilon_l)]].$$

For both kernels $K^{(1)}(t)$ and $K^{(2)}(t)$, one energy-integration can easily performed which leads to

$$K^{(1)}(t) = \frac{\rho_{0r}\rho_{0l}}{2} \int d\omega \frac{L_c^2}{(\omega + V)^2 + L_c^2} e^{i(\omega + V)t} \left[\omega \coth\left(\frac{\beta\omega}{2}\right)\right],$$

$$K^{(2)}(t) = \frac{\rho_{0r}\rho_{0l}}{2} \int d\omega \frac{L_c^2}{(\omega + V)^2 + L_c^2} e^{i(\omega + V)t}[-\omega].$$

With that we can find exact analytical expressions for the kernels $\mathcal{K}_{+/-}^{(1/2)}(t)$ and $\tilde{\mathcal{K}}_{+/-}^{(1/2)}(t)$ by solving the following integrals ($\alpha_1, \alpha_2 \in \{-1, 1\}$)

$$
\begin{aligned}
\mathcal{L}^{(1)}(\alpha_1, \alpha_2, t) &= \int_0^t d\tau K^{(1)}(\alpha_1 \tau) e^{i\alpha_2 \Omega \tau} \\
&= \frac{\rho_{0r}\rho_{0l}}{2} \int d\omega \frac{iL_c^2[1 - e^{it(\alpha_1(\omega+V)+\alpha_2\Omega)}]}{[(\omega+V)^2 + L_c^2][\alpha_1(w+V)+\alpha_2\Omega]} \left[\omega \coth\left(\frac{\beta\omega}{2}\right)\right] , \quad (5.18) \\
\mathcal{L}^{(2)}(\alpha_1, \alpha_2, t) &= \int_0^t d\tau K^{(2)}(\alpha_1 \tau) e^{i\alpha_2 \Omega \tau} \\
&= \frac{\rho_{0r}\rho_{0l}}{2} \int d\omega \frac{iL_c^2[1 - e^{it(\alpha_1(\omega+V)+\alpha_2\Omega)}]}{[(\omega+V)^2 + L_c^2][\alpha_1(w+V)+\alpha_2\Omega]} \left[-\omega\right] .
\end{aligned}
$$

For both functions $\mathcal{L}^{(1/2)}(\alpha_1, \alpha_2, t)$ the integration over ω can be done with the residue theorem. The integrand of function $\mathcal{L}^{(2)}(\alpha_1, \alpha_2, t)$ has poles at $\omega_{1/2} = -V \pm iL_c$ and $\omega_3 = -V - \alpha_2/\alpha_1 \Omega$. For the integral in Eq. (5.18) we write

$$
\coth\left(\frac{\beta\omega}{2}\right) = \sum_{n=-\infty}^{\infty} \frac{2}{\beta} \frac{\omega}{\omega^2 + \nu_n^2} ,
$$

where ν_n are the Matsubara frequencies $\nu_n = 2\pi n/\beta$, i.e., for the integrand in Eq. (5.18) we have additional poles at $\omega_{4/5} = \pm i\nu_n$. Having solved the integral with the residue theorem, we are left with an infinite sum over the Matsubara frequencies for which we can also find an analytical expression. This solution is however, too lengthy to be presented here. Finally, the kernels $\mathcal{K}_{+,-}^{(1/2)}(t)$ and $\tilde{\mathcal{K}}_{+/-}^{(1/2)}(t)$ are given by

$$
\begin{aligned}
\mathcal{K}_+^{(1)}(t) &= \frac{1}{2}\gamma_x^2 \left[\mathcal{L}^{(1)}(+,+,t) + \mathcal{L}^{(1)}(-,-,t) + \mathcal{L}^{(1)}(+,-,t) + \mathcal{L}^{(1)}(-,+,t)\right] , \\
\tilde{\mathcal{K}}_+^{(1)}(t) &= \frac{1}{2i}\frac{\gamma_x^2}{m\Omega} \left[\mathcal{L}^{(1)}(+,+,t) - \mathcal{L}^{(1)}(-,-,t) - \mathcal{L}^{(1)}(+,-,t) + \mathcal{L}^{(1)}(-,+,t)\right] , \\
\mathcal{K}_-^{(2)}(t) &= \frac{1}{2}\gamma_x^2 \left[\mathcal{L}^{(2)}(+,+,t) - \mathcal{L}^{(2)}(-,-,t) + \mathcal{L}^{(2)}(+,-,t) - \mathcal{L}^{(2)}(-,+,t)\right] , \\
\tilde{\mathcal{K}}_-^{(2)}(t) &= \frac{1}{2i}\frac{\gamma_x^2}{m\Omega} \left[\mathcal{L}^{(2)}(+,+,t) + \mathcal{L}^{(2)}(-,-,t) - \mathcal{L}^{(2)}(+,-,t) - \mathcal{L}^{(2)}(-,+,t)\right] .
\end{aligned}
$$

5.3.2 Entanglement in the non-Markovian regime

We now investigate the system's dynamics, where we take the vacuum state as an initial state, which is Gaussian, allowing us to use the logarithmic negativity $E_N(t)$ as a measure of entanglement. We will study the dependence of the entanglement on the electronic temperature in the reservoir T, the finite correlation time in the reservoir L_c, and the applied bias voltage V.

In Fig. 5.3, we show the logarithmic negativity for two finite electronic temperatures and for each temperature we probe the bias dependence of the logarithmic negativity. First, we see very little entanglement for high electronic temperatures (as compared to low electronic temperatures, cf. Fig. 5.4 and 5.5) which also vanishes rather quickly. Furthermore, for very
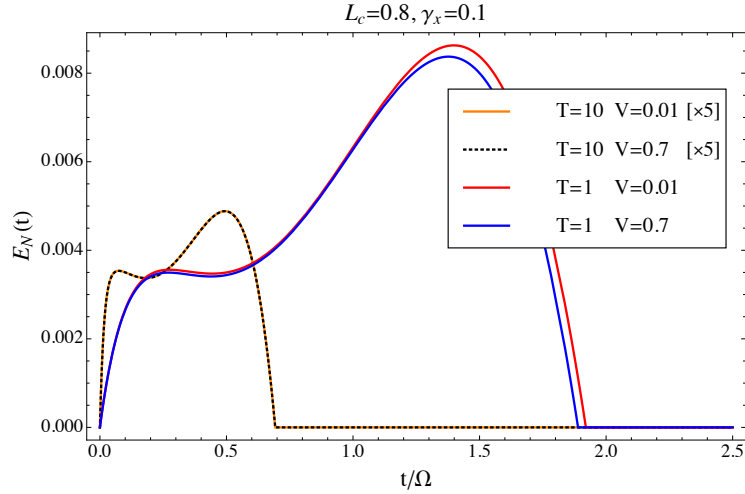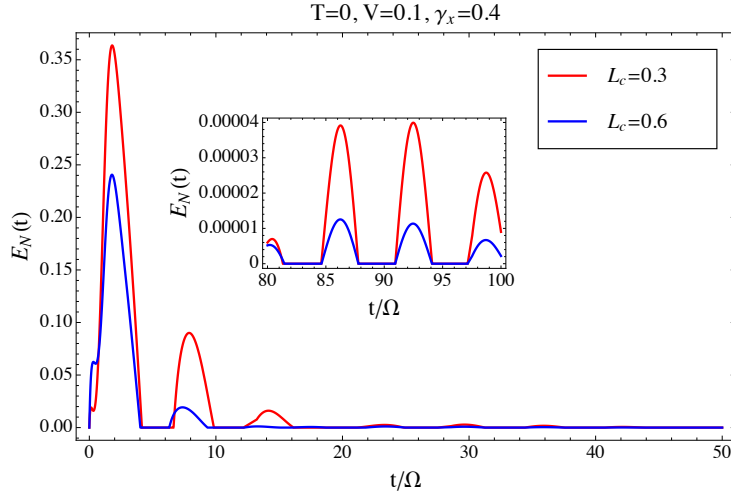
Figure 5.3: Logarithmic negativity for finite electronic temperatures. We show $E_N(t)$ for $T = 10\,\Omega$ (black and orange) and $T = \Omega$ (red and blue). High electronic temperatures lead to a fast decay of the entanglement. The dependence on the bias voltage for high electronic temperatures is negligible.

high electronic temperatures, here we show $T = 10\,\Omega$ (black and orange lines in Fig. 5.3), the bias dependence of the logarithmic negativity can be neglected. As soon as $T \approx \Omega$ (red and blue lines in Fig. 5.3), the bias dependence on the logarithmic dependence gets more pronounced (red and blue lines in Fig. 5.3), and we see less entanglement for higher V. This also reflects the fact that the tunnel junction can be assigned with an effective temperature which is proportional to the applied bias voltage [Mozyrsky02]. We can say that the influence of the bias voltage in the high temperature regime is negligible since in most cases we have $V < T$. A higher temperature of the electronic reservoir (than the effective temperature of the oscillator) might be hard to achieve in an experimental setup. When aiming to study this regime, it is necessary to actively cool the nanomechanical resonator to its ground state by applying techniques as for instance in Ref. [O'Connell10], where a qubit is coupled to the resonator and excitations can be swapped from the oscillator to the qubit.

For low electronic temperatures, we show in Fig. 5.4 and 5.5 the logarithmic negativity for $\gamma_x = 0.4\sqrt{m\Omega}$ and $\gamma_x = 0.1\sqrt{m\Omega}$, respectively, and its dependence on L_c. In both cases, we clearly see that the initially separable state becomes entangled right after the interactions have been suddenly switched on. Due to this quench, energy conservation can be violated for a short time, which is the cause for the entanglement. Experimentally, the switching in this tunneling setup can be achieved by gates controlling the tunnel coupling via a resonance. Physically this means, that the rise time of the gates has to be shorter than $1/\Omega$, the time scale of the oscillators. Typical rise times of electronic gates can be as short as $60\,\text{ps}$ [Dovzhenko11]. For an oscillator with a resonance frequency of $\sim 500\,\text{MHz}$ (which can be brought into its ground state at low temperatures) these rise times are sufficient to accomplish the sudden switching. In its subsequent evolution, the entanglement oscillates in time, before it slowly decays. We find that low bias voltages show an increased logarithmic negativity compared to high bias voltages (not shown in the figure). When we compare Figs. 5.4 and 5.5, we find that the entanglement decays faster with an increased coupling

Figure 5.4: Logarithmic negativity for $L_c = 0.3\,\Omega$ (red) and $L_c = 0.6\,\Omega$ (blue). Here, the temperature $T = 0$, $V = 0.1\,\Omega$, and $\gamma_x = 0.4\sqrt{m\Omega}$.
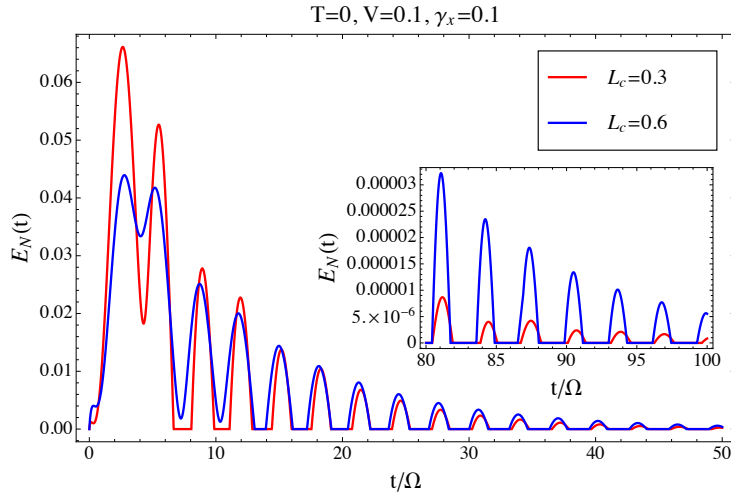
Figure 5.5: (Color online) Logarithmic negativity for $L_c = 0.3\,\Omega$ (red) and $L_c = 0.6\,\Omega$ (blue). Here, the temperature $T = 0$, $V = 0.1\,\Omega$, and $\gamma_x = 0.1\sqrt{m\Omega}$.

parameter γ_x. For a large coupling γ_x, the entanglement for small L_c is more pronounced than for large L_c. However, we see from Fig. 5.5 that entanglement for small L_c decreases faster compared to entanglement in the case of large L_c. Intuitively, we might guess that a small L_c is favorable for the time evolution of the entanglement, because a large L_c means a more rapid loss of coherence in the reservoir (as it is the case for larger coupling, cf. Fig. 5.4).

However, this counter intuitive dependence of $E_N(t)$ on the parameter L_c can be understood with the help of the toy model of two directly coupled harmonic oscillators, described by the

Hamiltonian

$$H_{TM} = \sum_{i=1,2} \frac{\hat{p}_i^2}{2m_i} + \frac{1}{2}m_i\Omega_i^2\hat{x}_i^2 + \lambda\hat{x}_1\hat{x}_2 \,.$$

We will briefly discuss this toy model, firstly, by employing a rotating wave approximation (RWA), and secondly without the RWA. Within the RWA, only energy conserving processes are allowed, i.e., we only can swap excitations from one oscillator to the other one. When taking the vacuum state as an initial state, there won't be any excitations regarding the oscillators, which is not favorable for entanglement. To conclude, in the RWA, the two oscillators in the toy model initially prepared in their ground state won't get entangled. This is different for the case when we do not employ the RWA because then, processes which can violate energy conservation for a short time after the interaction has been suddenly switched on, are present. To sum up, these processes are favorable for entanglement when the initial state is the Gaussian vacuum state. This argument can now also be made for Setup (A). In this case, the processes which favor a violation of energy conservation are the ones with a large L_c, i.e., for larger L_c the entanglement generated by a sudden switching on of interactions lasts longer than for smaller L_c.

In summary, we showed that Setup (A) indeed is suitable for generating entanglement between two indirectly coupled nanomechanical oscillators. We see from the various plots of the logarithmic negativity that there is a competition of processes favoring entanglement and processes leading to damping and/or decoherence. Due to the nontrivial dependence of the symplectic eigenvalue $\tilde{\lambda}_-$ on the involved parameters, the dependence of $E_N(t)$ on the parameters can be counter intuitive as we just discussed for L_c. Although this setup is rather academic, it serves us as a model and provides us with new insight into the situation where two nanomechanical oscillators are effectively coupled through two common fermionic baths. This is a less studied case compared to the more established case of coupling two oscillators to a common bosonic bath, for instance, within a Caldeira-Leggett model [Liu07]. In the next section, we analyze a second possible realization where we circumvent the need of a common macroscopic reservoir (i.e., the right reservoir in Fig. 5.1).

5.4 Coupling in an Andreev entangler setup – Setup (B)

Since Setup (A) relies on a long coherence time of two macroscopic reservoirs, we introduce another realization that gives rise to an effective coupling of the two oscillators mediated by tunneling of a split Cooper-pair. This realization, Setup (B), is of an Andreev entangler type of setup. The process where a spin-singlet is split in the superconductor and one electron tunnels to the lower oscillator and the other one tunnels to the upper oscillator gives rise to an effective coupling between the two nanomechanical oscillators, cf. Fig. 5.6. The major improvements of Setup (B) over Setup (A) are:

1. the right common reservoir of Setup (A) is now cut into two halves; the resulting two normal metal leads are entirely *independent*

2. both normal metal leads see the same tunneling processes; therefore their independence does not result in which-path information

3. phase coherence lengths of superconductors are typically much longer than of normal metals which allows for a larger spatial extend of the center reservoir.
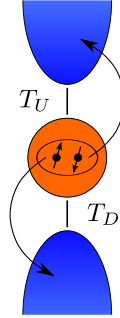
Figure 5.6: Schematics of the process we focus on. A Cooper-pair is split on on the superconducting island (orange). The two electrons of the Cooper-pair tunnel to different oscillators acting as leads (blue) which leads to an effective coupling between the two oscillators. The tunneling amplitudes are defined as $T_\alpha = \gamma_{0\alpha} + \gamma_{x\alpha}\hat{x}_\alpha$.

Processes where one Cooper-pair tunnels to the upper/lower lead are not taken into account since they won't lead to any entanglement, but rather to a background tunneling current. As for instance described in Ref. [Recher01], such processes are also energetically not favorable due to interaction effects in the leads and/or tunneling via a dot with a finite charging energy. Another possibility to favor the tunneling process where a Cooper-pair is split, is to couple the superconductor to two Luttinger liquid leads as described in Ref. [Recher02]. In NEMS this could be achieved by modeling the oscillators as one-dimensional nanowires or carbon nanotubes.

Below, we study the Setup (B) in two different regimes: First, the non-Markovian regime as we also did for Setup (A), and additionally in the Markovian regime in the limit of low bias voltages. The non-Markovian regime of Setup (B) is very similar to the non-Markovian regime of Setup (A). For Setup (B) we will see that the master equation for the reduced system in the Markovian regime is of Lindblad form which allows us study the system dynamics on a very intuitive level.

The system is again described by the Hamiltonian in Eq. (5.2) with H_S given in Eq. (5.7). Here, the bath consists of three independent reservoirs, two normal metal leads, and a central superconducting region. We focus here on transport at energies in the superconducting gap Δ, which is the largest energy scale of the problem. The bath Hamiltonian reads

$$H_B = H_I + H_U + H_D \,,$$

where

$$H_\alpha = \sum_{k\sigma} \varepsilon_{\alpha k} b^\dagger_{\alpha k\sigma} b_{\alpha k\sigma} \,,$$
$$H_I = \sum_{k\sigma} E_k \beta^\dagger_{k\sigma} \beta_{k\sigma}$$

with $\alpha = U, D$. Here, $E_k = \sqrt{(\varepsilon_k - \mu_S)^2 + \Delta^2}$ is the quasiparticle energy and $\beta_{k\sigma}$ is the quasiparticle annihilation operator. The quasiparticle operators are related to electron annihilation operators through the Bogoliubov transformation

$$c_{k\uparrow} = u_k \beta_{k\uparrow} + v_k \beta_{-k\downarrow}^\dagger ,$$
$$c_{-k\downarrow} = u_k \beta_{-k\downarrow} - v_k \beta_{k\uparrow}^\dagger ,$$

where $u_k = \sqrt{1/2 + \xi_k/(2E_k)}$ and $v_k = \sqrt{1/2 - \xi_k/(2E_k)}$ with $\xi_k = \varepsilon_k - \mu_S$. We take the superconductor to be grounded and each lead to be held at bias voltage V. The system-bath interaction is mediated by tunneling of a split Cooper-pair, i.e., we want one electron of the Cooper pair to tunnel to the upper oscillator and the other electron to tunnel to the lower oscillator. The process we want to focus on is therefore described by the following Hamiltonian

$$H_{SB} = \sum_{\{k_i\}} T_U T_D b_{D-k_1\downarrow}^\dagger b_{Uk_2\uparrow}^\dagger c_{I-k_3\downarrow} c_{Ik_4\uparrow} + T_U T_D b_{Dk_1\uparrow}^\dagger b_{U-k_2\downarrow}^\dagger c_{I-k_3\downarrow} c_{Ik_4\uparrow} + \text{H.c.} \qquad (5.19)$$

with $T_\alpha = \gamma_{0\alpha} + \gamma_{x\alpha} \hat{x}_\alpha$. We introduce the following system and bath operators

$$S_0 = \gamma_{0U} \gamma_{0D} ,$$
$$S_1 = \gamma_{0D} \gamma_{xU} \hat{x}_U ,$$
$$S_2 = \gamma_{0U} \gamma_{xD} \hat{x}_D ,$$
$$S_3 = \gamma_{xU} \gamma_{xD} \hat{x}_D \hat{x}_U ,$$

and

$$E = b_{D-k_1\downarrow}^\dagger b_{Uk_2\uparrow}^\dagger c_{I-k_3\downarrow} c_{Ik_4\uparrow} , \qquad (5.20)$$

respectively, which allow us to write the system-bath coupling Hamiltonian in a similar way as in Eq. (5.8)

$$H_{SB} = \sum_{\{k_i\}} \left[S_0 + S_1 + S_2 + S_3 \right] \left[E + E^\dagger \right] .$$

5.4.1 Equation of motion and memory kernels in the Andreev entangler setup

The equation of motion for the reduced density matrix can then be written as (note that we switched from U, D to $1, 2$)

$$
\begin{aligned}
\dot{\rho_S}(t) = &- i \left[H_S + i\mathcal{K}_-^{(2)}(t)(\hat{x}_1 + \hat{x}_2)^2, \rho_S(t) \right] \\
&- \mathcal{K}_+^{(1)}(t) \left[\hat{x}_1 + \hat{x}_2, [\hat{x}_1 + \hat{x}_2, \rho_S(t)] \right] \\
&+ \tilde{\mathcal{K}}_+^{(1)}(t) \left[\hat{x}_1 + \hat{x}_2, [\hat{p}_1 + \hat{p}_2, \rho_S(t)] \right] \\
&+ \tilde{\mathcal{K}}_-^{(2)}(t) \left[\hat{x}_1 + \hat{x}_2, \{\hat{p}_1 + \hat{p}_2, \rho_S(t)\} \right] \\
&- \mathcal{K}_+^{(3,1)}(t) \left[\hat{x}_1 \hat{x}_2, [\hat{x}_1 \hat{x}_2, \rho_S(t)] \right] \\
&- \mathcal{K}_+^{(3,2)}(t) \left[\hat{x}_1 \hat{x}_2, [\hat{p}_1 \hat{p}_2, \rho_S(t)] \right] \\
&+ \mathcal{K}_+^{(3,3)}(t) \left[\hat{x}_1 \hat{x}_2, [\hat{x}_1 \hat{p}_2 + \hat{x}_2 \hat{p}_1, \rho_S(t)] \right] \\
&- \mathcal{K}_-^{(3,1)}(t) \left[\hat{x}_1 \hat{x}_2, \{\hat{x}_1 \hat{x}_2, \rho_S(t)\} \right] \\
&- \mathcal{K}_-^{(3,2)}(t) \left[\hat{x}_1 \hat{x}_2, \{\hat{p}_1 \hat{p}_2, \rho_S(t)\} \right] \\
&+ \mathcal{K}_-^{(3,3)}(t) \left[\hat{x}_1 \hat{x}_2, \{\hat{x}_1 \hat{p}_2 + \hat{x}_2 \hat{p}_1, \rho_S(t)\} \right] .
\end{aligned}
\tag{5.21}
$$

Already at this stage, it is important to comment on the decisive difference between Setup (A) and (B). The effective Hamiltonian in Eq. (5.19), exhibits two important but different contributions. The first contribution stems from terms of order $\gamma_0 \gamma_x$. These terms are qualitatively similar to terms of order γ_x in Setup (A), meaning that to second order in γ_x we expect qualitatively the same behavior for the logarithmic negativity. The second contribution of the effective Hamiltonian is due to terms of order γ_x^2 which give rise to a direct coupling between the two oscillators, and are new in the Andreev entangler setup (terms five to nine in Eq. (5.21)). We will treat these two contributions independently, by focusing on different regimes where only one of them is dominant. Finally, the time-dependent memory kernels in Eq. (5.21) are defined as (for simplicity, we again assume symmetric coupling and identical oscillators)

$$
\begin{aligned}
\mathcal{K}_+^{(1)}(t) &= \int_0^t d\tau \left[K^{(1)}(\tau) + K^{(1)}(-\tau) \right] \gamma_0^2 \gamma_x^2 \cos(\Omega\tau) , \\
\tilde{\mathcal{K}}_+^{(1)}(t) &= \int_0^t d\tau \left[K^{(1)}(\tau) + K^{(1)}(-\tau) \right] \frac{\gamma_0^2 \gamma_x^2}{m\Omega} \sin(\Omega\tau) , \\
\mathcal{K}_-^{(2)}(t) &= \int_0^t d\tau \left[K^{(2)}(\tau) - K^{(2)}(-\tau) \right] \gamma_0^2 \gamma_x^2 \cos(\Omega\tau) , \\
\tilde{\mathcal{K}}_-^{(2)}(t) &= \int_0^t d\tau \left[K^{(2)}(\tau) - K^{(2)}(-\tau) \right] \frac{\gamma_0^2 \gamma_x^2}{m\Omega} \sin(\Omega\tau) , \\
\mathcal{K}_+^{(3,1)}(t) &= \int_0^t d\tau \left[K^{(1)}(\tau) + K^{(1)}(-\tau) \right] \gamma_x^4 \cos(\Omega\tau) \cos(\Omega\tau) , \\
\mathcal{K}_+^{(3,2)}(t) &= \int_0^t d\tau \left[K^{(1)}(\tau) + K^{(1)}(-\tau) \right] \frac{\gamma_x^4}{m^2\Omega^2} \sin(\Omega\tau) \sin(\Omega\tau) ,
\end{aligned}
$$

$$\mathcal{K}_+^{(3,3)}(t) = \int_0^t d\tau \left[K^{(1)}(\tau) + K^{(1)}(-\tau) \right] \frac{\gamma_x^4}{m\Omega} \cos(\Omega\tau)\sin(\Omega\tau)\,,$$

$$\mathcal{K}_-^{(3,1)}(t) = \int_0^t d\tau \left[K^{(2)}(\tau) - K^{(2)}(-\tau) \right] \gamma_x^4 \cos(\Omega\tau)\cos(\Omega\tau)\,,$$

$$\mathcal{K}_-^{(3,2)}(t) = \int_0^t d\tau \left[K^{(2)}(\tau) - K^{(2)}(-\tau) \right] \frac{\gamma_x^4}{m^2\Omega^2} \sin(\Omega\tau)\sin(\Omega\tau)\,,$$

$$\mathcal{K}_-^{(3,3)}(t) = \int_0^t d\tau \left[K^{(2)}(\tau) - K^{(2)}(-\tau) \right] \frac{\gamma_x^4}{m\Omega} \cos(\Omega\tau)\sin(\Omega\tau)\,.$$

The kernels $K^{(1/2)}(t)$ are given in Eq. (5.5) and (5.6) with E given in Eq. (5.20). The actual calculation of the kernels for the Andreev entangler setup goes along the same lines as for Setup (A). Therefore, we only sketch the calculation briefly. The kernels $K^{(m)}(t,t')$, ($m=1,2$) in the superconducting case become

$$K^{(m)}(t,t_1) = \frac{1}{2} \sum_{\{k_i\}} e^{i(\varepsilon_{k_1}^D + \varepsilon_{k_2}^U)(t-t_1)} u_{k_3} v_{k_3} u_{k_4} v_{k_4} \Big\{ n(\varepsilon_{k_1}^D)[1 - 2n(E_{k_3})]n(\varepsilon_{k_2}^U)[1 - 2n(E_{k_4})]$$

$$- (-1)^m [1 - n(\varepsilon_{k_1}^D)][1 - 2n(E_{k_3})][1 - n(\varepsilon_{k_2}^U)][1 - 2n(E_{k_4})] \Big\}\,, \qquad (5.22)$$

where we introduced the superconducting Green's functions

$$\langle c_{I-k\downarrow}(t) c_{Ik\uparrow}(t') \rangle = u_k v_k \left\langle \beta_{-k\downarrow}(t)\beta_{-k\downarrow}^\dagger(t') - \beta_{k\uparrow}^\dagger(t')\beta_{k\uparrow}(t) \right\rangle$$

$$= u_k v_k \left[e^{iE_k(t-t')}(1 - n(E_k)) - e^{-iE_k(t-t')}n(E_k) \right]\,,$$

and

$$\left\langle c_{Ik\uparrow}^\dagger(t) c_{I-k\downarrow}^\dagger(t') \right\rangle = u_k v_k \left[e^{iE_k(t-t')}(1 - n(E_k)) - e^{-iE_k(t-t')}n(E_k) \right]\,.$$

Now, we proceed along the lines of the calculation we already did in the case of Setup (A). In Eq. (5.22), we first take the sum over the momenta to an integral and introduce an energy-dependent density of states for the normal metal leads. Since we only focus on the regime within the superconducting gap, the density of states in the superconductor is constant. We furthermore assume zero temperature in the superconductor, therefore no quasiparticles in the superconductor can be excited, leading to $n(E_{k_i}) = 0$. For $K^{(m)}(t',t'') = K^{(m)}(t'-t'') \equiv K^{(m)}(t)$ we then have

$$K^{(m)}(t) = \frac{1}{2} \int d\varepsilon_{k_1}^D d\varepsilon_{k_2}^U d\varepsilon_{k_3} d\varepsilon_{k_4} e^{i(\varepsilon_{k_1}^D + \varepsilon_{k_2}^U)t} u_{k_3} v_{k_3} u_{k_4} v_{k_4} J(\varepsilon_{k_1}^D, \varepsilon_{k_2}^U)\rho_S\rho_S \times$$

$$\Big\{ n(\varepsilon_{k_1}^D)n(\varepsilon_{k_2}^U) - (-1)^m [1 - n(\varepsilon_{k_1}^D)][1 - n(\varepsilon_{k_2}^U)] \Big\}\,.$$

Here, the spectral function $J(\varepsilon_{k_1}^D, \varepsilon_{k_2}^U)$ is the same as for Setup (A) and given in Eq. (5.17). Both normal metal leads are held at the same chemical potential μ and the superconductor

is at $\mu_S = 0$. Next, we write $K^{(m)}(t)$ as

$$K^{(m)}(t) = \frac{\tilde{\rho}}{2} \left\{ \int d\varepsilon_{k_3} d\varepsilon_{k_4} u_{k_3} v_{k_3} u_{k_4} v_{k_4} \right\} \int d\omega \int d\omega_D e^{i(\omega+2\mu)t} \frac{L_c^2}{(\omega+2\mu)^2 + L_c^2}$$
$$\times \left\{ n(\omega_D) n(\omega - \omega_D) - (-1)^m [1 - n(\omega_D)][1 - n(\omega - \omega_D)] \right\},$$

where we defined $\tilde{\rho} = \rho_U \rho_D \rho_S \rho_S$ with $\rho_U = \rho_U = 1/L_c$. We still have to perform the integration over the momenta of the superconductor. In oder to include the free propagation of electrons in the superconducting island we now include a factor of $1/E_k$ in the tunnel amplitudes. Therefore, we have to evaluate

$$(*) = \int d\varepsilon_k \frac{u_k v_k}{E_k} = \int d\varepsilon_k \frac{\Delta}{E_k^2} = \int_a^b d\varepsilon_k \frac{\Delta}{(\varepsilon_k - \mu_S)^2 + \Delta^2} = \arctan\left(\frac{\varepsilon_k - \mu_S}{\Delta}\right)\Big|_a^b.$$

Using $b \to \infty$ and $a \to 0$, we get

$$(*) = \left[\frac{\pi}{2} + \arctan(\frac{\mu_{SC}}{\Delta})\right]$$

which for $\mu_S = 0$ gives just a factor $\pi/2$. In the end, we find for $K^{(m)}(t)$

$$K^{(1)}(t) = \frac{\tilde{\rho}}{2} \frac{\pi^2}{4} 4 \int d\omega e^{i(\omega+2\mu)t} \frac{L_c^2}{(\omega+2\mu)^2 + L_c^2} \left[\omega \coth\left(\frac{\beta\omega}{2}\right)\right],$$
$$K^{(2)}(t) = \frac{\tilde{\rho}}{2} \frac{\pi^2}{4} 4 \int d\omega e^{i(\omega+2\mu)t} \frac{L_c^2}{(\omega+2\mu)^2 + L_c^2} [-\omega],$$

where the factor 4 is due to the spin. The calculation of the kernels $\mathcal{K}_{+/-}^{(1/2)}(t)$, $\tilde{\mathcal{K}}_{+/-}^{(1/2)}$, $\mathcal{K}_+^{(3,i)}(t)$, and $\mathcal{K}_-^{(3,i)}(t)$ can then be done with the residue theorem as for Setup (A) .

5.4.2 Entanglement in the non-Markovian regime

Here, we will only consider the leading contribution in the master equation Eq. (5.21) which are terms of order $\gamma_0^2 \gamma_x^2$ ($\gg \gamma_x^4$). In Figs. 5.7 and 5.8 we present the results for the logarithmic negativity $E_N(t)$ for Setup (B). From these figures we already see the similarity between Setup (A) and (B) and conclude that it is possible to entangle two nanomechanical resonators which are coupled to three independent reservoirs within an Andreev entangler setup. Similar to Setup (A) we see a faster decay of the entanglement for larger couplings γ_x. The dependence on the parameter L_c is analogous to Setup (A) where we explained with the help of a toy model the counter intuitive behavior of the logarithmic negativity.
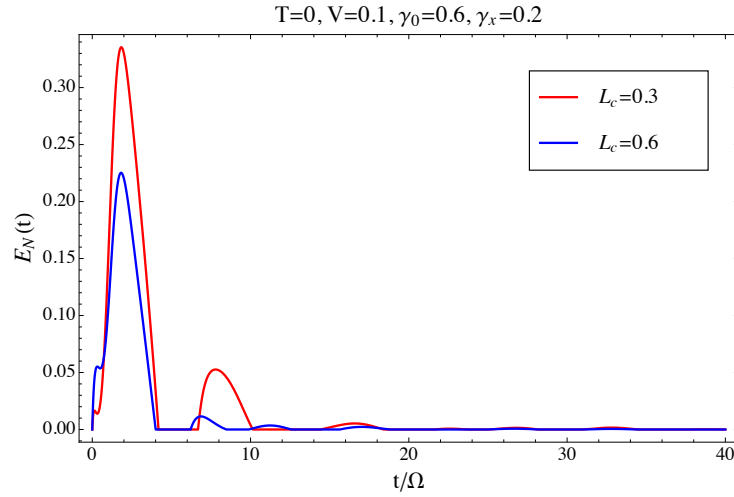
Figure 5.7: Logarithmic negativity for $L_c = 0.3\,\Omega$ (red) and $L_c = 0.6\,\Omega$ (blue). Here, the temperature $T = 0$, $V = 0.1\,\Omega$, $\gamma_0 = 0.6$, and $\gamma_x = 0.2\,\sqrt{m\Omega}$.
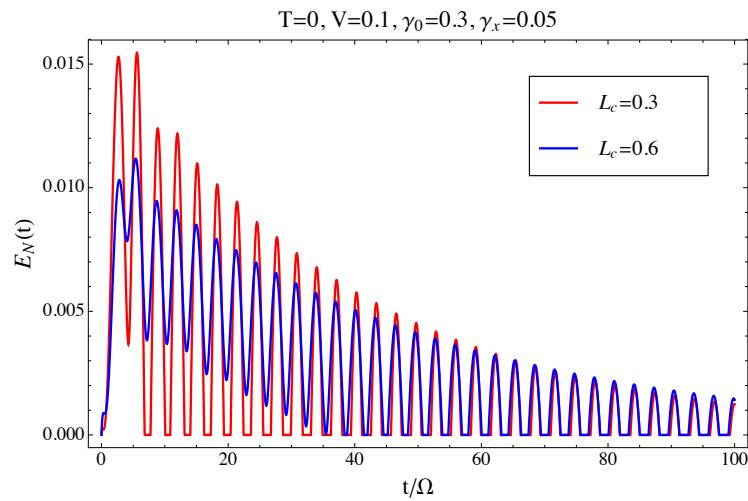
Figure 5.8: Logarithmic negativity for $L_c = 0.3\,\Omega$ (red) and $L_c = 0.6\,\Omega$ (blue). Here, the temperature $T = 0$, $V = 0.1\,\Omega$, $\gamma_0 = 0.3$, and $\gamma_x = 0.05\,\sqrt{m\Omega}$.

5.4.3 Entanglement in the Markovian regime

As we already mentioned, the master equation for the reduced system's density matrix has two distinct contributions, terms of order $\gamma_0^2 \gamma_x^2$ and of order γ_x^4. In this section, we want to focus on terms that are of order γ_x^4 only because they give rise to a direct coupling between the two oscillators and are a new element in the Andreev entangler setup. Interestingly, these terms can even generate entanglement in the Markovian regime. The regime, where they are the dominant contributions, is the low bias limit, i.e., $V \ll \Omega$ because then it is not possible to excite the oscillator due to the applied bias. Excitations are still possible due to the quench stemming from the sudden switching on of the interaction. In addition, we apply the Markov approximation, meaning we take the wide band limit, $L_c \to \infty$ (energy-independent density of states), and we let the upper integration limit in the expressions for the kernels $\mathcal{K}_{+/-}^{(1/2)}(t)$, $\tilde{\mathcal{K}}_{+/-}^{(1/2)}$, $\mathcal{K}_+^{(3,i)}(t)$, and $\mathcal{K}_-^{(3,i)}(t)$ go to $t \to \infty$. With

$$\int_0^\infty dt\, e^{\pm i\omega t} = \pi \delta(\omega) \pm i P \frac{1}{\omega}\,,$$

where P stands for the Cauchy principal value, we can perform the time integration in the expressions for the kernels $\mathcal{K}_{+/-}^{(1/2)}(t)$, $\tilde{\mathcal{K}}_{+/-}^{(1/2)}$, $\mathcal{K}_+^{(3,i)}(t)$, and $\mathcal{K}_-^{(3,i)}(t)$ which then become time-independent. The resulting master equation in the limit of $T \to 0$ and in the RWA is of Lindblad form and given by

$$\dot{\rho_S}(t) = - i\left[H_S, \rho_S(t)\right] + \frac{\tilde{\rho}\pi^3 \gamma_x^4 V}{(m\Omega)^2}\left[A\rho_S(t)A - \frac{1}{2}\left\{AA, \rho_S(t)\right\}\right]\,, \tag{5.23}$$

where the Lindblad operator $A = \hat{a}_1^\dagger \hat{a}_2 + \hat{a}_1 \hat{a}_2^\dagger$, and $\tilde{\rho} = \rho_U \rho_D \rho_S \rho_S$ with ρ_α and ρ_S being constant density of states in lead α and the superconductor, respectively. We also introduced bosonic creation (annihilation) operators $\hat{a}_i^\dagger$ $(\hat{a}_i)$ for both oscillators in the usual way

$$\hat{x}_i = \frac{1}{\sqrt{2m_i\Omega_i}}(\hat{a}_i + \hat{a}_i^\dagger)$$

$$\hat{p}_i = -i\sqrt{\frac{m_i\Omega_i}{2}}(\hat{a}_i - \hat{a}_i^\dagger)\,.$$

As we mentioned earlier, processes which violate energy conservation for a short time are favorable for entanglement. In Lindblad form, there are no such terms, i.e., if the initial state of the system would be the vacuum state, we do not expect any entanglement. However, if we choose a different initial state, things are different. To exemplify the dynamics generated by the Lindblad operator A for a different initial state, we choose $|n_1 = 1, n_2 = 1\rangle$ with n_i being the occupation number of oscillator i. Due to Eq. (5.23) the dynamics will only generate states $|n_1 = 2, n_2 = 0\rangle$ and $|n_1 = 0, n_2 = 2\rangle$. The system will stay in this three-dimensional Hilbert space. The initial state evolves to

$$p_1(t)|1,1\rangle + p_2(t)\left(|2,0\rangle + |0,2\rangle\right)\,.$$

A definite indicator for entanglement in this case is the prefactor $p_2(t)$ in front of the Bell state. Here, we just want to make the point that within the Andreev entangler setup we can generate an entangled state even in the Markovian regime.

5.5 Concluding remarks

We introduced two setups, where we have shown that it is possible to generate entanglement between two spatially separated nanoelectromechanical oscillators, even if these two oscillators are not directly coupled to each other. In Setup (A), the two oscillators are indirectly coupled via two common fermionic baths which should have a rather long coherence time. With Setup (B), we introduced an entirely new way of entangling two nanomechanical oscillators in an electric setup based on the working principle of an Andreev entangler. Here, the coherent process where a Cooper-pair is split leads to an effective coupling of the two nanomechanical oscillators. For both setups, the generated entanglement persists over many oscillator periods, before the system becomes separable again. Further investigations on these kinds of setups could deal with the question how it might be possible to generate steady state entanglement of the oscillators, by for instance applying an AC or pulsed bias voltage.

Part IV

Summary and outlook

Summary

Since we have in each chapter given a detailed summary and conclusion, we here only mention the main aspects of the work covered in this thesis.

With recent nanomechanical experiments already being in the quantum regime, the focus of this thesis was on the quantum regime of nanoelectromechanical systems. We studied different aspects of the quantum regime, such as non-Markovian effects of a nanomechanical oscillator coupled to a tunnel junction detector where we employed non-equilibrium methods to calculate transport properties. Since the electronic degrees of freedom couple to the mechanical ones, the transport quantities such as the average tunnel current or the current noise are directly related to the properties of the nanomechanical oscillator, allowing for its characterization via transport measurements. Furthermore, we presented a novel possibility to detect new states of matter using a nanomechanical resonator. This naturally could lead to the application of a nanomechanical oscillator as a detector for other physical degrees of freedom and make nanomechanical systems even more promising detectors also for other quantities than just mass and force. Finally, we studied the generation of entanglement between two mesoscopic resonators in an electric setup. We investigated two different kinds of setups where the two oscillators are not directly coupled to each other, but an effective coupling is mediated between them by common electronic reservoirs or by tunneling Cooper-pairs. If both oscillators are initially in their ground states (a separable state of the composite system), it is possible by running a current through the device to bring the oscillators into an entangled state. Since quantum mechanics in general also allows for entanglement of objects with length scales larger than atomic or subatomic, such studies allow for testing quantum mechanics on an entirely new length scale. This intermediate regime between classical and quantum also allows to investigate fundamental questions of quantum theory and the quantum to classical transition.

Outlook

Nanoelectromechanical systems as we studied in this thesis, i.e., where a rather massive conducting beam is coupled to a tunnel junction detector, have a major disadvantage which is the trouble that comes with manufacturing these devices. In my opinion, experimental realizations comparable to the vibrating membrane in Ref. [Teufel11] are the ones to be studied in the future since such setups are more flexible with respect to control, read out, and weak or strong electromechanical coupling of the oscillator to the electronics. Suspended carbon nanotubes or graphene sheets and ribbons comprise, due to their stiffness, also very high quality resonators which can be coupled to electronic devices. Moreover, a quantum dot can be formed on the vibrating carbon nanotube and one could imagine, coupling the mechanical degree of freedom directly to the occupation number of the dot, or even to the spin degree of freedom of an electron on the quantum dot.

Future theoretical work which could directly result from the work presented here, is the need of a feasible detection scheme for the entanglement of the two nanomechanical oscillators in Chap. 5. As we discussed in Chap. 5 we need information of the second moments of the conjugate variables $\hat{x}_i$ and $\hat{p}_i$, i.e., the covariance matrix. In case of Setup (A) we could

imagine following a detection scheme similar to the one proposed in Ref. [Schmidt10]. In this case we would have to add a third tunnel junction to Setup (A), thereby generating two Aharonov Bohm loops and in turn it would possible to gain information on the position and momentum (cf. Chap. 3) of the two oscillators. Entanglement can then be verified by information gained in current noise measurements which can be used to calculate the logarithmic negativity. In the case of the Andreev entangler such a detection scheme for entanglement is not feasible. However, it could be possible that a measurement of current cross-correlation leads to enough information to verify entanglement via an entanglement witness. If in the case of the Andreev entangler we are not able to fully obtain the covariance matrix, there are certain bounds that can be used to estimate the amount of entanglement. For instance we could use the bound $E_N \geq \max\{0, -\log_2[\langle (\hat{x}_1 - \hat{x}_2)^2 \rangle /2 + \langle (\hat{p}_1 + \hat{p}_2)^2 \rangle /2]\}$, where we already see that less information is needed to verify entanglement.

Another unaddressed issue so far is the calculation of the current noise of the nanomechanical Majorana bound state detector, cf. Chap. 4. This would of course be a natural extension since the current noise can be experimentally measured fairly easy and contains more information than the differential conductance. In this setup, we can also attached a second oscillating lead left of the topological superconductor which couples to the left Majorana bound state. The interplay between the two oscillating leads and the tunneling through the nonlocal Majorana bound state might reveal new transport features of the Majorana bound state which can be probed with current cross-correlations.

To summarize, due to their enormous potential for technical applications and the possibility to study fundamental questions of quantum mechanics, the field of nanoelectromechanical systems will definitively evolve further and we expect more interesting physics to come.

Bibliography

[Akhmerov09] A. Akhmerov, J. Nilsson, and C. Beenakker. *Electrically Detected Interferometry of Majorana Fermions in a Topological Insulator.* Phys. Rev. Lett. **102**, 216404 (2009).

[Alicea10] J. Alicea. *Majorana fermions in a tunable semiconductor device.* Phys. Rev. B **81**, 125318 (2010).

[Alicea11] J. Alicea, Y. Oreg, G. Refael, F. v. Oppen, and M. P. A. Fisher. *Non-Abelian statistics and topological quantum information processing in 1D wire networks.* Nat. Phys. **7**, 412 (2011).

[Alicea12] J. Alicea. *New directions in the pursuit of Majorana fermions in solid state systems.* Rep. Prog. Phys. **75**, 076501 (2012).

[Armour04a] A. Armour. *Current noise of a single-electron transistor coupled to a nanomechanical resonator.* Phys. Rev. B **70**, 165315 (2004).

[Armour04b] A. Armour, M. Blencowe, and Y. Zhang. *Classical dynamics of a nanomechanical resonator coupled to a single-electron transistor.* Phys. Rev. B **69**, 125313 (2004).

[Aspect81] A. Aspect, P. Grangier, and G. Roger. *Experimental tests of realistic local theories via Bell's theorem.* Phys. Rev. Lett. **47**, 460 (1981).

[Aspect82] A. Aspect, P. Grangier, and G. Roger. *Experimental realization of Einstein-Podolsky-Rosen-Bohm Gedankenexperiment: A New violation of Bell's inequalities.* Phys. Rev. Lett. **49**, 91 (1982).

[Aspelmeyer10] M. Aspelmeyer, S. Groeblacher, K. Hammerer, and N. Kiesel. *Quantum optomechanics—throwing a glance [Invited].* J. Opt. Soc. Am. B **27**, A189 (2010).

[Bagrets12] D. Bagrets and A. Altland. *Class D spectral peak in Majorana quantum wires.* arXiv:1206.0434 (2012).

[Bardeen57] J. Bardeen, L. N. Cooper, and J. R. Schrieffer. *Theory of superconductivity.* Phys Rev **108**, 1175 (1957).

[Barzanjeh11] S. Barzanjeh, D. Vitali, P. Tombesi, and G. Milburn. *Entangling optical and microwave cavity modes by means of a nanomechanical resonator.* Phys. Rev. A **84**, 042342 (2011).

[Beenakker11] C. W. J. Beenakker. *Search for Majorana fermions in superconductors.* arXiv:1112.1950 (2011).

[Bell64] J. S. Bell. *On the Einstein-Podolsky-Rosen paradox.* Physics **1**, 195 (1964).

[Bellomo10] B. Bellomo, R. L. Franco, S. Maniscalco, and G. Compagno. *Two-qubit entanglement dynamics for two different non-Markovian environments.* Phys. Scripta **T140**, 014014 (2010).

[Bennett12] S. D. Bennett, S. Kolkowitz, Q. P. Unterreithmeier, P. Rabl, A. C. B. Jayich, J. G. E. Harris, and M. D. Lukin. *Measuring mechanical motion with a single spin.* arXiv:1205.6740 (2012).

[Béri12] B. Béri. *Nonlocal conductance reveals helical superconductors.* Phys. Rev. B **85**, 140501 (2012).

[Blanter00] Y. Blanter and M. Büttiker. *Shot noise in mesoscopic conductors.* Phys. Rep. **336**, 1 (2000).

[Blencowe05a] M. P. Blencowe. *Nanoelectromechanical systems.* Contemp. Phys. **46**, 249 (2005).

[Blencowe05b] M. P. Blencowe, J. Imbers, and A. D. Armour. *Dynamics of a nanomechanical resonator coupled to a superconducting single-electron transistor.* New J. Phys. **7**, 236 (2005).

[Bolech07] C. Bolech and E. Demler. *Observing Majorana bound States in p-Wave Superconductors Using Noise Measurements in Tunneling Experiments.* Phys. Rev. Lett. **98**, 237002 (2007).

[Børkje11] K. Børkje, A. Nunnenkamp, and S. Girvin. *Proposal for Entangling Remote Micromechanical Oscillators via Optical Measurements.* Phys. Rev. Lett. **107**, 123601 (2011).

[Born28] M. Born and V. Fock. *Beweis des Adiabatensatzes.* Z. Phys. A Hadron. Nucl. **51**, 165 (1928).

[Bose06] S. Bose and G. S. Agarwal. *Entangling pairs of nano-cantilevers, Cooper-pair boxes and mesoscopic teleportation.* New J. Phys. **8**, 34 (2006).

[Bose11] S. Bose and P. Sodano. *Nonlocal Hanbury–Brown–Twiss interferometry and entanglement generation from Majorana bound states.* New J. Phys. **13**, 085002 (2011).

[Breuer02] H. P. Breuer and F. Petruccione. *The Theory of Open Quantum Systems.* Oxford University Press, Oxford, 2002.

[Budich12] J. C. Budich, S. Walter, and B. Trauzettel. *Failure of protection of Majorana based qubits against decoherence.* Phys. Rev. B **85**, 121405 (2012).

[Chaturvedi79] S. Chaturvedi and F. Shibata. *Time-Convolutionless Projection Operator Formalism for Elimination of Fast Variables - Applications to Brownian-Motion.* Z. Phys. B Con. Mat. **35**, 297 (1979).

[Chen11a] P.-W. Chen, C.-C. Jian, and H.-S. Goan. *Non-Markovian dynamics of a nanomechanical resonator measured by a quantum point contact.* Phys. Rev. B **83**, 115439 (2011).

[Chen11b] X. Chen, Z.-C. Gu, Z.-X. Liu, and X.-G. Wen. *Symmetry protected topological orders and the cohomology class of their symmetry group.* arXiv:1106.4772 (2011).

[Chiu08] H.-Y. Chiu, P. Hung, H. W. C. Postma, and M. Bockrath. *Atomic-Scale Mass Sensing Using Carbon Nanotube Resonators.* Nano Lett. **8**, 4342 (2008).

[Cirac95] J. Cirac and P. Zoller. *Quantum computations with cold trapped ions.* Phys. Rev. Lett. **74**, 4091 (1995).

[Cleland02] A. N. Cleland. *Foundations of Nanomechanics.* From Solid-State Theory to Device Applications. Springer, 2002.

[Cleland04] A. Cleland and M. Geller. *Superconducting Qubit Storage and Entanglement with Nanomechanical Resonators.* Phys. Rev. Lett. **93**, 070501 (2004).

[Clerk04a] A. Clerk. *Quantum-limited position detection and amplification: A linear response perspective.* Phys. Rev. B **70**, 245306 (2004).

[Clerk04b] A. Clerk and S. Girvin. *Shot noise of a tunnel junction displacement detector.* Phys. Rev. B **70**, 121303 (2004).

[Clerk05] A. A. Clerk and S. Bennett. *Quantum nanoelectromechanics with electrons, quasi-particles and Cooper pairs: effective bath descriptions and strong feedback effects.* New J. Phys. **7**, 238 (2005).

[Craig68] R. A. Craig. *Perturbation Expansion for Real-Time Green's Functions.* J. Math. Phys. **9**, 605 (1968).

[Das12] A. Das, Y. Ronen, Y. Most, Y. Oreg, M. Heiblum, and H. Shtrikman. *Evidence of Majorana fermions in an Al - InAs nanowire topological superconductor.* arXiv:1205.7073 (2012).

[De Chiara11] G. De Chiara, M. Paternostro, and G. Palma. *Entanglement detection in hybrid optomechanical systems.* Phys. Rev. A **83** (2011).

[Deng12] M. T. Deng, C. L. Yu, G. Y. Huang, M. Larsson, P. Caroff, and H. Q. Xu. *Observation of Majorana Fermions in a Nb-InSb Nanowire-Nb Hybrid Quantum Device.* arXiv:1204.4130 (2012).

[Dicarlo06] L. Dicarlo, Y. Zhang, D. T. McClure, C. M. Marcus, L. N. Pfeiffer, and K. W. West. *System for measuring auto- and cross correlation of current noise at low temperatures.* Rev. Sci. Instrum. **77**, 073906 (2006).

[Dirac28] P. A. M. Dirac. *The quantum theory of the electron.* Proc. R. Soc. A **117**, 610 (1928).

[Doiron07] C. Doiron, B. Trauzettel, and C. Bruder. *Improved position measurement of nanoelectromechanical systems using cross correlations.* Phys. Rev. B **76**, 195312 (2007).

[Doiron08] C. Doiron, B. Trauzettel, and C. Bruder. *Measuring the Momentum of a Nanomechanical Oscillator through the Use of Two Tunnel Junctions.* Phys. Rev. Lett. **100**, 027202 (2008).

[Domański08] T. Domański and A. Donabidowicz. *Interplay between particle-hole splitting and the Kondo effect in quantum dots.* Phys. Rev. B **78**, 073105 (2008).

[Dovzhenko11] Y. Dovzhenko, J. Stehlik, K. Petersson, J. Petta, H. Lu, and A. Gossard. *Nonadiabatic quantum control of a semiconductor charge qubit.* Phys. Rev. B **84**, 161302 (2011).

[Duan00] L. Duan, G. Giedke, J. Cirac, and P. Zoller. *Inseparability criterion for continuous variable systems.* Phys. Rev. Lett. **84**, 2722 (2000).

[Edamatsu04] K. Edamatsu, G. Oohata, R. Shimizu, and T. Itoh. *Generation of ultraviolet entangled photons in a semiconductor.* Nature **431**, 167 (2004).

[Eisert04] J. Eisert, M. Plenio, S. Bose, and J. Hartley. *Towards Quantum Entanglement in Nanoelectromechanical Devices.* Phys. Rev. Lett. **93**, 190402 (2004).

[Faust12] T. Faust, J. Rieger, M. Seitner, P. Krenn, J. Kotthaus, and E. Weig. *Nonadiabatic Dynamics of Two Strongly Coupled Nanomechanical Resonator Modes.* Phys. Rev. Lett. **109**, 037205 (2012).

[Feynman60] R. P. Feynman. *There's Plenty of Room at the Bottom.* Engineering and Science **23**, 22 (1960).

[Fidkowski11] L. Fidkowski and A. Kitaev. *Topological phases of fermions in one dimension.* Phys. Rev. B **83**, 075103 (2011).

[Flensberg10] K. Flensberg. *Tunneling characteristics of a chain of Majorana bound states.* Phys. Rev. B **82**, 180516 (2010).

[Flensberg11] K. Flensberg. *Non-Abelian Operations on Majorana Fermions via Single-Charge Control.* Phys. Rev. Lett. **106**, 090503 (2011).

[Flowers-Jacobs07] N. Flowers-Jacobs, D. Schmidt, and K. Lehnert. *Intrinsic Noise Properties of Atomic Point Contact Displacement Detectors.* Phys. Rev. Lett. **98**, 096804 (2007).

[Fu08] L. Fu and C. Kane. *Superconducting Proximity Effect and Majorana Fermions at the Surface of a Topological Insulator.* Phys. Rev. Lett. **100**, 096407 (2008).

[Fu09a] L. Fu and C. Kane. *Josephson current and noise at a superconductor/quantum-spin-Hall-insulator/superconductor junction.* Phys. Rev. B **79**, 161408 (2009).

[Fu09b] L. Fu and C. Kane. *Probing Neutral Majorana Fermion Edge Modes with Charge Transport.* Phys. Rev. Lett. **102**, 216403 (2009).

[Fu10] L. Fu. *Electron Teleportation via Majorana Bound States in a Mesoscopic Superconductor.* Phys. Rev. Lett. **104**, 056402 (2010).

[Gao11] M. Gao, Y.-X. Liu, and X.-B. Wang. *Coupling Rydberg atoms to superconducting qubits via nanomechanical resonator.* Phys. Rev. A **83**, 022309 (2011).

[Gavish00] U. Gavish, Y. Levinson, and Y. Imry. *Detection of quantum noise.* Phys. Rev. B **62**, 10637 (2000).

[Gell-Mann51] M. Gell-Mann and F. Low. *Bound states in quantum field theory.* Phys Rev **84**, 350 (1951).

[Geller05] M. Geller and A. Cleland. *Superconducting qubits coupled to nano-electromechanical resonators: An architecture for solid-state quantum-information processing.* Phys. Rev. A **71**, 032311 (2005).

[Genes08] C. Genes, D. Vitali, and P. Tombesi. *Emergence of atom-light-mirror entanglement inside an optical cavity.* Phys. Rev. A **77** (2008).

[Goldstein11] G. Goldstein and C. Chamon. *Decay rates for topological memories encoded with Majorana fermions.* Phys. Rev. B **84**, 205109 (2011).

[Golub11a] A. Golub and B. Horovitz. *Shot noise in a Majorana fermion chain.* Phys. Rev. B **83**, 153415 (2011).

[Golub11b] A. Golub, I. Kuzmenko, and Y. Avishai. *Kondo Correlations and Majorana Bound States in a Metal to Quantum-Dot to Topological-Superconductor Junction.* Phys. Rev. Lett. **107**, 176802 (2011).

[Hammerer09] K. Hammerer, M. Aspelmeyer, E. Polzik, and P. Zoller. *Establishing Einstein-Poldosky-Rosen Channels between Nanomechanics and Atomic Ensembles.* Phys. Rev. Lett. **102**, 020501 (2009).

[Hassler10]   F. Hassler, A. Akhmerov, C. Hou, and C. Beenakker. *Anyonic interfer-ometry without anyons: how a flux qubit can read out a topological qubit.* New J. Phys. **12**, 125002 (2010).

[Hassler11]   F. Hassler, A. Akhmerov, and C. Beenakker. *Top-transmon: hybrid superconducting qubit for parity-protected quantum computation.* New J. Phys. **13**, 095004 (2011).

[Hong12]   S. Hong, M. S. Grinolds, P. Maletinsky, R. L. Walsworth, M. D. Lukin, and A. Yacoby. *Coherent, mechanical control of a single electronic spin.* arXiv:1202.1823 (2012).

[Horodecki97]   P. Horodecki. *Separability criterion and inseparable mixed states with positive partial transposition.* Phys. Lett. A **232**, 333 (1997).

[Horodecki09]   R. Horodecki, M. Horodecki, and K. Horodecki. *Quantum entanglement.* Rev. Mod. Phys. **81**, 865 (2009).

[Isar10]   A. Isar. *Continuous variable entanglement in open quantum dynamics.* Phys. Scripta **2010**, 014023 (2010).

[Jensen08]   K. Jensen, K. Kim, and A. Zettl. *An atomic-resolution nanomechanical mass sensor.* Nat. Nanotechnol. **3**, 533 (2008).

[Joshi10]   C. Joshi, A. Hutter, F. Zimmer, M. Jonson, E. Andersson, and P. Öhberg. *Quantum entanglement of nanocantilevers.* Phys. Rev. A **82**, 043846 (2010).

[Kadanoff62]   L. Kadanoff and G. Baym. *Quantum statistical mechanics: Green's function methods in equilibrium and nonequilibrium problems.* W.A. Benjamin, New York, 1962.

[Katz07]   I. Katz, A. Retzker, R. Straub, and R. Lifshitz. *Signatures for a Classical to Quantum Transition of a Driven Nonlinear Nanomechanical Resonator.* Phys. Rev. Lett. **99**, 040404 (2007).

[Katz08]   I. Katz, R. Lifshitz, A. Retzker, and R. Straub. *Classical to quantum transition of a driven nonlinear nanomechanical resonator.* New J. Phys. **10**, 125023 (2008).

[Keldysh65]   L. V. Keldysh. *Diagram Technique for Nonequilibrium Processes.* Sov. Phys. JETP **20**, 1018 (1965).

[Kippenberg07]   T. J. Kippenberg and K. J. Vahala. *Cavity Opto-Mechanics.* Opt. Express **15**, 17173 (2007).

[Kippenberg08]   T. J. Kippenberg and K. J. Vahala. *Cavity optomechanics: Back-action at the mesoscale.* Science **321**, 1172 (2008).

[Kitaev01] A. Kitaev. *Unpaired Majorana fermions in quantum wires.* Phys.-Usp. **44**, 131 (2001).

[Kitaev06] A. Kitaev and J. Preskill. *Topological Entanglement Entropy.* Phys. Rev. Lett. **96**, 110404 (2006).

[Kitaev09] A. Kitaev. *Periodic table for topological insulators and superconductors.* AIP Conf. Proc. **1134**, 22 (2009).

[Kleckner06] D. Kleckner and D. Bouwmeester. *Sub-kelvin optical cooling of a micromechanical resonator.* Nature **444**, 75 (2006).

[Kovalev11] A. Kovalev, L. Hayden, G. Bauer, and Y. Tserkovnyak. *Macrospin Tunneling and Magnetopolaritons with Nanomechanical Interference.* Phys. Rev. Lett. **106**, 147203 (2011).

[Lassagne08] B. Lassagne, D. Garcia-Sanchez, A. Aguasca, and A. Bachtold. *Ultrasensitive Mass Sensing with a Nanotube Electromechanical Resonator.* Nano Lett. **8**, 3735 (2008).

[Law09] K. Law, P. Lee, and T. Ng. *Majorana Fermion Induced Resonant Andreev Reflection.* Phys. Rev. Lett. **103**, 237001 (2009).

[Lee08] M.-T. Lee and W.-M. Zhang. *Non-Markovian suppression of charge qubit decoherence in the quantum point contact measurement.* J. Chem. Phys. **129**, 224106 (2008).

[Leggett05] A. J. Leggett. *The Quantum Measurement Problem.* Science **307**, 871 (2005).

[Leijnse11a] M. Leijnse and K. Flensberg. *Quantum Information Transfer between Topological and Spin Qubit Systems.* Phys. Rev. Lett. **107**, 210502 (2011).

[Leijnse11b] M. Leijnse and K. Flensberg. *Scheme to measure Majorana fermion lifetimes using a quantum dot.* Phys. Rev. B **84**, 140501 (2011).

[Lesovik97] G. Lesovik and R. Loosen. *On the detection of finite-frequency current fluctuations.* JETP Lett. **65**, 295 (1997).

[Levin06] M. Levin and X.-G. Wen. *Detecting Topological Order in a Ground State Wave Function.* Phys. Rev. Lett. **96**, 110405 (2006).

[Li08] T. Li, Y. Pashkin, O. Astafiev, Y. Nakamura, J. Tsai, and H. Im. *High-frequency metallic nanomechanical resonators.* Appl. Phys. Lett. **92**, 043112 (2008).

[Liu07] K.-L. Liu and H.-S. Goan. *Non-Markovian entanglement dynamics of quantum continuous variable systems in thermal environments.* Phys. Rev. A **76**, 022312 (2007).

[Liu11a] C.-X. Liu and B. Trauzettel. *Helical Dirac-Majorana interferometer in a superconductor/topological insulator sandwich structure.* Phys. Rev. B **83**, 220510 (2011).

[Liu11b] D. Liu and H. Baranger. *Detecting a Majorana-fermion zero mode using a quantum dot.* Phys. Rev. B **84**, 201308 (2011).

[Liu12] J. Liu, A. C. Potter, K. T. Law, and P. A. Lee. *Zero-bias peaks in spin-orbit coupled superconducting wires with and without Majorana end-states.* arXiv:1206.1276 (2012).

[Loss98] D. Loss and D. DiVincenzo. *Quantum computation with quantum dots.* Phys. Rev. A **57**, 120 (1998).

[Ludwig10] M. Ludwig, K. Hammerer, and F. Marquardt. *Entanglement of mechanical oscillators coupled to a nonequilibrium environment.* Phys. Rev. A **82**, 012333 (2010).

[Lutchyn10] R. Lutchyn, J. Sau, and S. Das Sarma. *Majorana Fermions and a Topological Phase Transition in Semiconductor-Superconductor Heterostructures.* Phys. Rev. Lett. **105**, 077001 (2010).

[Mahan00] G. D. Mahan. *Many Particle Physics.* Kluwer Academic/Plenum Publishers, New York, 2000.

[Majorana37] E. Majorana. *Theory of the symmetry of electrons and positrons.* Nuovo Cimento **14**, 71 (1937).

[Mamin01] H. Mamin and D. Rugar. *Sub-attonewton force detection at millikelvin temperatures.* Appl. Phys. Lett. **79**, 3358 (2001).

[Mancini02] S. Mancini, V. Giovannetti, D. Vitali, and P. Tombesi. *Entangling Macroscopic Oscillators Exploiting Radiation Pressure.* Phys. Rev. Lett. **88**, 120401 (2002).

[Marquardt09] F. Marquardt and S. Girvin. *Optomechanics.* Physics **2**, 40 (2009).

[Martin12] I. Martin and A. F. Morpurgo. *Majorana fermions in superconducting helical magnets.* Phys. Rev. B **85**, 144505 (2012).

[Mourik12] V. Mourik, K. Zuo, S. M. Frolov, S. R. Plissard, E. P. A. M. Bakkers, and L. P. Kouwenhoven. *Signatures of Majorana Fermions in Hybrid Superconductor-Semiconductor Nanowire Devices.* Science **336**, 1003 (2012).

[Mozyrsky02] D. Mozyrsky and I. Martin. *Quantum-Classical Transition Induced by Electrical Measurement.* Phys. Rev. Lett. **89**, 018301 (2002).

[Mozyrsky04] D. Mozyrsky, I. Martin, and M. Hastings. *Quantum-Limited Sensitivity of Single-Electron-Transistor-Based Displacement Detectors.* Phys. Rev. Lett. **92**, 018303 (2004).

[Murakawa04] H. Murakawa, K. Ishida, K. Kitagawa, Z. Mao, and Y. Maeno. *Measurement of the Ru101-Knight Shift of Superconducting Sr2RuO4 in a Parallel Magnetic Field.* Phys. Rev. Lett. **93**, 167004 (2004).

[Naik09] A. K. Naik, M. S. Hanay, W. K. Hiebert, X. L. Feng, and M. L. Roukes. *Towards single-molecule nanomechanical mass spectrometry.* Nat. Nanotechnol. **4**, 445 (2009).

[Nakajima58] S. Nakajima. *On Quantum Theory of Transport Phenomena Steady Diffusion.* Prog. Theor. Phys. **20**, 948 (1958).

[Nayak08] C. Nayak, A. Stern, M. Freedman, and S. Das Sarma. *Non-Abelian anyons and topological quantum computation.* Rev. Mod. Phys. **80**, 1083 (2008).

[Neeley10] M. Neeley, R. C. Bialczak, M. Lenander, E. Lucero, M. Mariantoni, A. D. O'Connell, D. Sank, H. Wang, M. Weides, J. Wenner, Y. Yin, T. Yamamoto, A. N. Cleland, and J. M. Martinis. *Generation of three-qubit entangled states using superconducting phase qubits.* Nature **467**, 570 (2010).

[Nielsen00] M. A. Nielsen and I. L. Chuang. *Quantum Computation and Quantum Information.* Cambridge University Press, Cambridge, 2000.

[Nilsson08] J. Nilsson, A. Akhmerov, and C. Beenakker. *Splitting of a Cooper Pair by a Pair of Majorana Bound States.* Phys. Rev. Lett. **101**, 120403 (2008).

[Nozieres64] P. Nozieres. *Theory of Interacting Fermi Systems.* Westview Press, 1964.

[O'Connell10] A. D. O'Connell, M. Hofheinz, M. Ansmann, R. C. Bialczak, M. Lenander, E. Lucero, M. Neeley, D. Sank, H. Wang, M. Weides, J. Wenner, J. M. Martinis, and A. N. Cleland. *Quantum ground state and single-phonon control of a mechanical resonator.* Nature **464**, 697 (2010).

[Olivares12] S. Olivares. *Quantum optics in the phase space.* Eur. Phys. J.-Spec. Top. **203**, 3 (2012).

[Oreg10] Y. Oreg, G. Refael, and F. v. Oppen. *Helical Liquids and Majorana Bound States in Quantum Wires.* Phys. Rev. Lett. **105**, 177002 (2010).

[Paz02] J. P. Paz and W. H. Zurek. *Environment-Induced Decoherence and the Transition from Quantum to Classical.* Lecture Notes in Physics **587**, 77 (2002).

[Penrose96] R. Penrose. *On gravity's role in quantum state reduction.* Gen. Rel. Grav. **28**, 581 (1996).

[Peres96] A. Peres. *Separability criterion for density matrices.* Phys. Rev. Lett. **77**, 1413 (1996).

[Pinard07]   M. Pinard, A. Dantan, D. Vitali, O. Arcizet, T. Briant, and A. Heidmann. *Entangling movable mirrors in a double-cavity system.* Europhys. Lett. **72**, 747 (2007).

[Pirandola06]   S. Pirandola, D. Vitali, P. Tombesi, and S. Lloyd. *Macroscopic Entanglement by Entanglement Swapping.* Phys. Rev. Lett. **97**, 150403 (2006).

[Pirandola09]   S. Pirandola, A. Serafini, and S. Lloyd. *Correlation matrices of two-mode bosonic systems.* Phys. Rev. A **79**, 052327 (2009).

[Rabl09]   P. Rabl, P. Cappellaro, M. Dutt, L. Jiang, J. Maze, and M. Lukin. *Strong magnetic coupling between an electronic spin qubit and a mechanical resonator.* Phys. Rev. B **79**, 041302 (2009).

[Rabl10]   P. Rabl, S. J. Kolkowitz, F. H. L. Koppens, J. G. E. Harris, P. Zoller, and M. D. Lukin. *A quantum spin transducer based on nanoelectromechanical resonator arrays.* Nat. Phys. **6**, 602 (2010).

[Rainis12]   D. Rainis and D. Loss. *Majorana qubit decoherence by quasiparticle poisoning.* Phys. Rev. B **85**, 174533 (2012).

[Rammer07]   J. Rammer. *Quantum field theory of non-equilibrium states.* Cambridge University Press, 2007.

[Rastelli10]   G. Rastelli, M. Houzet, and F. Pistolesi. *Resonant magneto-conductance of a suspended carbon nanotube quantum dot.* Europhys. Lett. **89**, 57003 (2010).

[Read00]   N. Read and D. Green. *Paired states of fermions in two dimensions with breaking of parity and time-reversal symmetries and the fractional quantum Hall effect.* Phys. Rev. B **61**, 10267 (2000).

[Recher01]   P. Recher, E. Sukhorukov, and D. Loss. *Andreev tunneling, Coulomb blockade, and resonant transport of nonlocal spin-entangled electrons.* Phys. Rev. B **63**, 165314 (2001).

[Recher02]   P. Recher and D. Loss. *Superconductor coupled to two Luttinger liquids as an entangler for electron spins.* Phys. Rev. B **65**, 165327 (2002).

[Redfield57]   A. G. Redfield. *On the Theory of Relaxation Processes.* IBM J. Res. Dev. **1**, 19 (1957).

[Rieger12]   J. Rieger, T. Faust, M. J. Seitner, J. P. Kotthaus, and E. M. Weig. *Frequency and Q factor control of nanomechanical resonators.* Appl. Phys. Lett. **101**, 103110 (2012).

[Rokhinson12]   L. P. Rokhinson, X. Liu, and J. K. Furdyna. *Observation of the Fractional Ac Josephson Effect: the Signature of Majorana Particles.* Nat. Phys. DOI:10.1038/NPHYS2429 (2012).

[Sau10] J. D. Sau, R. M. Lutchyn, S. Tewari, and S. Das Sarma. *Generic New Platform for Topological Quantum Computation Using Semiconductor Heterostructures.* Phys. Rev. Lett. **104**, 040502 (2010).

[Schmidt10] T. L. Schmidt, K. Børkje, C. Bruder, and B. Trauzettel. *Detection of Qubit-Oscillator Entanglement in Nanoelectromechanical Systems.* Phys. Rev. Lett. **104**, 177205 (2010).

[Schmidt12] M. Schmidt, D. Rainis, and D. Loss. *Decoherence of Majorana qubits by noisy gates.* Phys. Rev. B **86**, 085414 (2012).

[Schoelkopf97] R. Schoelkopf, P. Burke, A. Kozhevnikov, D. Prober, and M. Rooks. *Frequency dependence of shot noise in a diffusive mesoscopic conductor.* Phys. Rev. Lett. **78**, 3370 (1997).

[Schrödinger35a] E. Schrödinger. *Die gegenwartige Situation in der Quantenmechanik.* Naturwissenschaften **23**, 807 (1935).

[Schrödinger35b] E. Schrödinger. *Die gegenwartige Situation in der Quantenmechanik.* Naturwissenschaften **23**, 823 (1935).

[Schumaker86] B. L. Schumaker. *Quantum mechanical pure states with Gaussian wave functions.* Phys. Rep. **135**, 317 (1986).

[Schwinger61] J. Schwinger. *Brownian motion of a quantum oscillator.* J. Math. Phys. **2**, 407 (1961).

[Semenoff07] G. Semenoff and P. Sodano. *Stretched quantum states emerging from a Majorana medium.* J. Phys. B: At., Mol. Opt. Phys. **40**, 1479 (2007).

[Shibata77] F. Shibata, Y. Takahashi, and N. Hashitsume. *A generalized stochastic liouville equation. Non-Markovian versus memoryless master equations.* J. Stat. Phys. **17**, 171 (1977).

[Shibata80] F. Shibata and T. Arimitsu. *Expansion formulas in nonequilibrium statistical mechanics.* J. Phys. Soc. Jpn. **49**, 891 (1980).

[Shivamoggi10] V. Shivamoggi, G. Refael, and J. E. Moore. *Majorana fermion chain at the quantum spin Hall edge.* Phys. Rev. B **82**, 041405 (2010).

[Simon00] R. Simon. *Peres-Horodecki separability criterion for continuous variable systems.* Phys. Rev. Lett. **84**, 2726 (2000).

[Smirnov03] A. Smirnov, L. Mourokh, and N. Horing. *Nonequilibrium fluctuations and decoherence in nanomechanical devices coupled to the tunnel junction.* Phys. Rev. B **67**, 115312 (2003).

[Stanescu11] T. Stanescu, R. Lutchyn, and S. Das Sarma. *Majorana fermions in semiconductor nanowires.* Phys. Rev. B **84**, 144522 (2011).

[Steane98]   A. Steane. *Quantum Computing.* Rep. Prog. Phys. **61**, 117 (1998).

[Steffen06]   M. Steffen, M. Ansmann, R. C. Bialczak, N. Katz, E. Lucero, R. Mc-Dermott, M. Neeley, E. M. Weig, A. N. Cleland, and J. M. Martinis. *Measurement of the entanglement of two superconducting qubits via state tomography.* Science **313**, 1423 (2006).

[Stevenson06] R. M. Stevenson, R. J. Young, P. Atkinson, K. Cooper, D. A. Ritchie, and A. J. Shields. *A semiconductor source of triggered entangled photon pairs.* Nature **439**, 179 (2006).

[Strübi11]   G. Strübi, W. Belzig, M.-S. Choi, and C. Bruder. *Interferometric and Noise Signatures of Majorana Fermion Edge States in Transport Experiments.* Phys. Rev. Lett. **107**, 136403 (2011).

[Teufel11]   J. D. Teufel, T. Donner, D. Li, J. W. Harlow, M. S. Allman, K. Cicak, A. J. Sirois, J. D. Whittaker, K. W. Lehnert, and R. W. Simmonds. *Sideband cooling of micromechanical motion to the quantum ground state.* Nature **475**, 359 (2011).

[Tewari08]   S. Tewari, C. Zhang, S. Das Sarma, C. Nayak, and D.-H. Lee. *Testable Signatures of Quantum Nonlocality in a Two-Dimensional Chiral p-Wave Superconductor.* Phys. Rev. Lett. **100**, 027001 (2008).

[Treutlein07] P. Treutlein, D. Hunger, S. Camerer, T. Hänsch, and J. Reichel. *Bose-Einstein Condensate Coupled to a Nanomechanical Resonator on an Atom Chip.* Phys. Rev. Lett. **99**, 140403 (2007).

[Utami04]   D. Utami, H.-S. Goan, and G. Milburn. *Charge transport in a quantum electromechanical system.* Phys. Rev. B **70**, 075303 (2004).

[vanHeck11]   B. van Heck, F. Hassler, A. Akhmerov, and C. Beenakker. *Coulomb stability of the 4π-periodic Josephson effect of Majorana fermions.* Phys. Rev. B **84**, 180502 (2011).

[Vidal02]   G. Vidal and R. Werner. *Computable measure of entanglement.* Phys. Rev. A **65**, 032314 (2002).

[Vitali07a]   D. Vitali, S. Gigan, A. Ferreira, H. Böhm, P. Tombesi, A. Guerreiro, V. Vedral, A. Zeilinger, and M. Aspelmeyer. *Optomechanical Entanglement between a Movable Mirror and a Cavity Field.* Phys. Rev. Lett. **98** (2007).

[Vitali07b]   D. Vitali, P. Tombesi, M. Woolley, A. Doherty, and G. Milburn. *Entangling a nanomechanical resonator and a superconducting microwave cavity.* Phys. Rev. A **76**, 042336 (2007).

[Wabnig05]   J. Wabnig, D. V. Khomitsky, J. Rammer, and A. L. Shelankov. *Statistics of charge transfer in a tunnel junction coupled to an oscillator.* Phys. Rev. B **72**, 165347 (2005).

[Wabnig07] J. Wabnig, J. Rammer, and A. Shelankov. *Noise spectrum of a tunnel junction coupled to a nanomechanical oscillator.* Phys. Rev. B **75**, 205319 (2007).

[Wallraff04] A. Wallraff, D. I. Schuster, A. Blais, L. Frunzio, R. S. Huang, J. Majer, S. Kumar, S. M. Girvin, and R. J. Schoelkopf. *Strong coupling of a single photon to a superconducting qubit using circuit quantum electrodynamics.* Nature **431**, 162 (2004).

[Walter11a] S. Walter, T. L. Schmidt, K. Børkje, and B. Trauzettel. *Detecting Majorana bound states by nanomechanics.* Phys. Rev. B **84**, 224510 (2011).

[Walter11b] S. Walter and B. Trauzettel. *Momentum and position detection in nano-electromechanical systems beyond the Born and Markov approximations.* Phys. Rev. B **83**, 155411 (2011).

[Walter12] S. Walter, J. C. Budich, and B. Trauzettel. *Entanglement of nano-electromechanical oscillators by Cooper-pair tunneling.* arXiv:1210.0665 (2012).

[Werner01] R. F. Werner and M. M. Wolf. *Bound Entangled Gaussian States.* Phys. Rev. Lett. **86**, 3658 (2001).

[Williams12] J. Williams, A. Bestwick, P. Gallagher, S. Hong, Y. Cui, A. Bleich, J. Analytis, I. Fisher, and D. Goldhaber-Gordon. *Unconventional Josephson Effect in Hybrid Superconductor-Topological Insulator Devices.* Phys. Rev. Lett. **109**, 056803 (2012).

[Wingreen94] N. S. Wingreen and Y. Meir. *Anderson model out of equilibrium: Noncrossing-approximation approach to transport through a quantum dot.* Phys. Rev. B **49**, 11040 (1994).

[Xia06] J. Xia, Y. Maeno, P. Beyersdorf, M. Fejer, and A. Kapitulnik. *High Resolution Polar Kerr Effect Measurements of Sr2RuO4: Evidence for Broken Time-Reversal Symmetry in the Superconducting State.* Phys. Rev. Lett. **97**, 167002 (2006).

[Xiao10] X. Xiao, M.-F. Fang, and Y.-L. Li. *Non-Markovian dynamics of two qubits driven by classical fields: population trapping and entanglement preservation.* J. Phys. B: At., Mol. Opt. Phys. **43**, 185505 (2010).

[Yang06] Y. Yang, C. Callegari, X. Feng, K. Ekinci, and M. Roukes. *Zeptogram-scale nanomechanical mass sensing.* Nano Lett. **6**, 583 (2006).

[Ying-Hua10] J. Ying-Hua and H. Ju-Ju. *Entanglement and decoherence of coupled superconductor qubits in a non-Markovian environment.* Chinese Phys. B **19**, 060304 (2010).

[Zazunov11] A. Zazunov, A. Yeyati, and R. Egger. *Coulomb blockade of Majorana-fermion-induced transport.* Phys. Rev. B **84**, 165440 (2011).

[Zhu05] Y. Zhu, J. Maciejko, T. Ji, H. Guo, and J. Wang. *Time-dependent quantum transport: Direct analysis in the time domain.* Phys. Rev. B **71** (2005).

[Zurek03] W. H. Zurek. *Decoherence, einselection, and the quantum origins of the classical.* Rev. Mod. Phys. **75**, 715 (2003).

[Zwanzig60] R. Zwanzig. *Ensemble Method in the Theory of Irreversibility.* J. Chem. Phys. **33**, 1338 (1960).

Acknowledgments

The last three years during which this thesis was worked out have been a real pleasure. Without the support from many sides this would not have been possible and I am thankful to a lot of people including not only colleagues but also friends and family for their constant help and support.

I would like to thank all the guys of TP4 here at Würzburg for making my time as a PhD student as delightful and pleasant as it has been. The very unique atmosphere in this one-of-a-kind research group, including scientific discussions as well as social get-togethers and activities created a supporting and enjoyable working environment which I am very thankful for. I always found help in Dietrich, Jörg, and Rolf seeking solutions for challenges with numerics, latex, and computers. I very much appreciate my office mates Anselm, Florian, Moritz, and Sebastian. In particular I would like to thank Moritz for many discussions on miscellaneous physics and math related problems. Another person who I especially would like to thank is Jan for sharing his tremendous knowledge and insight to various aspects of physics, numerous discussions, fruitful collaborations, and the occasional after work beer. Many thanks to Nelly for taking care of all administrative matters in a friendly and cordial manner, the fastest and most uncomplicated way possible. I also would like to thank a non-TP4 colleague, Thomas Schmidt, who shared his understandings of nanomechanics with me and was always a prime address for questions on long calculations and analytical technicalities.

I am very grateful to my advisor Björn Trauzettel who introduced me to the subject of my thesis and for his superb guidance throughout the three years. He always managed to have an open door to discuss and talk. His always positive nature encouraged me to stick to problems and try to solve them. I profited not only from his enormous expertise in divers fields of physics but also by the large number of opportunities he gave me to attend conferences, workshops, and scientific visits.

Most of all, I am deeply thankful for the constant support and love of my family during all these years of school and university, and raising me the way they did.

List of publications

The following articles have appeared in peer-reviewed journals:

1. Jan Carl Budich, Stefan Walter, and Björn Trauzettel.
   Failure of protection of Majorana based qubits against decoherence.
   Phys. Rev. B **85**, 121405(R) (2012).

2. Stefan Walter, Thomas L. Schmidt, Kjetil Børkje, and Björn Trauzettel.
   Detecting Majorana bound states by nanomechanics.
   Phys. Rev. B **84**, 224510 (2011).

3. Stefan Walter and Björn Trauzettel.
   Momentum and position detection in nanoelectromechanical systems beyond the Born and Markov approximations.
   Phys. Rev. B **83**, 155411 (2011).

4. Stefan Walter, Dominik Schneble, and Adam C. Durst.
   Bloch oscillations in lattice potentials with controlled aperiodicity.
   Phys. Rev. A **81**, 033623 (2010).

The following pre-print is under review:

5. Stefan Walter, Jan Carl Budich, and Björn Trauzettel.
   Entanglement of nanoelectromechanical oscillators by Cooper-pair tunneling.
   arXiv:1210.0665 (2012).
   (submitted to Physical Review Letters)

Curriculum Vitae

Persönliche Angaben:

Name:	Stefan Walter
Geburtsdatum:	8. Oktober 1984
Geburtsort:	Würzburg
Staatsangehörigkeit:	deutsch
Familienstand:	ledig

Schulbildung:

09/1995–07/2004:	Röntgen Gymnasium Würzburg Abschluss: Abitur

Universitätsbildung:

09/2005–09/2007:	Studium der Nanostrukturtechnik Julius-Maximilians-Universität Würzburg, Deutschland
09/2007–08/2008:	Studium der Physik Julius-Maximilians-Universität Würzburg, Deutschland
08/2008–09/2009:	Studium der Physik Stony Brook University, USA Abschluss: Master of Arts in Physics
seit 10/2009:	Doktorand unter Leitung von Prof. Dr. Björn Trauzettel Julius-Maximilians-Universität Würzburg, Deutschland

Würzburg, den . . . .

. . . .

(Stefan Walter)

Affidavit / Erklärung

Die vorliegende Dissertation wurde am Lehrstuhl für Theoretische Physik IV am Institut für Theoretische Physik und Astrophysik der Fakultät für Physik und Astronomie an der Bayerischen Julius-Maximilians-Universität Würzburg angefertigt und von Prof. Dr. Björn Trauzettel betreut. Hiermit versichere ich, Stefan Walter, geboren am 8. Oktober 1984 in Würzburg, an Eides statt, dass ich die vorliegende Dissertation eigenständig, d. h. insbesondere selbstständig und ohne Hilfe eines kommerziellen Promotionsberaters angefertigt und keine anderen als die angegebenen Quellen und Hilfsmittel benutzt habe. Ich erkläre außerdem, dass die vorliegende Dissertation weder in gleicher noch in anderer Form in einem anderen Prüfungsfach vorgelegen hat, und dass ich außer den mit dem Zulassungsgesuch urkundlich vorgelegten Graden keine weiteren akademischen Grade erworben oder zu erwerben versucht habe.

Würzburg, den . . . .

. . . .

(Stefan Walter)